



## Morphological model of the Rhine-Meuse delta

KPP Rivierkunde 2012 - Stabiele keringen





# **Morphological model of the Rhine-Meuse delta**

**KPP Rivierkunde 2012 - Stabiele keringen**

Kees Sloff  
Robin van der Sligte  
Ymkje Huismans  
Hinnerk Fuhrhop

1205961-001



**Title**  
Morphological model of the Rhine-Meuse delta

<b>Client</b>	<b>Project</b>	<b>Reference</b>	<b>Pages</b>
KPP Rivierkunde	1205961-001	1205961-001-ZWS-0005-	120

**Keywords**  
Rhine- Meuse Delta, morphological model, Delft3D, sand, mud, subsoil bookkeeping.

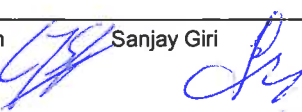
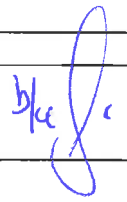
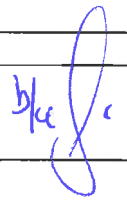
**Summary**

2D and 3D morphological models for the Rhine-Meuse Delta (RMM) are considered important tools for supporting management decisions, and evaluating long-term policy decisions for the delta branches in the Netherlands with respect to safety against flooding. The morphological model for RMM has been set-up and extended in several steps in previous phases of the KPP project, and has become an important part of the River Morphological Deltamodel (RMD). For this model Delft3D has been used, and it has been designed to simulate the tides, as well as the seasonal river-discharge variations. Sediment transport in this model includes two sand and two mud fractions, for which the lithographic profiles of the river bed have been transferred to the under-layer model for sediment composition.. In this project we further improved and extended the model for the Nieuwe Waterweg and Maas River. We derived a parameterisation for the 3D effect of the salt wedge in the Nieuwe Waterweg on the tidal-average sediment-transport rates, to be applied for the 2D simulations, and for computation-time reduction we applied a representative tide to replace the full spring-neap cycle. The calculated flow has been verified on basis of SOBEK simulations, and agreement is reasonable for discharge distribution. For morphological verification we have carried out simulations for dredging operations in the "Oversteek" at Moerdijk, which is the navigation channel from the Dordtsche Kil crossing the Haringvliet estuary. The sedimentation processes observed in this section are reproduced by the model, but the rate of sedimentation is still underestimated by the model. Further improvement is possible by calibration of the transport model and adjusting sediment inflow at boundaries.

A part of the model has also been applied to study the full 3D flow field in local scour holes in the Spui River. Good results for flow field in these holes can be obtained solely using a 3D z-layer model with non-hydrostatic pressure.

**References**

KPP, Deltamodel.

Versie	Datum	Auteur	Paraaf	Review	Paraaf	Goedkeuring	Paraaf
3.0	nov. 2012	Robin van der Sligte & Ymkje Huismans		Frans van der Knaap		Gerard Blom	
4.0	July. 2013	Kees Slooff, Robin van der Sligte & Ymkje Huismans		Sanjay Giri 	Gerard Blom		

**State**  
final



## Contents

<b>1 Introduction</b>	<b>1</b>
1.1 Background (in Dutch)	1
1.2 The Rhine-Meuse delta and the RMM model	2
<b>2 Model construction</b>	<b>5</b>
2.1 Domain description	5
2.2 The baseline model	9
2.3 Hydraulic model	9
2.3.1 Upstream hydrograph	10
2.3.2 Downstream morphological/representative tide	12
2.3.3 Lateral discharges	12
2.4 Morphological model	13
2.4.1 Sediment fractions	13
2.4.2 Bed composition	14
2.4.3 Sediment transport formulae	16
2.4.4 Fixed layers	17
2.4.5 Morphological boundary conditions	17
2.4.6 General simulation scheme for morphological simulations	19
2.4.7 Time reduction techniques	19
<b>3 Salt wedge and sediment transport</b>	<b>23</b>
3.1 Description of the system	23
3.2 From 3D to depth averaged 2D	26
3.3 Implementation	31
3.4 Result in RMM model	33
3.5 Discussion	39
<b>4 Hydraulic verification</b>	<b>41</b>
<b>5 Test-case Moerdijk</b>	<b>43</b>
<b>6 3D analysis of scour holes in the river Spui</b>	<b>49</b>
6.1 Introduction	49
6.2 Model	49
6.2.1 Grid extraction and refinement	49
6.2.2 Boundary conditions	50
6.2.3 Initial conditions	55
6.2.4 Vertical hydrodynamic grid	57
6.3 Results	58
6.4 Conclusions	67
<b>7 Conclusions and recommendations</b>	<b>69</b>
<b>8 References</b>	<b>73</b>

## Appendices

<b>A Hydraulic verification results</b>	<b>A-1</b>
<b>B Roughness definition file (ruw-karak)</b>	<b>B-1</b>
<b>C Haringvliet barrier</b>	<b>C-1</b>
<b>D Subsoil Noord, Oude Maas, Spui</b>	<b>D-1</b>
<b>E Toplayer RMM south</b>	<b>E-1</b>
<b>F Van Rijn (1984); adjusted</b>	<b>F-1</b>
<b>G Riemann boundaries and sea level rise</b>	<b>G-1</b>
<b>H Results 3D analysis scour holes</b>	<b>H-1</b>
H.1 Water-level results	H-1
H.2 Computed stresses and velocities for different discharge scenario's	H-4

# 1 Introduction

## 1.1 Background (in Dutch)

### Achtergrond

Door het sterke getij schuren met name de Oude Maas, Spui en Dordtsche Kil relatief sterk uit. Vanwege de heterogene ondergrond kunnen na het doorbreken van hardere maar dunneren veen en/of kleilagen onverwacht snel diepe ontgrondingskuilen ontwikkelen. Keringen in het rivierstuk met dergelijke kuilen verliezen lokaal tegendruk in de rivierondergrond en dat kan de stabiliteit van deze keringen sterk verminderen. Keringen langs het water vergen een stabiel fundament. In geval van zettingsgevoelige ondergrond is dit stabiliteitsverlies veelal aanleiding om de kering af te keuren en in te grijpen. Dus, in het voor zettingsvloeiing gevoelige Rijn-Maas-Mond gebied (RMM) is de stabiliteit van de keringen afhankelijk van de dynamiek in de rivierbodem.

### Vraag

Uit het bovenstaande volgt dat hoogwaterveiligheid in het RMM-gebied ook afhankelijk is van het beheer van de rivierbodem. Voor het RMM gebied ontbreekt echter een model waarmee trends en beheervarianten voor de verschillende takken in samenhang kunnen worden beschouwd. Doel van dit KPP onderdeel is het operationeel maken van een dergelijk RMM model.

### Doel

Om te bepalen wat rivierbodemontwikkelingen in de toekomst kunnen zijn en hoe de rivierfuncties het beste gehandhaafd kunnen worden is gereedschap nodig om de bodemdynamiek en de invloed van eventuele harde (technische) en zachte (storten, baggeren) maatregelen in het RMM-gebied goed te kunnen voorspellen. Dit gereedschap komt voor beheersvragen beschikbaar met voltooiing van het numerieke Delft3D RMM-model.

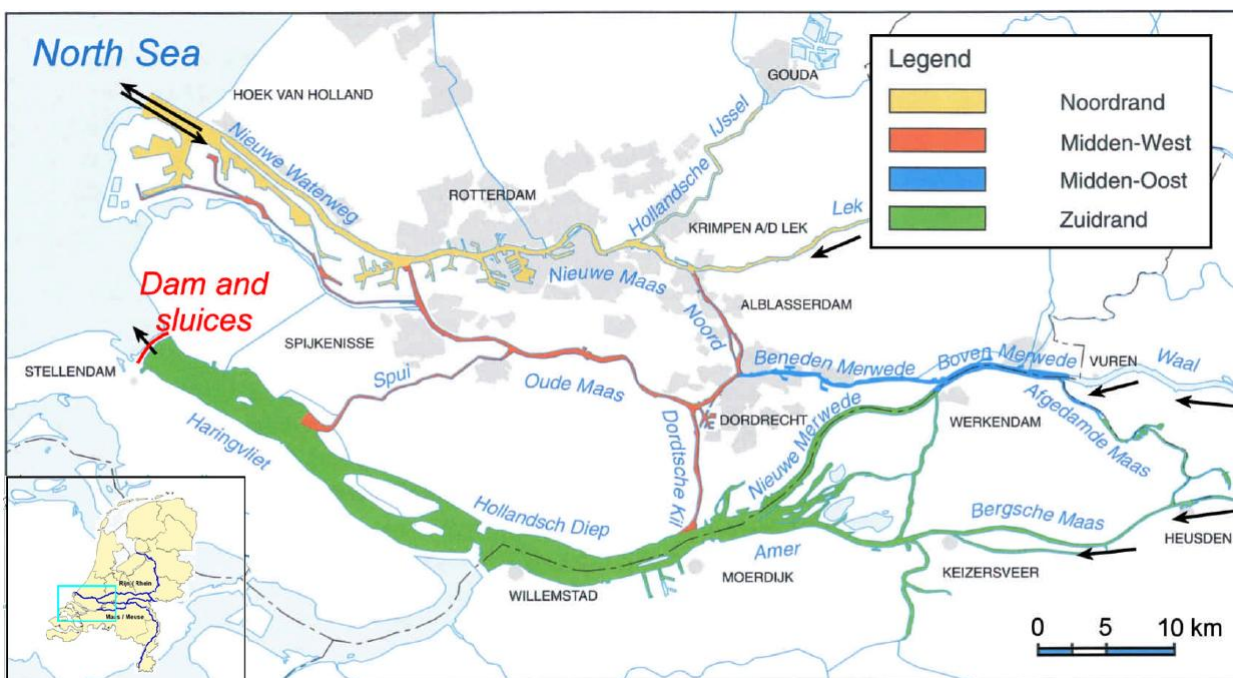
Voor de planning van 2012 is daarom binnen KPP Rivierkunde als onderdeel opgenomen de uitbreiding en toepassing van het numerieke Rijn-Maas-Monding model (RMM) voor 2D riviermorphologie. De betreffende activiteiten omvatten:

- i) de bouw van een op de bestaande modellen van RMM en Lek aansluitende schematisatie van het riviersysteem, tot aan een geschikte raai door de Noordzee-vaargeul.
- ii) de definitie van een rekenmethodiek waarin met voldoende frequentie de invloed van getij en gelaagdheid op grootte en richting van het sedimenttransport kan worden meegenomen voor de verschillende karakteristieke waterbewegingssituaties.
- iii) Het geschikt maken van de bagger-stort module voor het simuleren van sediment-management in de RMM.
- iv) Uitvoering van een test-case van een beheersvariant, met een simulatie van 40 jaar rivierbodemontwikkeling.
- v) Toepassing van een 3D variant van het model voor analyse van gedrag van stroming in de erosiekuilen in RMM.

In de voorliggende rapportage zijn de resultaten van deze activiteiten gepresenteerd. Tegelijkertijd heeft in het kader van de ontwikkeling van het Deltamodel verdere uitbreiding van het RMM model plaatsgevonden, project 1207054. De resultaten van de testsommen, genoemd in punt iv zijn daarom gecombineerd met de resultaten van het Deltamodel in het rapport 1207054 gepresenteerd.

## 1.2 The Rhine-Meuse delta and the RMM model

The mouth of the rivers Rhine and Meuse is located in the highly populated and economically important western part of the Netherlands. The rivers bifurcate into several branches before reaching the North sea, Figure 1.1. Around 1970 the large southern estuary branch, the Haringvliet, was closed by a barrier to, among other things, improve safety of the hinterland as the sixth construction of the Deltaworks. However, the construction of the barrier drastically altered the flow fields in the tidal rivers that used to connect the two estuary branches. The tidal volume is now exchanged entirely through these middle reaches, instead of the original mouth. As a result, large erosion occurs in the middle reaches, Spui, Oude Maas, Noord and Dordtsche Kil. Due to large spatial variations in the erodibility of the underlying alluvium, the river bed shows alternating stable or aggrading sections and deep erosion pits instead of a continuous degradation. As a matter of fact, the variable erodibility is a dominating factor for the present morphology of the river bed. Locally at deep pits the stability of river banks and adjacent dikes is at stake. To maintain a stable and safe river, the river manager is faced with difficult questions to keep the irregular bed-development within certain limits. (Slooff et al. 2011).



Kaartvervaardiging: Meetkundige Dienst; Afdeling GAT © 1995

Figure 1.1 Study area, branches of the Rhine and Meuse River Delta. In this area we distinguish the north-edge (Nieuwe Waterweg and Nieuwe Maas, yellow); the south-edge (Haringvliet and Hollandsch Diep) and the middle-reaches (Spui, Oude Maas, Noord and Dordtsche Kil).

As part of the constant effort of the Dutch government to 'keep dry feet', she asked a new Delta Committee to come up with recommendations on how the Netherlands can be made climate proof over the very long term: safe against flooding, while still remaining an attractive place to live, to reside and work, for recreation and investment (Findings of the Deltacommissie 2008). In the Delta Programme, the Delta Committee investigates possible strategies to meet the goal for future dry feet. In this program, the Rhine Meuse estuary has been appointed as a focus area. The on-going erosion in the river branches and accompanying risk of dike failure and effect on salt intrusion is, understandably, input for the program. On the other side, the planned measures in the river system are likely to affect the morphodynamics of the rivers in the estuary and thereby reduce or possibly accelerate the erosion processes.

Both the local management of the rivers and the national Delta Programme require a solid ground for their visions on sediment management and large scale future strategies. For this a numerical morphological model is developed that will:

- Increase understanding of the current and future sediment transport and morphodynamics.
- Predict the effects and effectiveness of sediment management strategies.
- Test the morphodynamic impact of large scale measures.

The morphological model of the Rhine Meuse estuary is in one way an extension of the successful Delft3D morphological model of the Rhine branches (Duurzame Vaardiepte Rijndelta, DVR, see Yossef 2006). This model covers the Rhine branches from Lobith to the Ketelmeer in the North and the rivers Lek and the Merwedes in the West of the Netherlands. The techniques developed in the DVR are extensively used in this model construction. However, the estuarine nature and the complex diversity of the subsoil of the lower branches of the rivers Rhine and Meuse demand special attention in the modelling process. More specific, this includes the physical modelling of the effect of the salt wedge onto the sediment transport, the incorporation of subsoil layer information, subsoil bookkeeping, and a general managing of the tidal boundary in a morphological river model.

The construction of the morphological model of the Rhine Meuse estuary has been commissioned by the KPP research program after questions from Dienst Zuid Holland. Since 2012 an impulse was given to the construction by the involvement of the Deltamodel. The model developed in this study, will be combined with the DVR model to form a morphological Deltamodel for the Dutch rivers (excluding the Meuse upstream of Lith).

It will be used in the analysis of policy measures, not as an operational tool. Specific examples of its application are the modeling of 'autonomous' bed erosion, testing of dredging or nourishment scenario's, opening of the Haringvliet connection to the sea, the effect of discharge distribution on river bifurcations, and the effect of barriers in the river branches.

### Project team

Dr. ir. Kees Sloff was the project leader for the KPP program; the model construction was in the hands of ir. Robin van der Sligte; Dr. Ymkje Huismans contributed on the salt wedge parameterization. Furthermore drs. Pieter Doornbal and drs. Marco de Kleine contributed in the lithographic analysis. During the final stage of the project Hinnerk Furhop from Delft University of Technology proved to be a useful extra hand in the model construction.

Programming of the activities and guidance from the Rijkswaterstaat Waterdienst was provided by Arjan Sieben, in co-operation with the senior staff of Rijkwaterstaat Directie Zuid Holland in Rotterdam.

## 2 Model construction

### 2.1 Domain description

The RMM model has a partial overlap with the DVR model. The Nieuwe Merwede domain from the DVR model was adjusted to incorporate the Biesbosch, Amer and a connection to the Bergsche Maas. From a previous RMM model (K. Sloff S. Giri 2009), the computational grids for the Dordtsche Kil, Hollandsch Diep, and Oude Maas are used with minor adjustments. All other morphologically important river sections were constructed following the directions for the construction of computational grids for morphological modelling with Delft3D as described in Mosselman 2005 and Yossef 2006. Table 2.1 gives a summary of the source and corresponding domain of the modelled river sections.

*Table 2.1 List of the river sections in the RMM morphological model, including their origin and corresponding model domain.*

River	Source	Domain
Boven Merwede	DVR Sloff 2009b	mw1
Beneden Merwede	DVR Sloff 2009b	mw2
Nieuwe Merwede	adjusted from DVR Sloff 2009b	mam
Amer	constructed	mam
Bergsche Maas	constructed	bem
Maas (until Lith)	constructed	bem
Dordtsche Kil	previous RMM Sloff 2009a	dom
Hollands Diep	previous RMM Sloff 2009a	dom
Haringvliet	constructed	hos
Spui	constructed	hos
Oude Maas	previous RMM Sloff 2009a	dom/hos
Nieuwe Maas	constructed	nim
Hartelkanaal	constructed	nim
Nieuwe Waterweg	constructed	nim
Noord	constructed	nod
Lek (until Hagestein)	DVR Van der Mark 2010	nr2

Six out of nine domains were constructed or adjusted for the RMM model. The positioning of the domain decomposition boundaries was preferably chosen at locations of minor morphological activity. Several river sections can therefore be within one domain and vice-versa. An overview of the domains is given in Figure 2.1.

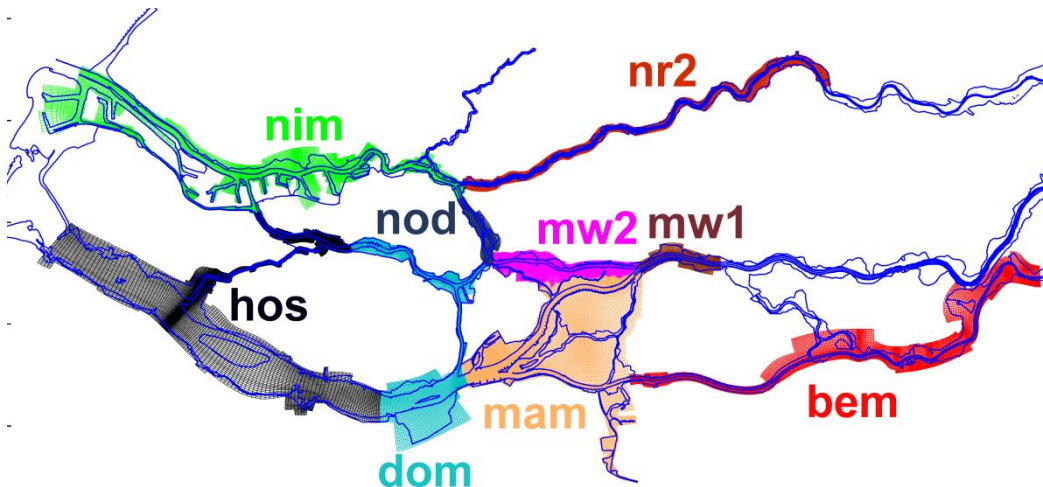


Figure 2.1 Location of the computational domains in RMM

Table 2.2 Description of the domains in the RMM, ordered in number of active grid cells.

Domain	Sections	Active grid cells	MxN	DD-boundaries	external boundaries
nod	Noord	2,865	125x41	mw2, dom, nim	-
mw1	Boven Merwede	3,442	33x139	mw2, mam	Waal (Gorinchem)
dom	Oude Maas, Dordtsche Kil, Hollands Diep	8,888	155x143	nod, mam, hos	-
mw2	Beneden Merwede	10,067	44x507	mw1, nod	-
bem	Bergsche Maas, Maas (until Lith)	12,497	89x242	mam	Maas (Lith)
mam	Nieuwe Merwede, Amer, Biesbosch	13,904	210x235	mw1, bem, dom	-
nim	Nieuwe Maas, Nieuwe Waterweg, Hartelkanaal	15,979	417x189	nr2, nod, hos	North Sea (Maasmond)
hos	Oude Maas, Haringvliet, Spui	16,937	51x619	dom, nim	Haringvliet (barrier)
nr2	Lek	17,615	465x211	nim	Lek (Hagestein)

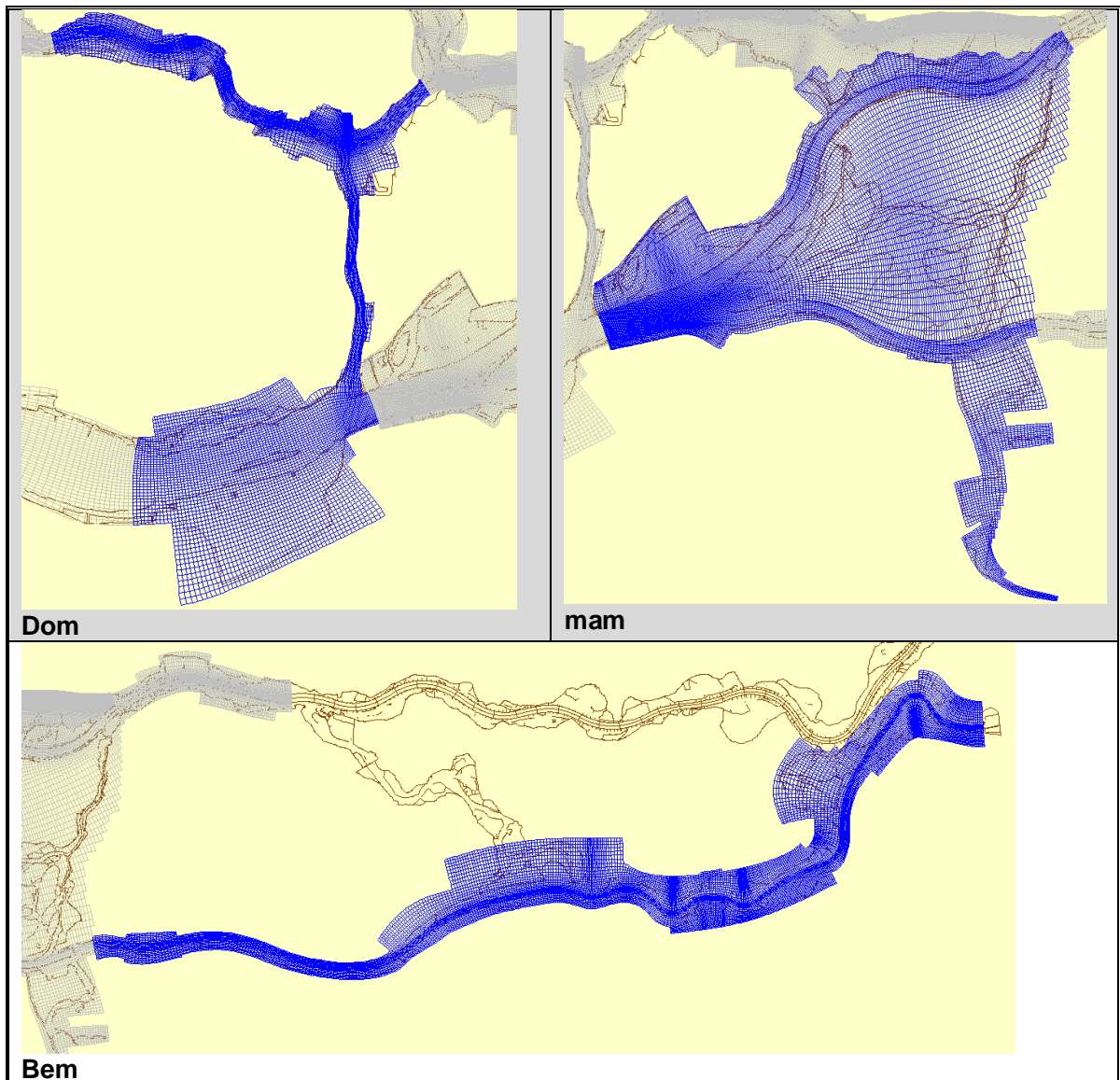


Figure 2.2 Curvi-linear grids for DO, MAM and BEM domains.

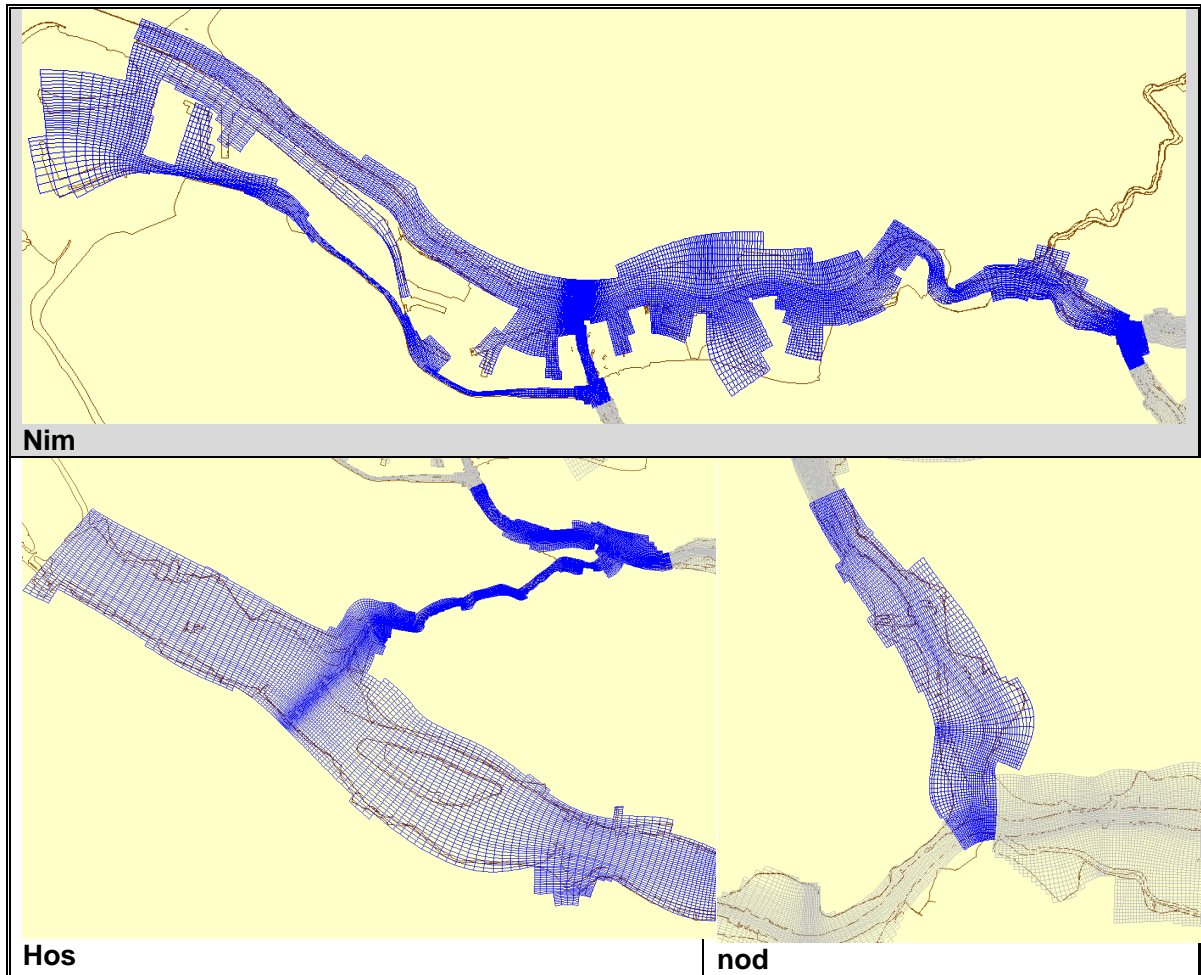


Figure 2.3 Curvi-linear grids for NIM, HOS and NOD domains.

In the nim-domain an internal transformation in coordinate direction is implemented to enable coupling with the other domains. This can be achieved during the grid construction at a location of a junction but this method has drawbacks in the morphological computation. Therefore, another solution is implemented in which the reduced morphological activity around the gravel bed in the Nieuwe Maas is utilised. Figure 2.4 shows a close up of the bend near the Noordereiland. The crossing of the grid lines inside the bend creates the necessary coordinate transformation.

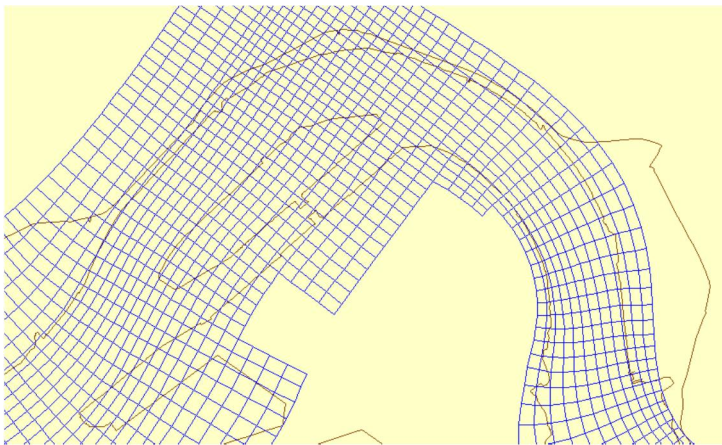


Figure 2.4 A close up of the computational grid of the nim domain. The grid lines cross in the bend to make connectivity to the other domains possible.

## 2.2 The baseline model

The geotechnical data of the model area is obtained from a Baseline database. Baseline is a program which runs in the ArcGis environment and enables the modeller to project geotechnical data onto the model grid. The model is setup using the fifth generation RMM Baseline model. The geotechnical data projected onto the model is: the bathymetry, weirs, thin dams, calibrated roughness codes, observation points, cross sections and the domain enclosure. A description of this model and the calibration procedure can be found in Struijk 2012 or Zagonjoli 2012. A summary of the Baseline model is given in table Table 2.3.

Table 2.3 Summary of the Baseline-tree

<b>Baseline Model</b>		
Name	RMM_j12_5	
Year bed levels	RMM (DZH)	2009
	RMM Maas*	2009
	Lek, Boven Merwede	2011
Roughness calibration	RMM (DZH)	F. Zijl, 2011
	Maas	A. Becker, 2012a
	Lek, Boven Merwede	A. Becker, 2012b

\*Measurements were performed by DZH

The roughness calibration on the WAQUA models is discharge dependent and includes directional dependency in the near sea region. These dependencies are not included in the Delft3D model. For the morphological analysis, the calibration set for the medium discharge is used.

## 2.3 Hydraulic model

The model has three inflow boundaries, two outflow boundaries and lateral discharges at the Haringvliet sluices. At the upstream boundaries discharges are prescribed by means of a stepwise hydrograph. A tidal water level is applied at the downstream boundaries.

The discretization of the upstream hydrograph is dependent on the tidal signal downstream, the morphological acceleration factor and the time step. Furthermore, durations of the low,

medium and high discharge must coincide, i.e. in the model the discharges of the Waal, Lek and Maas are fully correlated. Since the river Waal conveys most of the water into the RMM, it is considered leading in the discretization process.

### 2.3.1 Upstream hydrograph

The annual discharges from the three contributing branches of the RMM are schematized in a stepwise hydrograph as shown in Figure 2.5. Three discharge levels, low, medium and high are applied. The discharge levels are obtained from previous SOBEK computations, as shown in Table 2.4.

Table 2.4 Discharges RMM from SOBEK ndb1\_1\_0.

Discharge (m <sup>3</sup> /s)	Corresponding Boven-Rijn	Waal, Tiel	Lek, Hagestein	Maas, Lith
1	1000	804	25	88
2	2200	1504	390	264
3	6000	3997	1158	1156

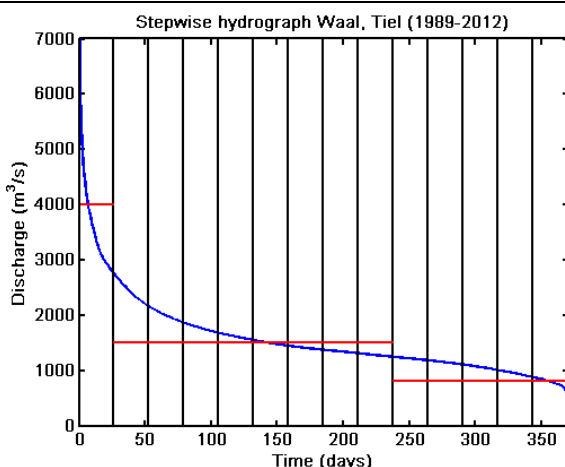


Figure 2.5 Leading hydrograph for the discretization steps in the RMM.

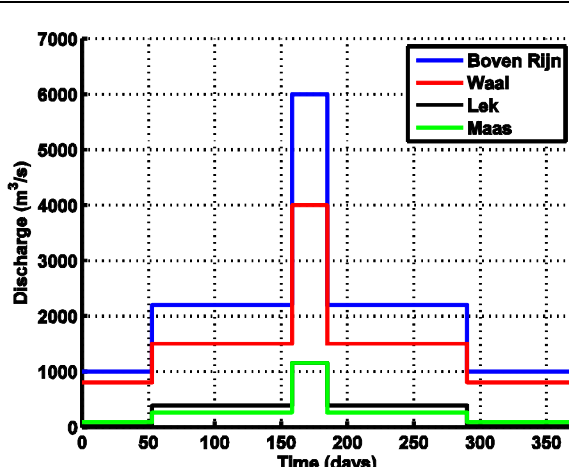


Figure 2.6 Discretized hydrographs for the RMM and the 'corresponding' Boven-Rijn Discharge.

With respect to the DVR hydrograph schematisations, an extra condition is added due to the presence of a tidal boundary. Therefore the morphological acceleration factor becomes part of the discretization of the hydrograph. The description on the morphological factor can be found in 2.4.7.

In the discretization of the hydrograph, the following conditions apply:

- The schematization represents the measured hydrograph.
- The duration of each step is a multiple of the tidal period.
- The tidal period is a multiple of the time step.
- The duration of each step divided by the morphological factor should be a multiple of the time step.

With a morphological factor of 51, and a tidal period of 12 hours and 25 minutes, the temporal resolution becomes approximately 26 days. All periods in the discretization of the hydrograph must therefore be a multiple of this temporal resolution. This also implies that the simulation year adds five days to the normal year.

*Table 2.5 Simulation parameters important for the hydraulic boundaries, due to the tidal signal downstream, the tidal period and morphological acceleration factor become important as well.*

<b>Simulation parameters</b>	
time step (min)	0,1
Morfac	51
main tidal period (hours:min)	12:25
Hydraulic spin up (hours:min)	12:25
Hydrograph step size (days)	26,39
simulation year (days)	369
Discharge levels (#)	3

## 2.3.2 Downstream morphological/representative tide

The outflow boundaries of the model are located at the Maasmond and the Haringvliet. The latter is modelled as a withdrawal of discharge and is discussed in 2.3.3. The model has two water-level boundaries at the Nieuwe Waterweg and the Hartelkanaal. In the morphological simulations the input at the boundary signal is reduced to enable time reduction techniques like the morphological factor and discretization of the hydrograph. The conditions at these locations are based on the harmonic components M2, M4, and M6 at Hoek van Holland. The M2-component is multiplied by 1.1 in order to obtain a correction for the spring-neap cycle (i.e. the morphological tide), see Lesser 2009 and Table 2.6.

Table 2.6 Components computed over 2003-2006, getijtafels, 2011.

Component	Celerity (°/hr)	Amplitude (m)	Phase (deg)
A0	-	0.09 (+NAP)	-
M2	28.984	0.80	85
M4	57.968	0.17	164
M6	86.952	0.05	129

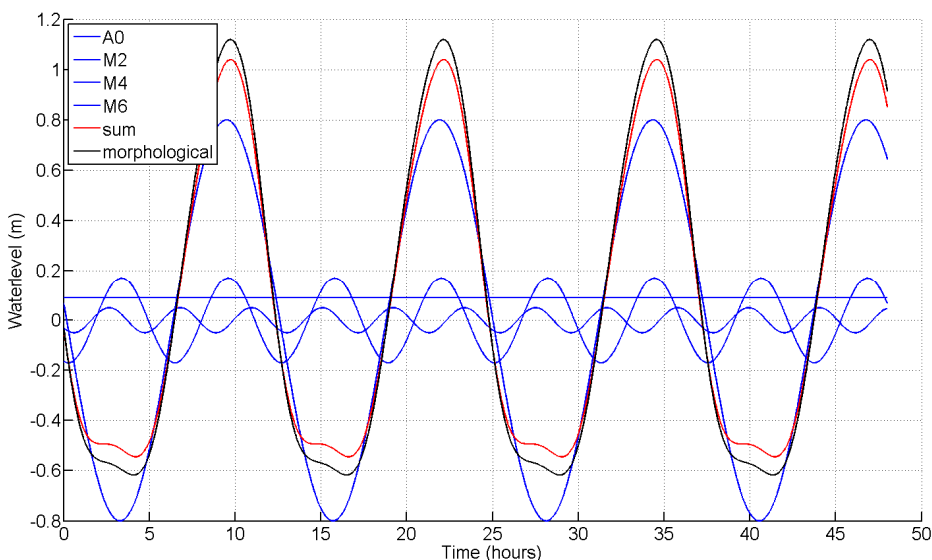


Figure 2.7 The waterlevel boundary condition at the Maasmond is a combination of the M2, M4, and M6 components with an enlarged M2 component to obtain a representative tide for morphology.

## 2.3.3 Lateral discharges

The discharge of fresh water from the Haringvliet into the North Sea is modelled as multiple sink terms at the location of the Haringvlietdam. In the hydraulic verification, discharges were obtained from the SOBEK model. For the morphological model, typical discharge time series were constructed based on the SOBEK model, see Figure 2.8 and for a discussion on the phase difference appendix C.

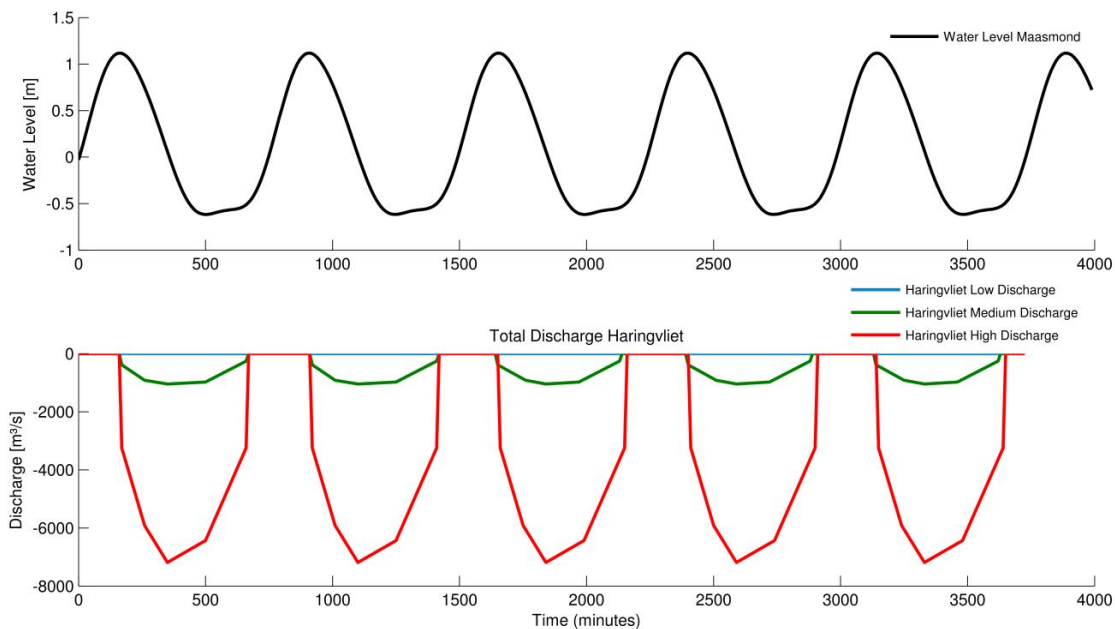


Figure 2.8 Water level at Maasmond and the discharge at the Haringvliet barrier.

## 2.4 Morphological model

The Holocene Rhine-Meuse delta is formed under the influence of sea-level rise, tectonics, variations in discharge and sediment supply, and storm events. Under the more or less natural conditions that have been prevailing for centuries, this area has been mostly a sediment trap, in which sediment from both the sea and the river were depositing. The varying presence of marshes, avulsions and infilling channels, and so on, has caused the substratum to be composed of alternating layers and patches of sand, clay and peat. As the erodibility of the (compacted) clay layers is much less than that of sand, the large-scale erosion in the middle reaches of the delta does not occur evenly. As indicated above stable (clay) reaches are interrupted by deep scour holes depending on the presence of sand patches in the subsoil. (Slooff et al. 2011)

For the morphological model of the Rhine Meuse estuary it is important to:

- Implement several fractions both cohesive and non-cohesive.
- Implement subsoil information for these fractions.
- Implement fixed layers at locations of tunnels, pipelines etc.
- Adjust for the 3D-effects of the salt wedge in the 2D simulation.

### 2.4.1 Sediment fractions

The RMM works with four sediment fractions: silt, sand, coarse sand, and clay. For the 'Walcheren' and 'Wormer' (Holocene) sub-soils the grain size is approximately 175 µm. For 'Pleistocene' sand we assume a median grain size of 350 µm. The median grain size of the sand in the area has been based on the basis of 33 borings by Hijma (2009), as other borings did not have a sufficient description of grain size per layer.

For the cohesive sediments a critical stress for erosion and sedimentation can be given. Following Chu et al. (2010) we assume a high critical shear stress for sedimentation ( $\tau_{crS}$ ) which effectively means that sedimentation occurs at all times (see also Winterwerp and Kesteren, 2004). The semi-fixed layers (peat and clay) are modelled by a clay fraction with a critical shear stress ( $\tau_{crE}$ ) of 1,8 Pa. The silt fraction is profoundly present, also by means of dredging activity, in the south side of the Rhine Meuse estuary. The (re)suspension of this fraction is schematized by a critical shear stress of 0,5 Pa following previous models into the siltation in the Rhine Meuse estuary (Meijers and Icke, 2006).

Sediment characteristics	Silt	Clay	Sand	Coarse Sand
Type	Mud	Mud	Sand	Sand
Settling velocity (mm/s)	1	1	-	-
$\tau_{crE}$ (Pa)	0,5**	1,8*	0,15*	0,30*
$\tau_{crS}$ (Pa)	1000***	1000***	-	-
Erosion parameter (kg/m <sup>2</sup> /s)	0,00001	0,00001	-	-
D <sub>50</sub> (μm)	-	-	175*	350*

\*Stouthamer and De Haas, 2011

\*\*Meijers and Icke, 2006

\*\*\*Winterwerp and Kesteren, 2004

## 2.4.2 Bed composition

A well modelled bed composition is crucial for the modelling of the initiation and growth of scour holes. For the rivers Noord, Spui, Oude Maas subsoil data is available from a study performed by Stouthamer en De Haas (2011). For the Dortsche Kil data has been used from TNO-NITG (processed by Giri 2010 and Smits 2011). P. Doornbal and M. de Kleine (geologists at Deltares) completed the available profiles at locations with missing data using available drillings from the DINO database and the Geotop model. For these river sections, subsoil information was implemented in the Delft3D model.

A Matlab tool was developed which facilitated the translation from bed composition profiles to Delft3D input files. Figure 2.9 shows the longitudinal profile of subsoil in the river Noord. It is composed of sand, clay, peat and coarse sand in the deep bottom. The top of the soil displays the surface level. The module determined the sand, coarse sand, and clay fractions within the figures. Peat was included as a clay fraction. After the projection of the grid and local depth, a virtual drilling collects the subsoil beneath each computational cell. Figure 2.10 illustrates the projection of the computational cells at their depth (known from the Baseline database) and the virtual drilling.

This procedure is repeated for each morphologically active computational cell. In general, this means that subsoil information included in the Delft3D model differs along the river profile in both longitudinal and transversal direction. However, most of the subsoil database is constructed based on measurement along the banks of the river. These measurements are combined to form a longitudinal profile and interpreted as representative in the transversal direction. Scarce measurements in the transversal direction show that subsoil content is not constant, which is readily understood by the fact that most of the subsoil content are river deposits of the past. This fact has to be taken into consideration when analysing the results or when creating scenario simulations.

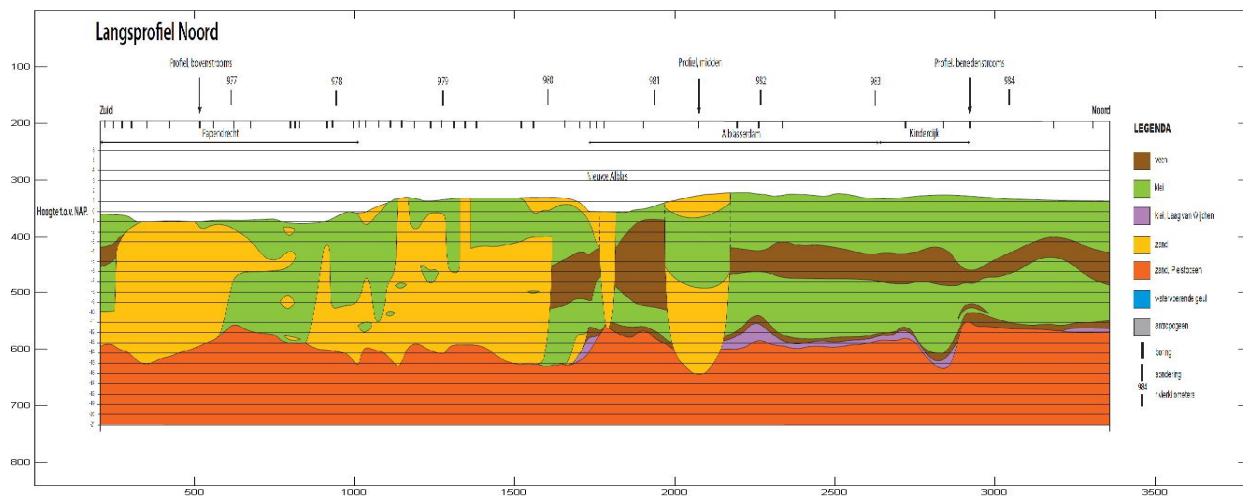


Figure 2.9 Illustration of one of the bed composition profiles. The profile shows the peat, clay, sand, and coarse sand content of the subsoil in the river Noord.

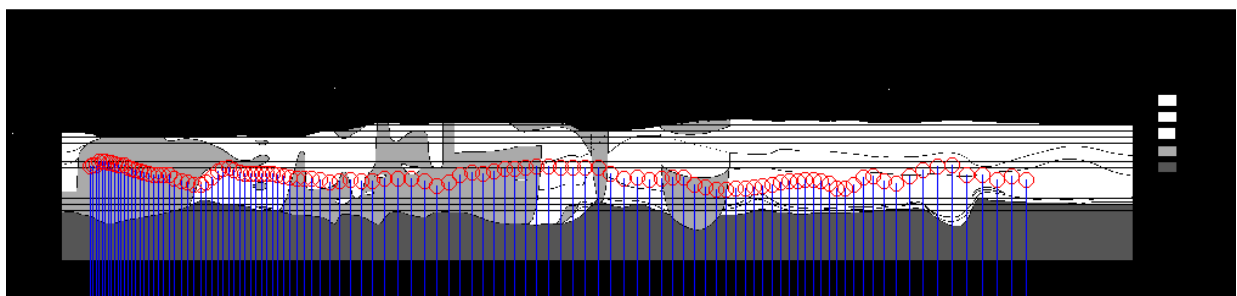


Figure 2.10 The color subsoil content is interpreted into the given fractions and presented in grayscale. Virtual drillings take place at each computational cell between the normal lines, and the subsoil administration saved.

For the Dordtsche Kil, subsoil information was taken from the study of Smits 2011 and Giri 2010. The southern part of the RMM has a silt rich soil which was mapped in the MEDUSA-study, see appendix E. Figure 2.11 shows the schematized silt percentage for the Haringvliet, Hollands Diep, Amer and Nieuwe Merwede. For the Nieuwe Maas and Nieuwe Waterweg a silt fraction of 0.6 was applied.

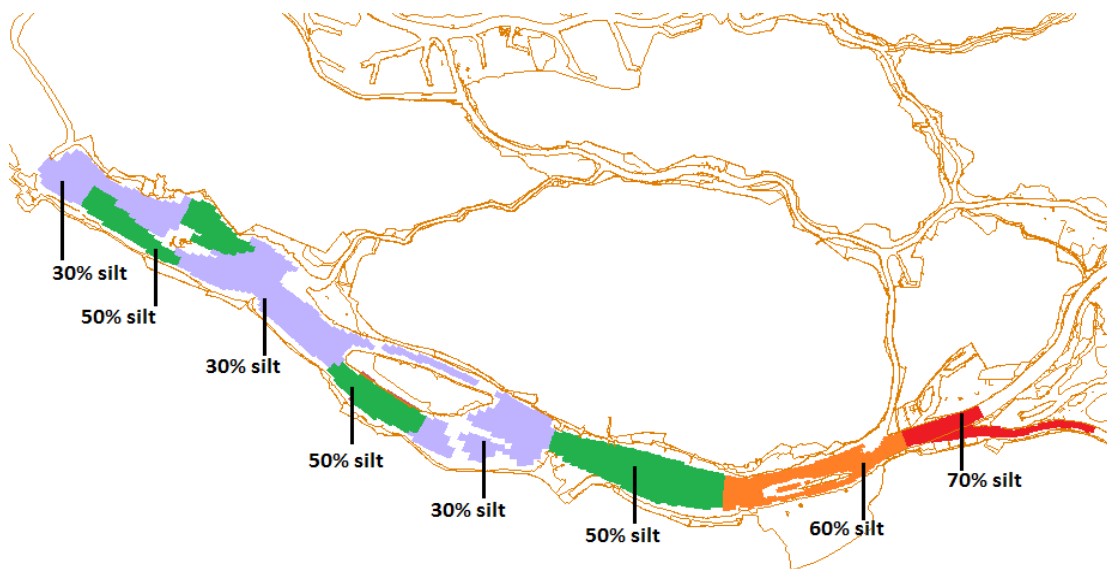


Figure 2.11 Schematized silt content in the Southern part of the RMM.

The Lek, Bergsche Maas, and remaining parts of the Merwedes have a complete sand fraction for the initial bed.

#### 2.4.3 Sediment transport formulae

##### **Non-cohesive**

The Van Rijn (1984) sediment transport formula is considered to be one of the most accurate and commonly used formulations. It has the advantage of having two separate expressions for bed load and suspended load. The formula of Van Rijn is presented in Appendix F. The RMM-model uses the same Van Rijn formulation as in the DVR-models except for the regions in which sediment transport is affected by the presence of the salt wedge. These adjustments are described in 2.4.5.

##### **Cohesive**

Silt and clay can have both a critical shear stress to erosion (lower limit) and a critical shear stress for sedimentation or deposition (upper limit). We use the Partheniades-Krone formulation for the erosion and deposition behaviour. In this research it is assumed that sedimentation can occur simultaneously with erosion and the critical sedimentation parameter can therefore be chosen sufficiently high.

The erosion of mud is zero below the threshold bottom shear stress and linear with bed shear stress at higher shear. The slope of this erosion function is determined by the combination of the critical shear stress and the so called erosion parameter (or erosion rate constant). The erosion parameter can therefore be used as a calibration parameter. Van Rijn (Van Rijn, 1993) mentions values between 1E-5 and 5E-4.

## 2.4.4 Fixed layers

Semi-fixed layers, clay or peat, are modelled as a cohesive clay fraction as described in 2.4.2. Fixed layers are present in the form of gravel reinforced river profiles, tunnels and pipelines. In total, 14 fixed layers are identified and implemented in the Delft3D model as regions depleted of active sediment, see Figure 2.12. A list of the locations can be found in Table 2.7.

Table 2.7 List of the identified fixed layers in the Rijn Meuse estuary.

1	<b>Oude Maas</b>	Botlek tunnel
2		Metrotunnel Spijkenisse
3		Leidingenstraat
4		Heinenoordtunnel
5		HSL tunnel at Zwijdrecht
6		Drechttunnel
7	<b>Dordtsche Kil</b>	Kiltunnel
8		HSL tunnel
9	<b>Noord</b>	Sophiatunnel
10		Noordtunnel at Alblasserdam
11	<b>Nieuwe Maas</b>	Gravel reinforced profile
12		Maastrunnel
13		Beneluxtunnel
14	<b>Calandkanaal</b>	Burgemeester Thomassentunnel

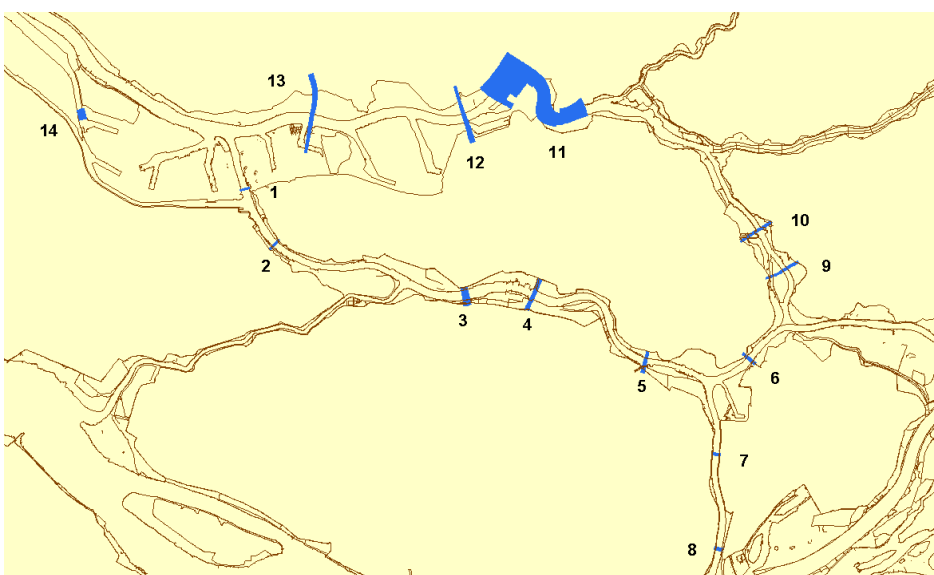


Figure 2.12 Fixed layers in the Noord, Oude Maas, Nieuwe Maas and the Dordtsche Kil.

## 2.4.5 Morphological boundary conditions

Both bed and suspended load have to be prescribed at the boundaries. The inflow boundary of both the Lek and the Maas are positioned at a weir which fixates the bed. The third inflow boundary is located at the Merwede, which is considered stable.

Suspended transport at the inflow boundaries contributes to the available silt and fine sand in the Rhine Meuse estuary. For the inflow boundaries we used relations obtained from Meijers and Icke (2006) en Mosselman et al. (2005). These relations lead to the suspended sediment load as depicted in Figure 2.13 and tabulated in Table 2.8. Snippen (2005) made a sediment balance of the Rhine Meuse estuary. The yearly averaged suspended inflow load, together with the applied suspended sediment inflow in the model are tabulated in Table 2.9. Following Mosselman et al. (2005) we assume a 62:38 silt/sand fraction, and the suspended sediment at the Maasmond is set at 10 mg/L.

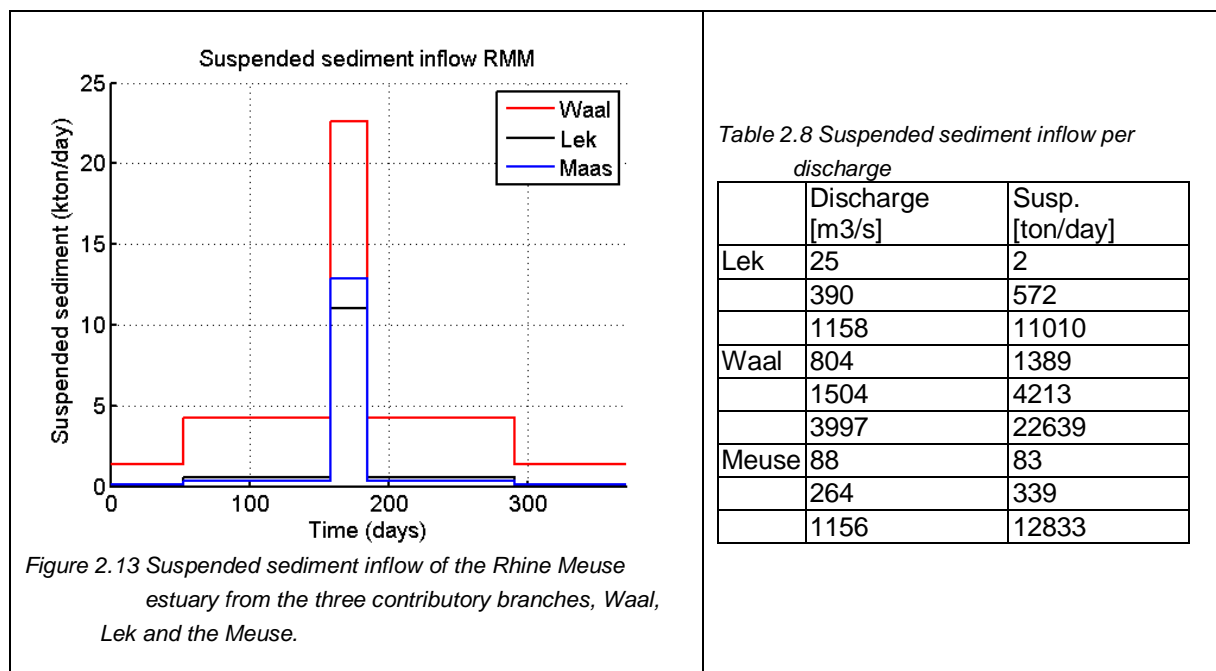


Table 2.9 Averaged yearly load in the Rhine Meuse estuary according to Snippen et al. 2005 and the total yearly model load for the three branches.

Location	Period		Suspended sediment [Mton/year]
<b>Lek, Hagestein</b>	1960 -	1969	0,34
	1970 -	1979	0,25
	1980 -	1989	0,44
	1990 -	1999	0,31
	Model		0,41
<b>Waal, Vuren</b>	1960 -	1969	2,41
	1970 -	1979	1,94
	1980 -	1989	2,06
	1990 -	1999	1,44
	Model		1,67
<b>Maas, Lith</b>	1960 -	1970	0,47
	1970 -	1980	0,26
	1980 -	1990	0,50
	1990 -	2000	0,42
	Model		0,42

## 2.4.6 General simulation scheme for morphological simulations

Since the model domain covers tidal and intertidal rivers, the common simulation techniques known from the non-tidal morphological river models (e.g. DVR) cannot be applied in the same manner.

In these non-tidal river models the annual river discharge is modelled by a stepwise hydrograph. Per discharge level, the most recent water levels and velocity fields are stored in a local database. At the beginning of a new step on the hydrograph, the bed of the previous simulation is combined with the hydraulic information from the local database stored for that particular discharge level. At the end of the simulation, the hydraulic conditions are stored in the local database and the morphological information is transferred to the next simulation. The simulation itself does not begin with morphological computations in the first time steps. At first, a hydraulic spin up simulation is performed in which the flow adapts to the new bed. After this phase, flow, sediment transport and bed updates are computed within the same simulation, the so called online computation of morphology.

The morphological simulations for the tidal influenced RMM domain are run in a similar way as for the non-tidal DVR. However, the hydraulic spin up time contains a full tidal period (745 min), and the morphological simulation has a hydraulic time period of an integer number of tidal periods ( $N \times 745$  min). The steps are schematized in Figure 2.14. The first two steps are general spin up steps and have to be performed once for each scenario set. At first, a hydraulic spin up period adjusts the model from an arbitrary water level and velocity field (e.g. water level at 2 m + N.A.P. in each domain and zero velocity).

In the second step, the bed composition of the top layer is allowed to change due to flow conditions but without bed level changes. After these two initial steps the morphological computation can begin at the first discharge in the schematized hydrograph. The figure shows that each morphological simulation is preceded by a hydraulic phase in which the hydrodynamics can adjust to the new bed.

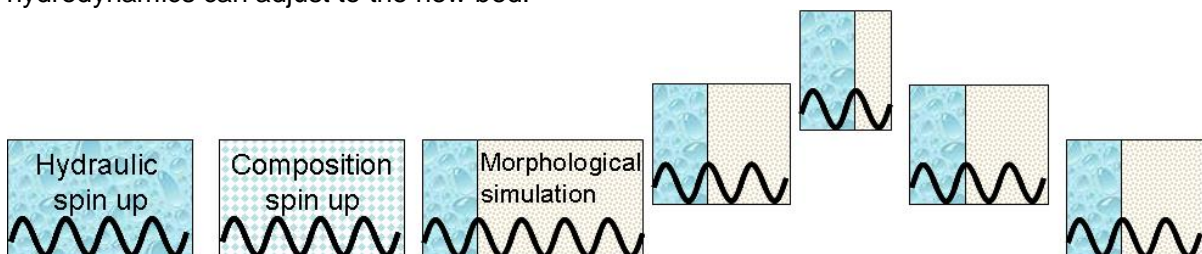


Figure 2.14 Steps performed in a morphological simulation in a tidal river. Due to the tide it is important that the hydraulics consists of full periods of the tidal signal. This holds for the hydraulic spin up, but also for the morphological simulation.

## 2.4.7 Time reduction techniques

### The morphological factor

One of the complications inherent in carrying out morphological projections on the basis of hydrodynamic flows is that morphological developments take place on a time scale several times longer than typical flow changes (for example, tidal flows change significantly in a period of hours, whereas the morphology will usually take weeks, months, or years to change significantly). One technique for approaching this problem is to use a morphological time scale factor whereby the speed of the changes in the morphology is scaled up to a rate that it begins to have a significant impact on the hydrodynamic flows.

In these models, simulation time is reduced by a multiplication of the computed sediment transport rates by a discharge dependent constant called the morphological factor. By the multiplication of the morphological effect during a time step, the simulated period is multiplied by the same factor.

The interpretation of the morphological factor differs for tidal and non-tidal river applications. For coastal applications with tidal motion, the morphological variations during a tidal cycle are often small and the hydrodynamics is not significantly affected by the bed level changes. By increasing the morphological factor to for instance 10, the morphological changes during one simulated tidal cycle are increased by this factor. From a hydrodynamical point of view this increase in morphological development rate is allowed if the hydrodynamics is not significantly influenced. In that case the morphological development after one tidal cycle can be assumed to represent the morphological development that would in real life only have occurred after 10 tidal cycles. In this example the number of hydrodynamic time steps required to simulate a certain period is reduced by a factor of 10 compared to a full 1:1 simulation. This leads to a significant reduction in simulation time. However, one should note that by following this approach the order of events is changed, possible conflicts may arise in combination with limited sediment availability. In non-tidal river applications there is no such periodicity as a tidal cycle. For such applications, the morphological factor should be interpreted as a speed-up factor for morphological development without changing the order of events. Effectively, it means that the morphological development is simulated using a, for instance 10 times, larger time step than the hydrodynamics, or phrased more correctly the hydrodynamics is simulated at a 10 times faster rate.

This means that in case of time-varying boundary conditions (e.g. river hydrograph) the time-scale of these forcings should be sped up: a 20 day flood peak will be compressed in 2 days. (Delft3D flow manual, 2011)

Currently, the Delft3D RMM model uses a morphological factor of 51. This implies that the whole year can be simulated by fourteen tidal cycles with a period of approximately half a day (excluding the hydraulic spin up before each simulation). However, this is a factor eight times smaller than the average morphological acceleration in the DVR and it is therefore worth investigating if the morphological factor can be increased. It is possible to vary the morphological factor during a simulation to speed up relatively quiet periods more than relatively active periods. There are limitations to this method. One of them is the relation to the hydrograph schematization as discussed in section 2.3.1. Another is determined by the physical correctness, which is tested by means of comparison. The optimal gain for improvements in the morphological factor is expected to be a total time reduction by a factor of two.

### Representative tide

The representative tide is an input reduction technique used in coastal studies (see Roelvink and Reniers 2012 and Lesser 2011). In this technique a representative boundary condition is chosen which represents the average condition for morphology. Roelvink and Reniers (2012) describe a method to obtain and verify the morphological tide by performing an analysis on the sediment transport during a spring neap cycle. Due to time limitations, Prof. Dr. ir. Roelvink was consulted for a good estimate of the representative tide. The study of Lesser (2011) showed a good agreement of the representativeness of the tide when multiplying the M2 by a factor of 1.1. The extended method can be used to verify and possibly adjust the tidal signal at the boundary.

**Time step**

The time step has a direct influence on total computational time. Compared to the DVR model, the RMM model has a low time step (0.4 min in the DVR and 0.1 min in the RMM) due to stability of the simulations. A similar time step would decrease the computation time by a factor four. With the detection of problematic or critical area(s) in the model improvements can be made. The possibility of a river discharge dependent time step could also be investigated.

**Hardware and domain decomposition**

The simulations are run on an i7 quadcore processor with hyper-threading which creates 8 threads out of the four cores. The nine domains in the model will run on these eight virtual computational units. Smaller domains are automatically clustered leaving dedicated threads open for the bigger domains. After an expert consult we can conclude that only little, if at all something, can be gained by grid modifications, combining of domains or different hardware architecture (like on the Lisa cluster). With respect to currently available hardware and domain decomposition techniques, we have quite an optimal setup.



### 3 Salt wedge and sediment transport

Analysis of sediment balances and previous studies show that in the Nieuwe Waterweg a net landward transport of sediment occurs. This landward component is driven by the salinity intrusion and its effect on the tidal-averaged near bed velocities. For long term morphological predictions it is necessary to include this effect in the model.

#### 3.1 Description of the system

In the Dutch Delta the interplay between the saline water from sea and the fresh water from the rivers results in a complex flow pattern. During flood, inflow of saline water can result in a flow pattern where the heavier saline water flows under the fresh river flow. Whether the system is well mixed, stratified or something in between, depends on a number of parameters, summarized by the Estuarine Richardson Number (ERN) , see Savenije (2005):

$$N_R = \frac{\Delta\rho}{\rho_{fw}} \frac{gh}{v^2} \frac{Q_f T}{P_t} \quad (1)$$

With the density difference  $\Delta\rho$  between the saline ( $\rho_{sw}$ ) and fresh water ( $\rho_{fw}$ ), the acceleration due to gravity  $g$ , the water depth  $h$ , the tidal velocity  $v$ , the fresh water discharge  $Q_f$ , the tidal period  $T$  and the flood volume  $P_t$ . The higher the value of  $N_R$ , the more stratified.

The ERN accounts for three effects. First for the relative density difference between fresh water and seawater, second for the ratio between the amplitude of the tidal velocity and the celerity of a finite amplitude wave ( $\sqrt{gh}$ ) and third for the ratio of the potential energy provided by the river discharge and the kinetic energy provided by the tide during a tidal period.

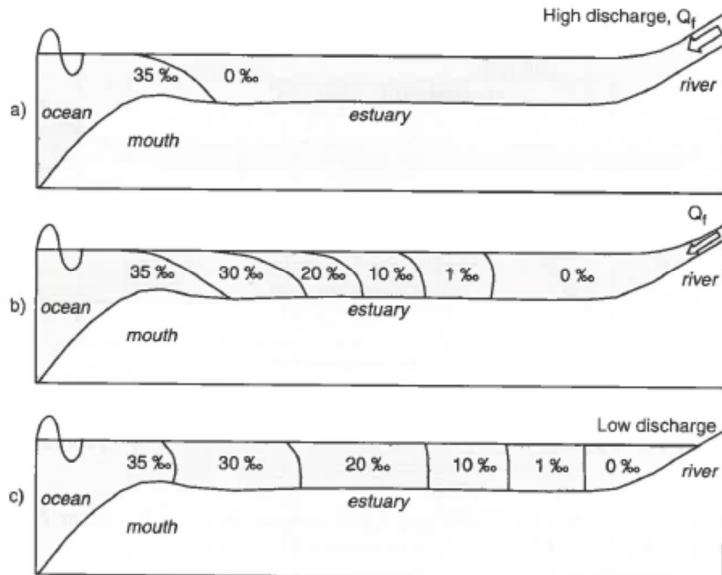


Figure 3.1. Longitudinal distribution of the salinity for a stratified estuary (a), a partially mixed estuary (b), and a well-mixed estuary (c). Figure taken from Savenije 2005.

In Figure 3.1 the three different cases – well mixed, partially mixed and stratified – are shown. Figure 3.1a, shows that a stratified estuary is characterized by a sharp transition between saline and fresh water, while on the other extreme a well-mixed estuary shows a gradual transition in salinity.

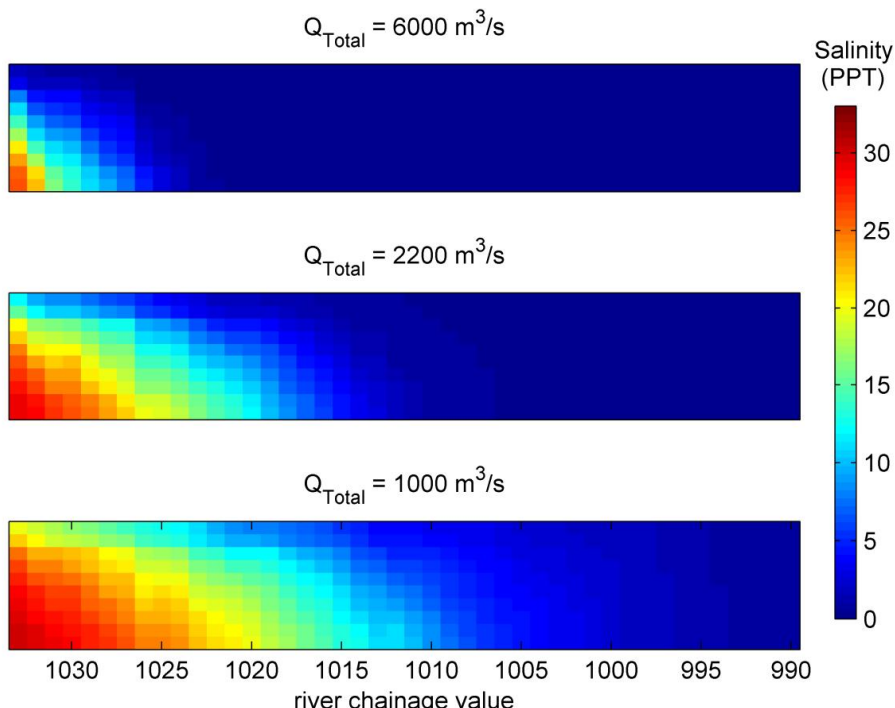
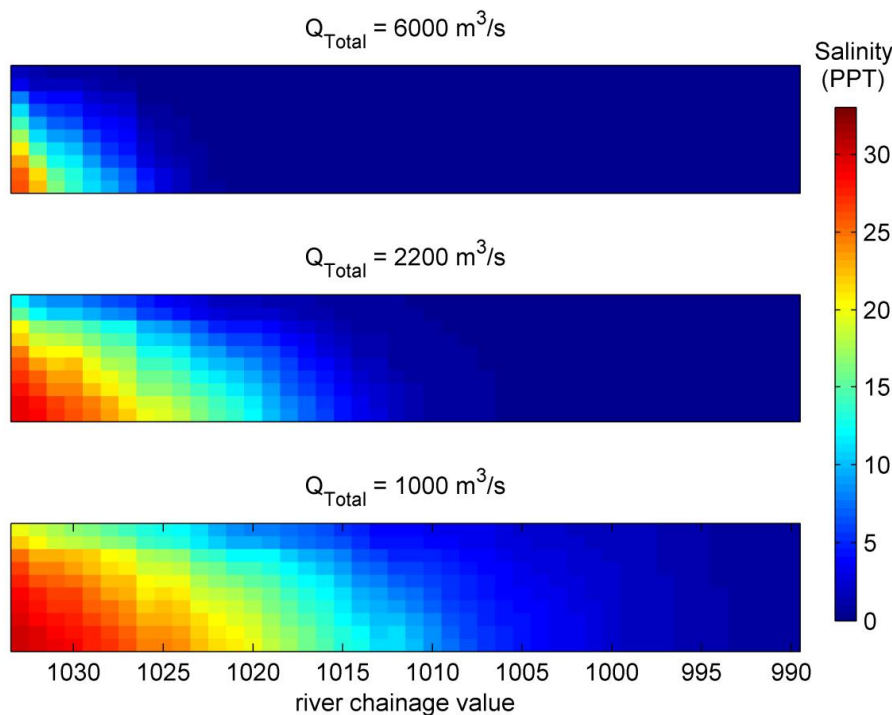


Figure 3.2 the tide-averaged salinities are shown for the Nieuwe Waterweg - Nieuwe Maas, for three different river discharges ( $1000 \text{ m}^3/\text{s}$ ,  $2200 \text{ m}^3/\text{s}$  and  $6000 \text{ m}^3/\text{s}$ ). The model results are obtained with the Delft3D three-dimensional “Zeedelta model” (Van der Kaaïj et al, 2010)

and show a partially mixed (low river discharges) to stratified (for high river discharges) estuary, in agreement with Abraham 1982.



*Figure 3.2. Spring-neap tide averaged salinities versus the river chainage value, where rkm 1033 is at the inlet of the Nieuwe Waterweg, rkm 1013 at the bifurcation with the Oude Maas and rkm 999 the location of the Noordereiland.*

The significance of a (partially) stratified estuary for sediment transport is its effect on the velocity field, of which an example is shown in Figure 3.3. This is a typical flow velocity field for low river discharges, shortly after low water slack.

This modified flow pattern has a drastic effect on the sediment transport. While in the example the net flow is directed towards sea, the flow close to the bottom is directed landward. Sand, which is mostly transported in the bottom layers, will in this case be transported landward instead of seaward.

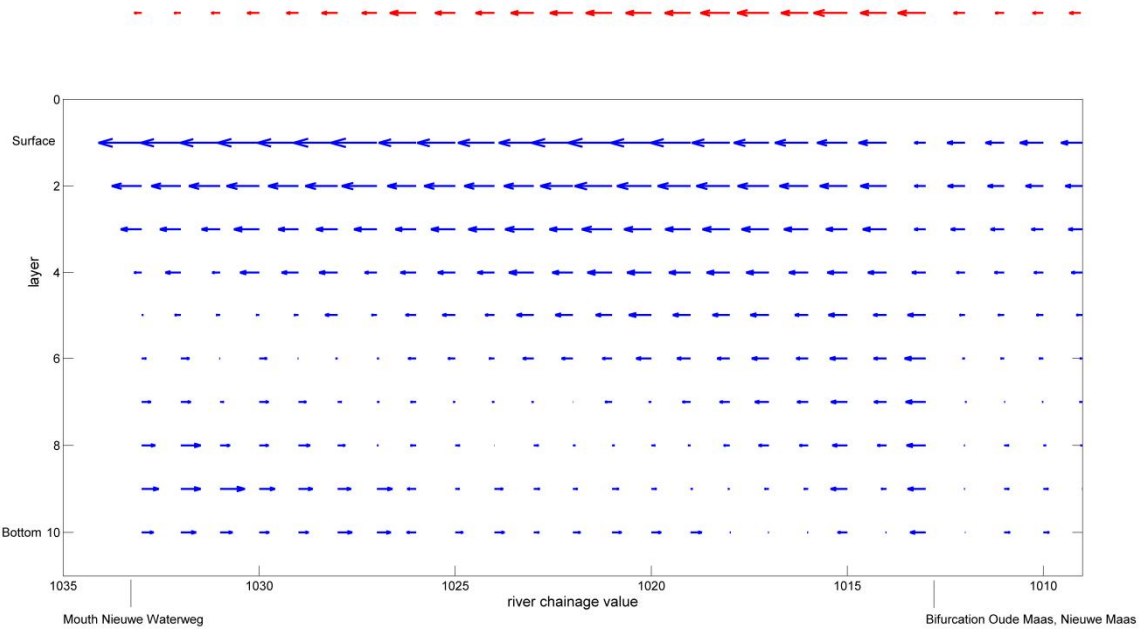


**Figure 3.3.** Flow velocity field of the horizontal velocities shortly after low water slack, for a river discharge of  $Q = 1000 \text{ kg/m}^3$ . The blue arrows indicate the flow velocity field for the 10 layers in the calculation. The red arrows represent the depth-averaged velocity.

### 3.2 From 3D to depth averaged 2D

The effect of the salt wedge on the flow pattern and consequently on the sediment transport is clearly a complex three-dimensional (3D) phenomenon. However, to limit computational time, it is desirable to work with a depth averaged two-dimensional model (2D) as is the case in the present study. To make this possible an effort has been undertaken to parameterize the effect of the salt wedge on the sediment transport.

The parameterization is particularly relevant for the coarse sediment fraction, notably sand, that is transported in the lower part of the water column. Fine silt and clay fractions are much more distributed over the vertical. Furthermore fine silt and clay are not only influenced by the flow pattern, but also particular 3D phenomena of this sediment, such as the development of an Estuarine Turbidity Maximum (ETB) at the tip of the salt wedge require different parameterization, which has not been considered in this project. In addition, flocculation of clay particles is not included.

Ideally, a parameterization is based on analytic expressions for the flow velocity fields, from which a relation between depth average velocity and depth-dependent velocity can be retrieved. Available expressions are however only for highly idealized cases (Prandle 2009, Chapter 4.2). Therefore, a phenomenological study was performed based on numerical 2D and 3D hydraulic computations with the Zeedelta model (Van der Kaaij et al, 2011).

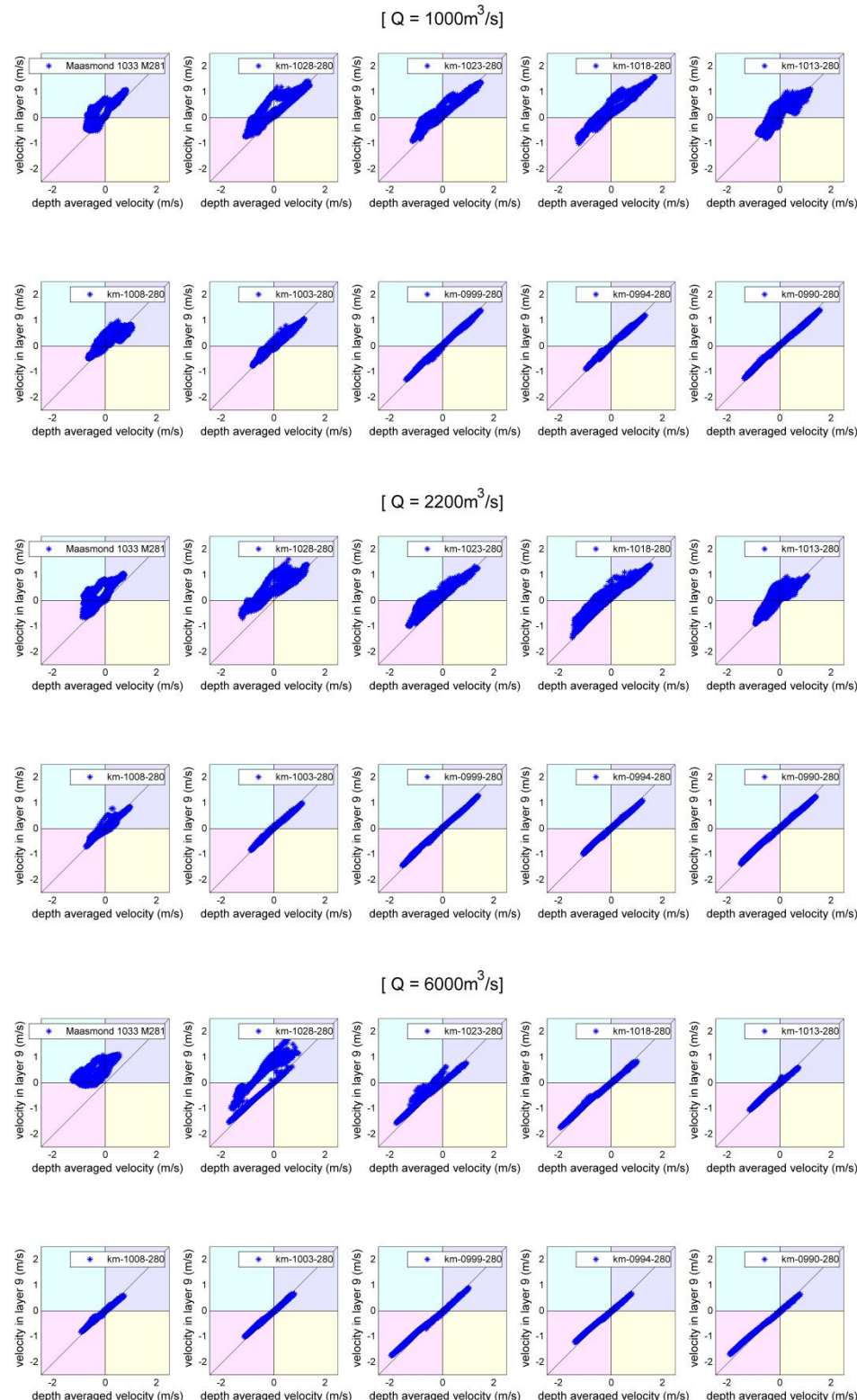


*Figure 3.4. Velocity-velocity ( $v$ - $v$ ) plots for all three river discharges and for different river chainage values. Negative velocity is seaward, positive velocity is landward.*

First, a comparison between the depth averaged velocity ( $v_{da}$ ) from the 2D computation and the velocity at the bottom has been made. As an estimate for the characteristic velocity at the bottom use has been made of the velocity in the ninth layer ( $v_9$ )(layer 10 is at the bottom).

In Figure 3.4 the results are shown for a full spring neap cycle, for all three river discharges. The four colored regions indicate four different regions of velocity-velocity relations:

- Bottom left/ pink: both  $v_{da}$  and  $v_9$  are negative (seaward).
- Top left/ light blue:  $v_{da}$  is seaward, while  $v_9$  is landward.
- Top right/ purple:  $v_{da}$  and  $v_9$  are both directed landward.
- Bottom right/ yellow:  $v_9$  is seaward, while  $v_{da}$  is landward.

The diagonal line indicates where  $v_{da}$  and  $v_9$  are identical.

A normal river flow without stratification is characterized by a logarithmic velocity profile, with lower velocities at the bottom (reduction factor of 0.91 for layer 9). In a v-v plot, this would look like a straight line with a small tilt, see Figure 3.5, furthermore, only seaward velocities are present.

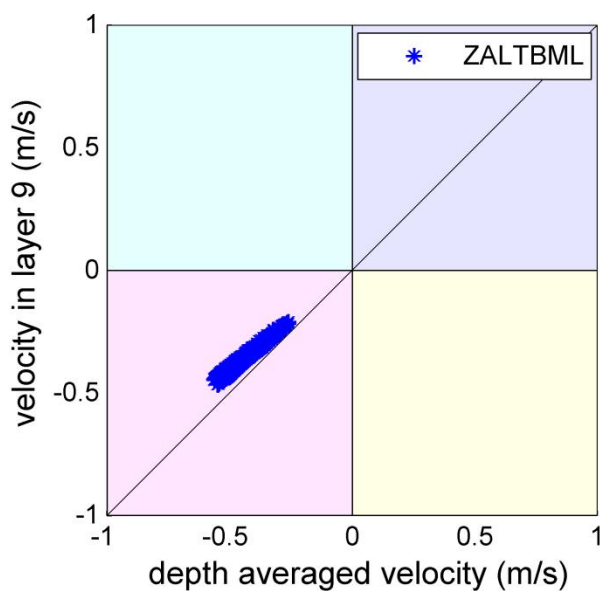


Figure 3.5. v-v plot for the Waal, close to Zaltbommel. The v-v plot shows a typical river flow velocity field.

The situation for the Nieuwe Waterweg – Nieuwe Maas is clearly different. Close to the mouth, many points are located in the top left/light blue area, indicating that the depth-averaged flow is directed seaward while the bottom velocity is directed landward. This is the typical effect of the salt wedge, and is strongest for the high river discharges, where stratification is strongest. The further upstream, the more linear the relation between the two velocity components gets. This linear relation sets in further upstream for low river discharges (around river chainage value 999) than for high river discharges (around chainage value 1018). Thus, along the line of expectations, the effect of the salt wedge on the stratification of the velocity profile is strongest (highest value for  $N_R$ ) for the high river discharges but intrudes less far.

In Figure 3.6 the sediment transport capacity as a result of the depth averaged and bottom velocity is calculated for a full spring neap cycle, with the modified van Rijn's formula from 1984, see appendix F. This formula is made for depth-averaged velocities, so when applying this formula for bottom velocities the bottom velocity  $v_9$  should be corrected by multiplying it by a factor. From analysis of velocity profiles it has been concluded that a factor of 1.1 (Van der Kaaij 2010) can be used for this model. In the ratio between 3D and 2D transport capacity, a negative sign indicates an opposite sign of the 3D transport. Because the residual 2D transport is mostly seaward (negative) this means that for negative ratios the residual 3D transport is landward. Note that at low values of the 2D transport these ratios can become very large (division by values close to zero).

For  $Q = 1000 \text{ m}^3/\text{s}$ , the net sediment transport capacity as a result of the velocity at the bottom is directed landward in the Nieuwe Waterweg, while net sediment transport capacity as a result of the depth averaged velocity is around zero. For river chainage values below 1010 (~32 kilometers from the mouth), the ratio between the two sediment transport capacities gets one, a bit earlier than that the v-v ratio becomes linear (around river chainage value 999, ~43 kilometers from the mouth).

For  $Q = 2200 \text{ m}^3/\text{s}$ , the net sediment transport capacity as a result of the velocity at the bottom is still directed landward in the Nieuwe Waterweg, while net sediment transport capacity as a result of the depth averaged velocity is now seaward. At about the same point as for  $Q = 1000 \text{ m}^3/\text{s}$  situation the, the ratio between the two sediment transport capacities gets one, which in this case more or less coincides with the location where the v-v ratio becomes linear.

For the highest discharge,  $Q = 6000 \text{ m}^3/\text{s}$ , the net sediment transport capacities for both cases are seaward and only close to the mouth there is a large difference between the two.

The effect of sea level rise on the sediment transport capacity has been studied for a river discharge of  $Q = 1000 \text{ m}^3/\text{s}$ . The results in Figure 3.7 show that the sea level rise has a marginal effect on the net transport of sand.

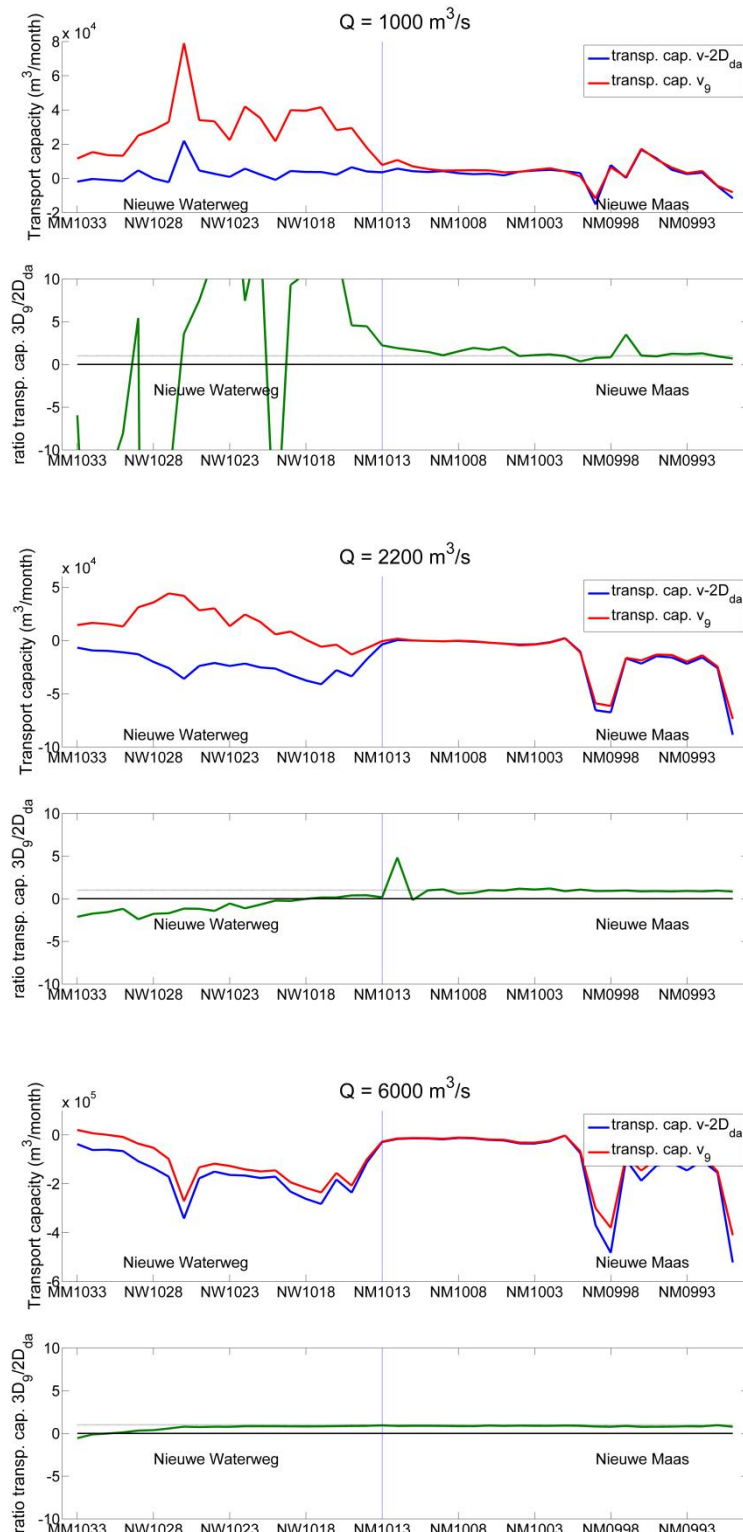


*Figure 3.6. Rough estimates for the residual sediment transport capacities for discharges of  $Q = 1000 \text{ m}^3/\text{s}$ ,  $Q = 2200 \text{ m}^3/\text{s}$  and  $Q = 6000 \text{ m}^3/\text{s}$ , based on a full spring-neap cycle. In blue the sediment transport capacity due to depth averaged velocities, in red sediment transport capacity due to bottom velocity (layer 9) and in green the ratio. Transport capacities have been calculated with the modified van Rijn 1984 (appendix F) for a sediment fraction with  $D_{50} = 300 \mu\text{m}$ .*

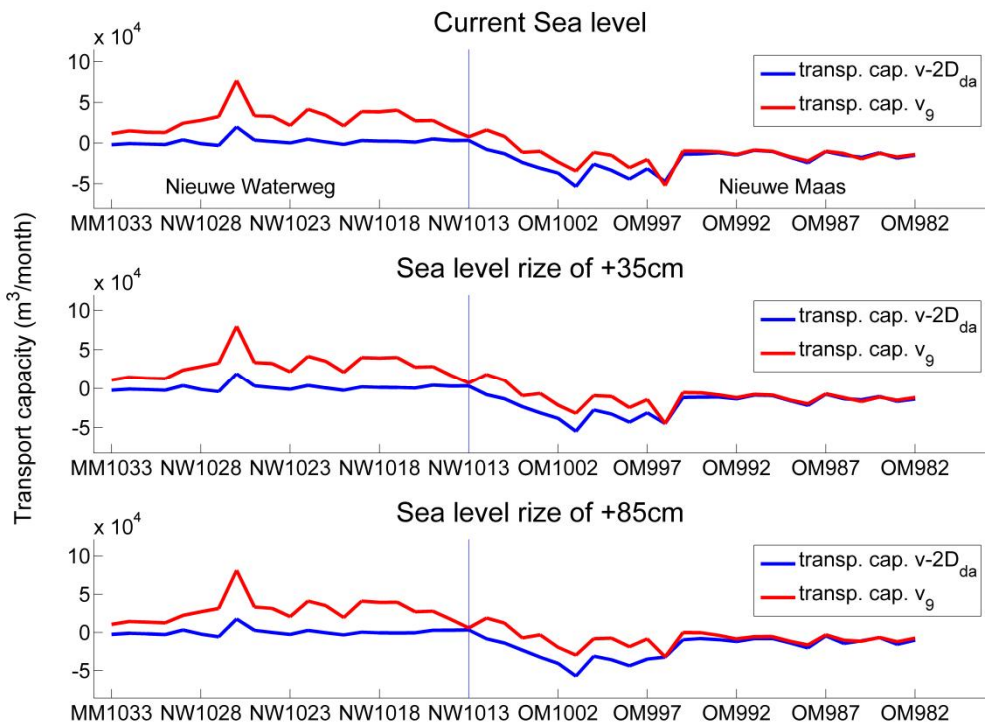


Figure 3.7. Rough estimates for the sediment transport capacities for different sea levels and a discharge of  $Q = 1000 \text{ m}^3/\text{s}$ , based on a full spring-neap cycle. In blue the sediment transport capacity due to depth averaged velocities, in red sediment transport capacity due to bottom velocity (layer 9) and in green the ratio. Transport capacities have been calculated with the modified van Rijn 1984 (appendix F) for a sediment fraction with  $D_{50} = 300\mu\text{m}$ .

### 3.3 Implementation

One approach to correct for the sediment transport in 2D would be to multiply the sediment transport capacity due to depth average velocities by a certain factor, which is dependent on the distance to the mouth and reflect the ratios observed in Figure 3.6. This method has two drawbacks. First, it is hard to correct the sediment transport capacity if the capacity due to the depth-averaged velocity is close to zero, while the capacity due to the velocity at the bottom has a significant value. Second, the ratio between the two sediment transport capacities depends strongly on the tidal period chosen (i.e. whether it is a full spring neap cycle or just one low water high water cycle during normal tide, neap tide or spring tide). It therefore is better to choose a correction method which is less sensitive to different time frames.

The method chosen compensates the sediment transport capacity for each time step by:

- Weakening the sediment transport due to negative (seaward) velocities and/ or changing its sign.
- Strengthening the sediment transport due to positive (landward) velocities.

The factors for weakening, changing sign and strengthening are dependent on the distance to the mouth and converge to a value of one when the sediment transport capacity ratio reaches one.

The correction is applied to the “total load” of sand as computed with the transport model of Van Rijn (1984). We have assumed that both bed-load and suspended-load components of this model can be found in the lower part of the water column and are therefore in a similar way affected by the salt wedge.

The correction method and the procedure for determining the correction values will be explained based on Figure 3.8, which shows the same v-v plots as in Figure 3.4, but with a different color marking:

- a1 - In the yellow region, the depth averaged velocity is (on average) more negative than the bottom velocity or has the same value. To compensate for a too negative velocity value, the sediment transport capacity is reduced by factor a1 with  $[0 < a1 < 1]$ .
- a2 - In the mint green region the depth averaged velocity is more negative than the bottom velocity or has an opposite value (i.e. bottom velocity is positive). To compensate for this the factor a2 has been introduced which either reduces the sediment transport capacity or changes its sign  $[a2 < 1]$ .
- a3 - In the blue region the depth averaged velocity is (on average) less positive than the bottom velocity or has the same value. To compensate for a too low positive velocity value, the sediment transport capacity is enhanced by factor a3 with  $[a3 > 1]$ .
- vl - vl is the parameter that marks the border between the yellow and mint green region.

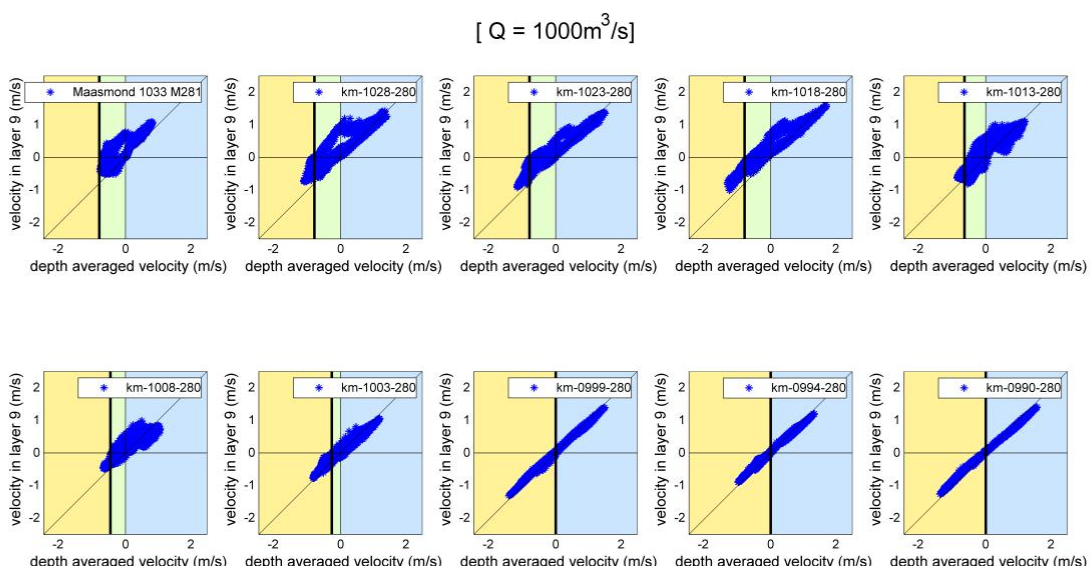


Figure 3.8. v-v plots as shown in Figure 3.4, but with different color marking to indicate the different regions for sediment transport correction.

The resulting sediment transport capacity plots are shown in Figure 3.9. The parameters  $a_1$ ,  $a_2$ ,  $a_3$  and  $v_l$  have been optimized for the representative tide described in 2.3.2, therefore the results in Figure 3.9 are based on a representative tide, and not on a full spring neap cycle as in Figure 3.6. However choice of a different period (like another tidal cycle or a full spring neap cycle), has only little effect on the quality of the correction. Furthermore, no different parameters are needed for different values of the grain size  $D_{50}$ .

The results in Figure 3.9 show that the new sediment transport capacity ratio is mostly close to one (value of one is indicated by the grey line in the transport capacity ration plots in Figure 3.9). Some extreme values occur, when both the sediment transport capacity due to the bottom velocity and the correct sediment transport capacity due to the depth-averaged velocity are close to zero. This is not a problem, as confirmed by the sediment transport capacity plots, which show that the blue and red lines have almost the same value at these points.

#### 3.4 Result in RMM model

For low discharges the result of the correction on sediment transport of sand particles ( $D_{50} = 300\mu\text{m}$ ) is shown in Figure 3.10. The lines show the results from the Zeedelta model (transport induced by depth averaged and bottom velocities), the stars show the results from the RMM model (net transport capacity without and with correction). The values from the RMM model in without correction are in general much more negative than the values for the depth averaged induced sediment transport of the Zeedelta model. This is due to the fact that the observed maximum negative (seaward) velocities in the RMM model are higher (on the order of -1.5 m/s) in the Nieuwe Waterweg than for the Zeedelta model (on the order of -1 m/s).

The modified RMM results are considerably less negative than the reference RMM results, so the modification acts in the correct direction (less strong seaward). However it does not result in the expected net sediment transport directed towards land. This is due to the fact that the parameters were derived for the obtained velocities in the Zeedelta model, which are different than the velocities in the RMM model. It remains to be checked from where the differences between the depth averaged velocities from the RMM- and Zeedelta model originate.

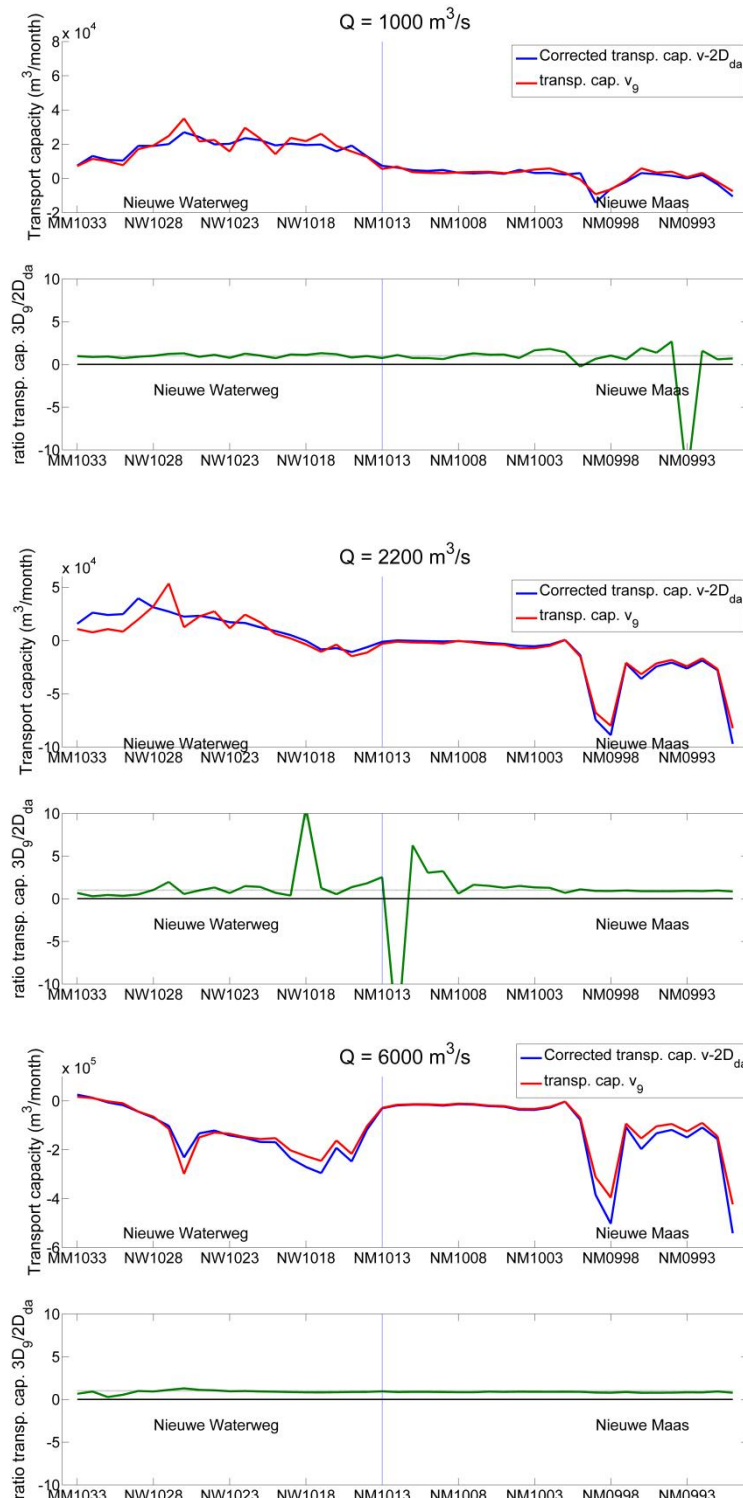
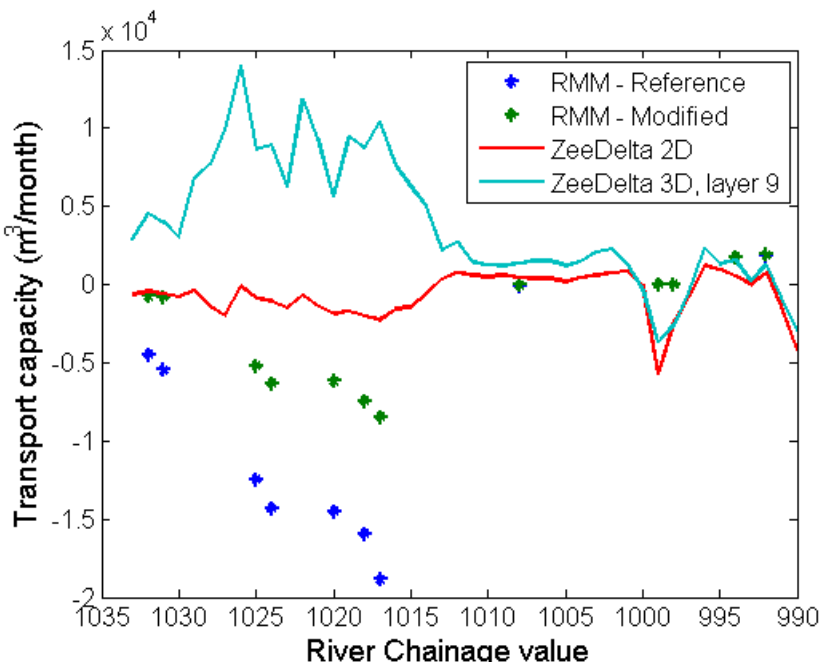


Figure 3.9. Rough estimates for the sediment transport capacities for discharges of  $Q = 1000 \text{ m}^3/\text{s}$ ,  $Q = 2200 \text{ m}^3/\text{s}$  and  $Q = 6000 \text{ m}^3/\text{s}$ , based on representative tide. In blue the corrected sediment transport capacity due to depth averaged velocities, in red sediment transport capacity due to bottom velocity (layer 9) and in green the ratio. Transport capacities have been calculated with the modified van Rijn 1984 (appendix F) for a sediment fraction with  $D_{50} = 300 \mu\text{m}$ .



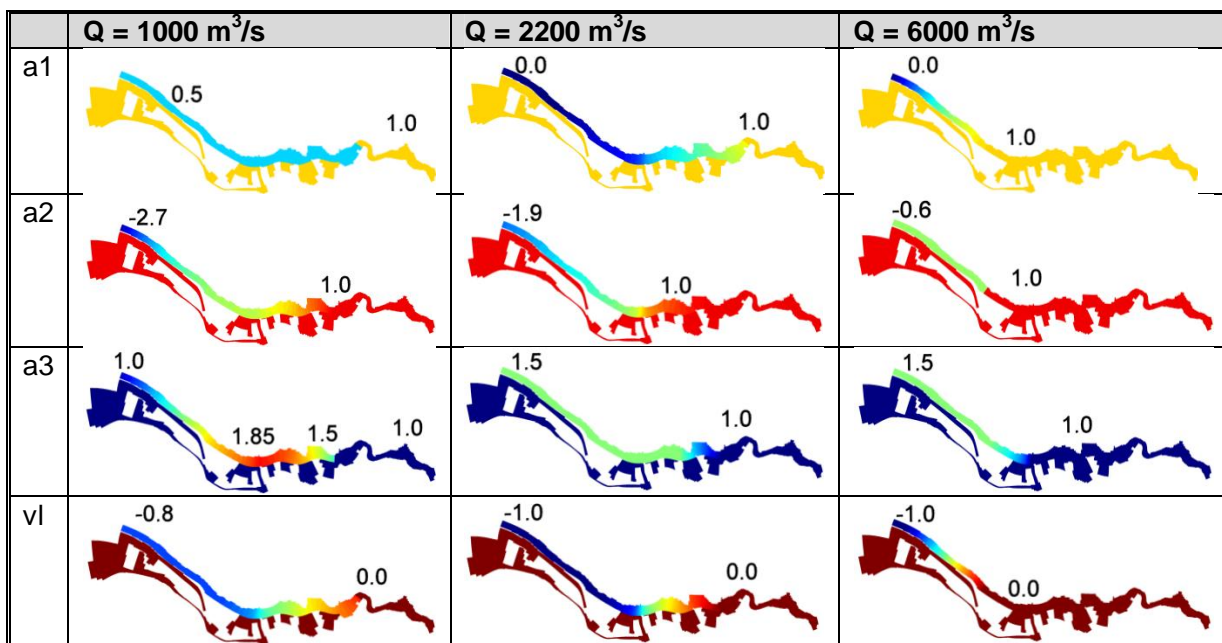
*Figure 3.10 Bedload transport capacity for sand particles ( $D_{50} = 300 \mu\text{m}$ ), for the RMM model and the Zeedelta model. Red line: transport capacities due to depth averaged velocities from the ZeeDelta model. Blue dots: transport capacities due to depth averaged velocities from the RMM model. Light blue line: transport capacities due to bottom velocities from the ZeeDelta model. Green dots: Modified transport capacities due to depth averaged velocities from the RMM model. Note that the transport capacity for the ZeeDelta model has been decreased with respect to previous results for low discharges. This is due to the fact that the initial sediment composition has been taken into account, which is 40% for the  $300 \mu\text{m}$  sand fraction.*

Test simulations with morphological changes have been carried out for testing the Delta Model. The results are presented in report Sloff, van der Sligte and Visser (2013). For the test simulations we applied the following settings, as indicated graphically in Table 3.1:

- Coefficient a1:
  - At low river discharge  $Q=1000 \text{ m}^3/\text{s}$  it is constant, equal to 0.5 from the Maasmond through the Nieuwe Waterweg and Nieuwe Maas until halfway the Noordereiland in Rotterdam.
  - At median discharge  $Q=2200 \text{ m}^3/\text{s}$  it increases gradually from 0 at the Maasmond, to 1.0 halfway the Noordereiland.
  - At high discharge  $Q=6000 \text{ m}^3/\text{s}$  increasing gradually from 0 at the Maasmond, to 1.0 halfway the Nieuwe Waterweg
- Coefficient a2:
  - At low river discharge it increases gradually from -2.7 at the Maasmond, to 1.0 at the Waalhaven (zero near 2e Petroleumhaven)
  - At median discharge it increases gradually from -1.9 at the Maasmond, to 1.0 at the Waalhaven (zero near Oude Maas)
  - At high discharges it remains -0.6 until Maassluis, and then suddenly increases to 1.0.
- Coefficient a3:
  - At low river discharge it increases gradually from 1.0 at the Maasmond, to 1.85 near the Oude Maas mouth, and reduces gradually to 1.5 at the Waalhaven where it jumps back to 1.0 near the Maashaven.

- At median discharge it has a value of 1.5 along the Nieuwe Waterweg, and the Nieuwe Maas until the Eemhaven, from where it gradually decreases to 1.0 west of the Waalhaven
- At high discharges it remains 1.5 until Maassluis, and then decreases gradually to 1.0 at the Oude Maas mouth (all other sections 1.0).
- Coefficient  $vl$ :
  - At low discharge it remains -0.8 in the Nieuwe Waterweg, and from the Botlekhaven till the Noordereiland it increases gradually to 0.0 (where it remains 0 in other sections as well).
  - At median discharges it remains -1.0 in the Nieuwe Waterweg, and from the Botlekhaven till the Noordereiland it increases gradually to 0.0 (where it remains 0 in other sections as well).
  - At high discharges it increases gradually from -1.0 at the Maasmond to 0.0 at Maassluis (and all other sections equal to 0).

Table 3.1 Settings for salt-wedge correction.



The outcomes of the model simulations with and without the salt-wedge correction are presented in the following figure. The results for the correction shows bed-level fluctuations in the Western part of the Nieuwe Waterweg (West of Maassluis) as can be seen from the bed-level changes in the figure. The cause of these variations could be traced back to the reversal of sediment-transport at certain velocities. It has been found that this reversal is not occurring simultaneously in all cells in a specific area, but causes reversals in individual cells with transport in neighboring cells still in opposite direction. These variations invoke a destabilizing transport gradient, which is strengthening itself.

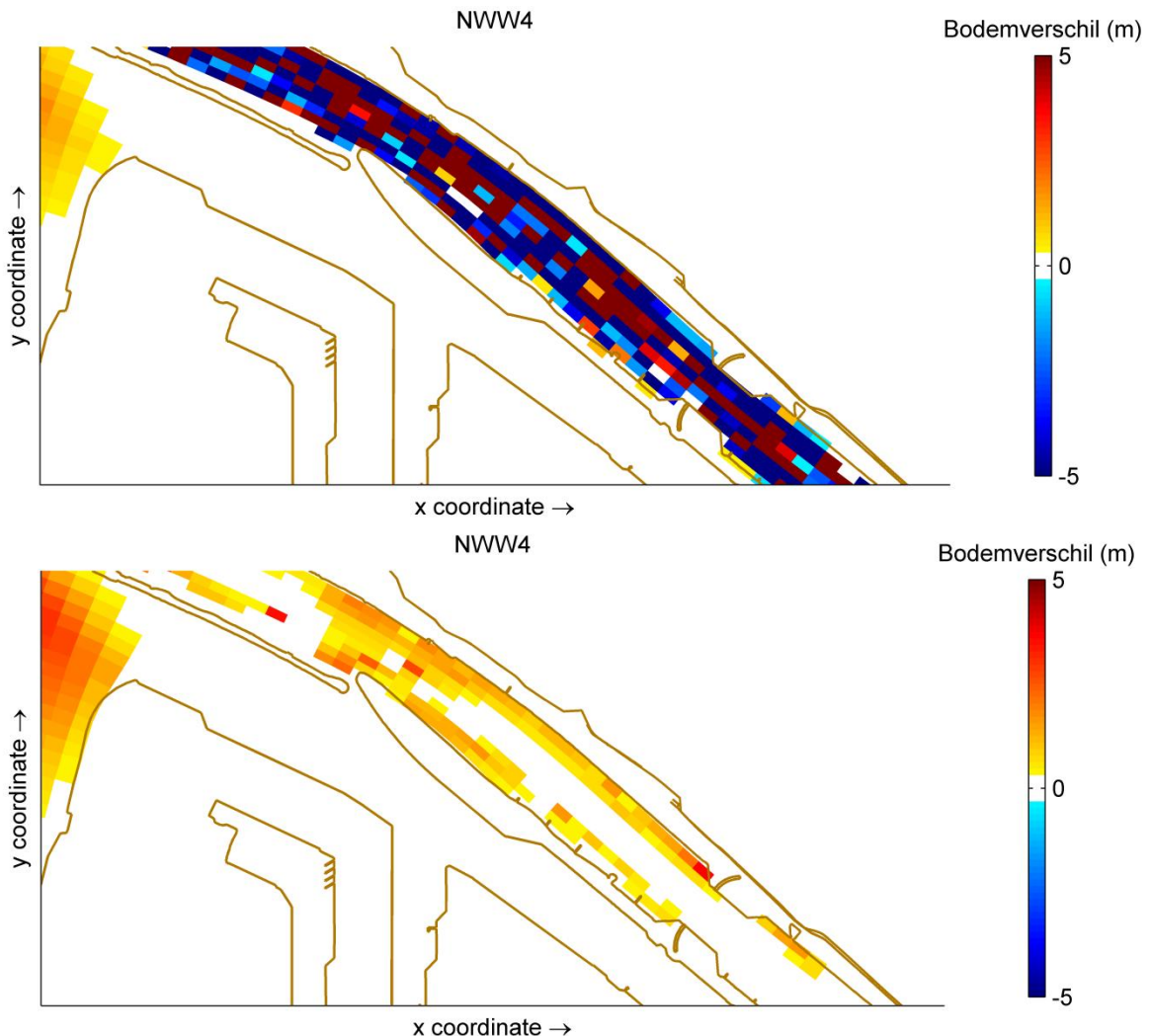
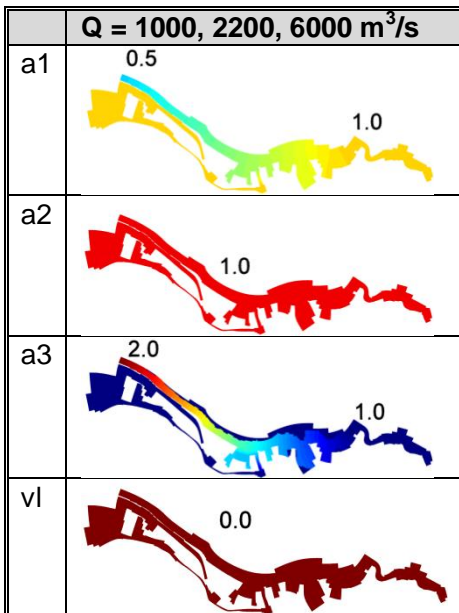


Figure 3.11 Bed-level change computed with salt-wedge correction (top-figure) and without salt-wedge correction (bottom figure) for a 10-year period.

The solution to this problem was to remove the coefficients that are related to reversal of the sediment transport relative to depth-average flow. Effectively the salt-wedge correction then increases the landward transports (upcoming flood tide) and reduces the seaward transport (outgoing tide). The changed settings, as indicated graphically in Table 3.2, are:

- Coefficient a1: for all discharges it increases gradually from 0.5 at the Maasmond to 1.0 at the Noordereiland;
- Coefficient a2: for all discharges it equals 1.0 everywhere.
- Coefficient a3: for all discharges it decreases gradually from 2 at the Maasmond to 1.0 at the Noordereiland
- Coefficient vl: all values equal to zero

Table 3.2 Settings for salt-wedge correction, adapted.



The resulting bed-level change after 10-years is indicated in Figure 3.12. The result is very well comparable to that computed without salt-wedge correction (Figure 3.11 lower figure). Still there are some relevant differences between the 2 simulations, which can be seen in Figure 3.13. Generally the salt-wedge correction causes the final bed to be somewhat higher (in the order of a decimeter) over a period of 10 years.

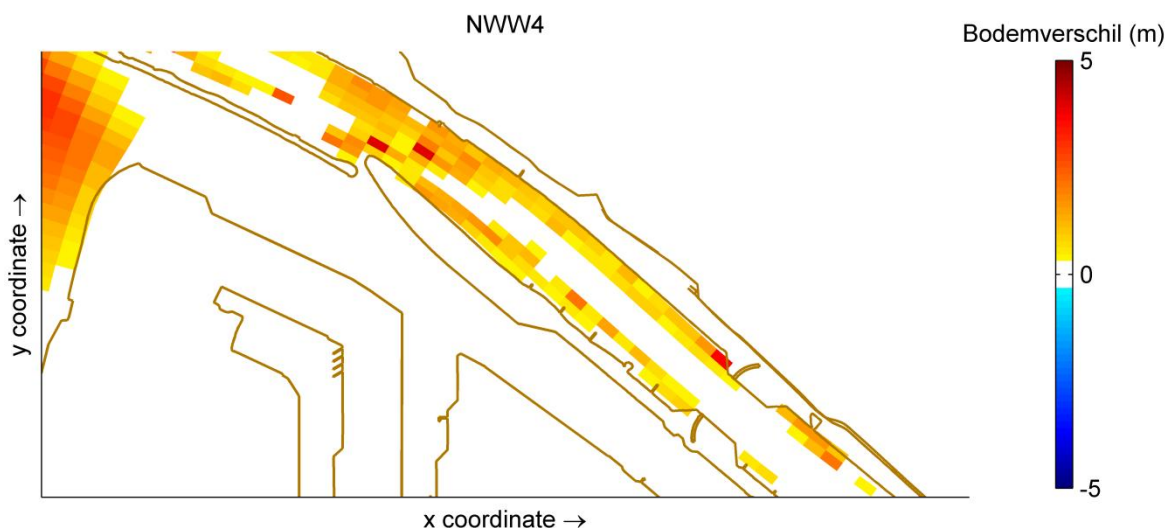
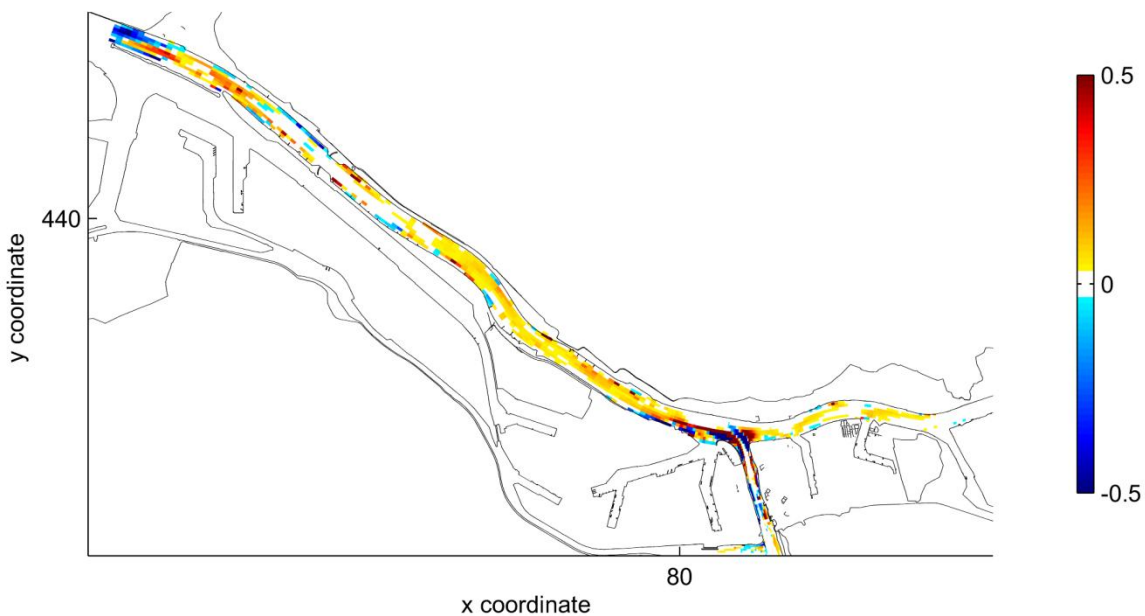


Figure 3.12 Bed-level change computed with adapted salt-wedge correction for a 10-year period.



*Figure 3.13 Difference (m) in computed bed-level for simulation with salt-wedge correction, minus bed-level for simulation without salt-wedge correction (after 10 years simulation). Positive values (red, yellow) mean higher bed level in salt-wedge simulation.*

### 3.5 Discussion

With the presented parameterization, the sediment transport capacity is on average correctly predicted for the Zeedelta model (see Figure 3.9) and gives values for the sediment transport that are in agreement with a previous study (van der Kaaij 2010). The correction is not optimized yet for the RMM model, which is due to the fact that the flow velocity fields are different from the 2D Zeedelta model on which the parameterization was optimized. Aside from the fact that this should be improved, it also shows that the drawback of the current parameterization is its dependence on the Zeedelta model as a reference model. This could be improved by deriving a parameterization which is independent on the boundary conditions. This could be achieved by deriving relations for the current profile in the three dimensional case and make a parameterization of the full velocity profile depending on the degree of stratification, the length of the salt intrusion (for which analytic expression are known) and the depth averaged velocities. Deriving relations for the current profile for non idealized situation has however never been done and might be rather complex, at the same time it will be extremely useful as it could improve 2D modeling of other delta regions too.

Another aspect that could be improved is the modelling of silt and clay. Currently no correction is made for this sediment fraction; however with the help of previous research by (De Nijs et al. 2010 and Van Maren et al. 2007) and the use of the 'flocculation module' in Delft3D (after the work of Van Maren) an improvement could probably be made on modelling silt in the RMM.



## 4 Hydraulic verification

In the hydraulic verification, the Delft3D RMM simulation results were compared to the SOBEK-RE NDB1\_1 results for low, medium and high discharge. Boundary conditions and the lateral outflow at the Haringvlietdam were obtained from the SOBEK model.

In general, the discharge, flow velocity and water level between the SOBEK and the Delft3D model are comparable. This implies that the prescribed phase difference between the tidal waterlevel at the Maasmond and the discharge outflow of the Haringvliet is good. The found discrepancies between the models can be interpreted as an over-preference for the Beneden Merwede and the Oude Maas. Therefore, a special focus in this analysis lies on the connecting branches. The discharge values mentioned in the text refer to the high discharge situation if not specified otherwise.

At the bifurcation at the Merwedes more discharge is conveyed into the Beneden Merwede at the expense of the discharge into the Nieuwe Merwede.

Following the Beneden Merwede, at the next bifurcation point, the river Noord receives around 25 m<sup>3</sup>/s less on average, although the mean discharge of the Beneden Merwede is increased. The total difference instead flows through the Oude Maas. This way, a relatively strong local deviation occurs around river kilometre 978.

Following the Nieuwe Merwede, the mean discharge sums up with the flow coming from the Bergsche Maas which shows accurate results. This way, the total mean discharge entering the Hollands Diep is around 3390 m<sup>3</sup>/s.

Around 2000 m<sup>3</sup>/s is conveyed from the Hollandsch Diep to the Oude Maas through the Dordtsche Kil. This is around 115 m<sup>3</sup>/s less than in the SOBEK model, but a reduction was expected because of the different discharge distribution at Bifurcation 1. The summation of the discharges of Dordtsche Kil and the initial section of the Oude Maas leads to a mean downstream discharge increase of about 140 m<sup>3</sup>/s in the Oude Maas.

The outflow at the Haringvliet barrier is in good agreement with the SOBEK model.

The Nieuwe Maas receives discharge from the Noord and the Lek, where the latter agrees with the SOBEK model. Because of the deficit in the Noord, the corresponding discharge through the Nieuwe Maas is also lower.

Besides the Haringvliet barrier, the Hartelkanaal and the Nieuwe Waterweg represent the other downstream boundaries. They receive the discharge through the Nieuwe Maas and the Oude Maas and show accurate results of the mean discharge distribution.

Near the mouth of the Nieuwe Waterweg and the Hartelkanaal, but also at some parts of the Oude Maas, the mean discharges do not add up perfectly due to the influence of the tidal cycles. The discharge distribution is schematized in Figure 4.1.

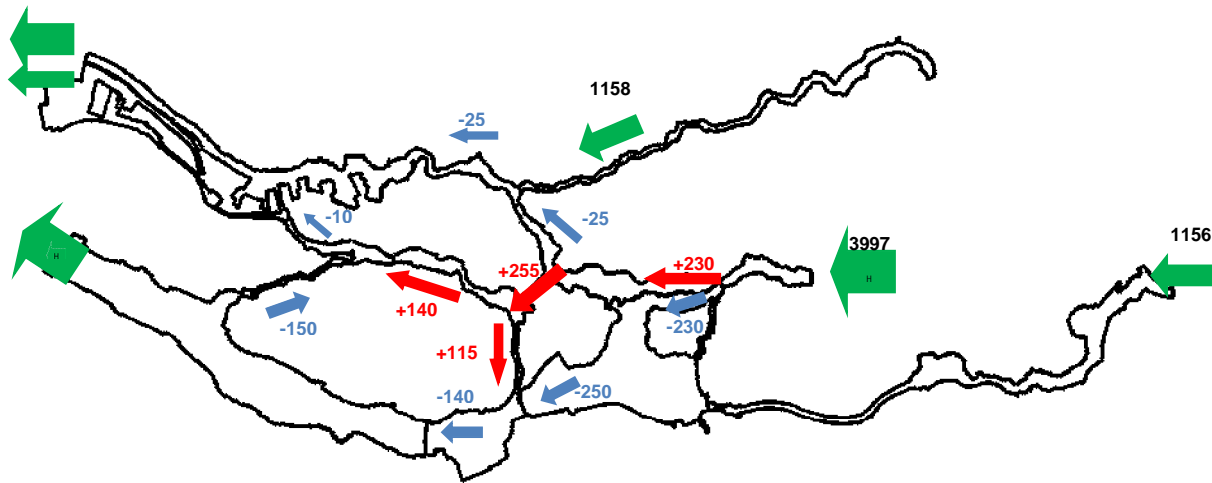


Figure 4.1 Figure of the average error in discharge over the individual branches at high river discharge inflow.

The verification shows an overall agreement of the SOBEK model, though the discharge distribution has a higher preference for the central way via the Beneden Merwede and the Oude Maas than in the prototype. Since the morphodynamics are the goal of this model it is recommended to investigate the effect of a higher roughness in these two rivers on the computed velocities rather than the water levels.

## 5 Test-case Moerdijk

The municipality Moerdijk is located south of the Hollandsch Diep across from the mouth of the Dordtsche Kil. Its industrial area and inland port are used by around 400 companies, including chemical industry and a power plant. They are supplied to a large extend by waterway transport.

In order to ensure safe accessibility to the port also for sea-going vessels, special attention has to be paid to the fairway, which connects the port to the Dordtsche Kil.

This connection is called 'Oversteek Moerdijk' and had to be dredged to the required navigational depth. As a consequence, a deeper trench crosses the Hollandsch Diep.

Because of potential morphodynamic changes of the bed level, it is of vital interest to gain knowledge and make predictions about future required amounts of maintenance dredging of the 'Oversteek Moerdijk'.



Figure 5.1 Google Earth map of Moerdijk and Dordtsche Kil, the "oversteek".

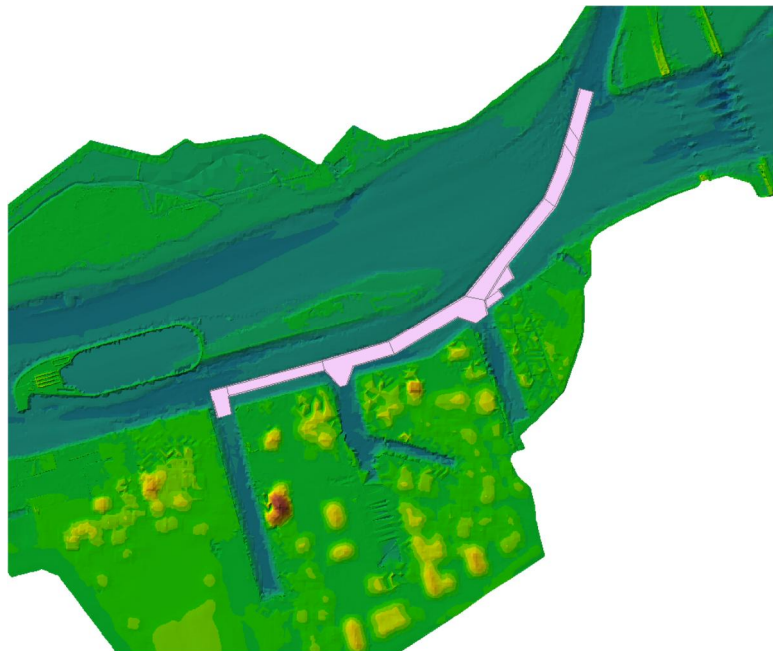


Figure 5.2 Topography and location of navigation channel, the “oversteeek”.

vak	2011 m <sup>3</sup> dredged	2012 m <sup>3</sup> dredged
B1	5,217	18,502
OVM-B	48,377	73,596
OVM-C	38,294	30,424
OVM-D	4,340	1,414
OVM-F	13,843	11,000
IHM-CO1	27,622	50,217
IHM-CO1a		2,654
IHM-CO2	3,257	609
IHM-M	1,310	3,144
IHM-W	756	1,560
totaal	143,016	193,120

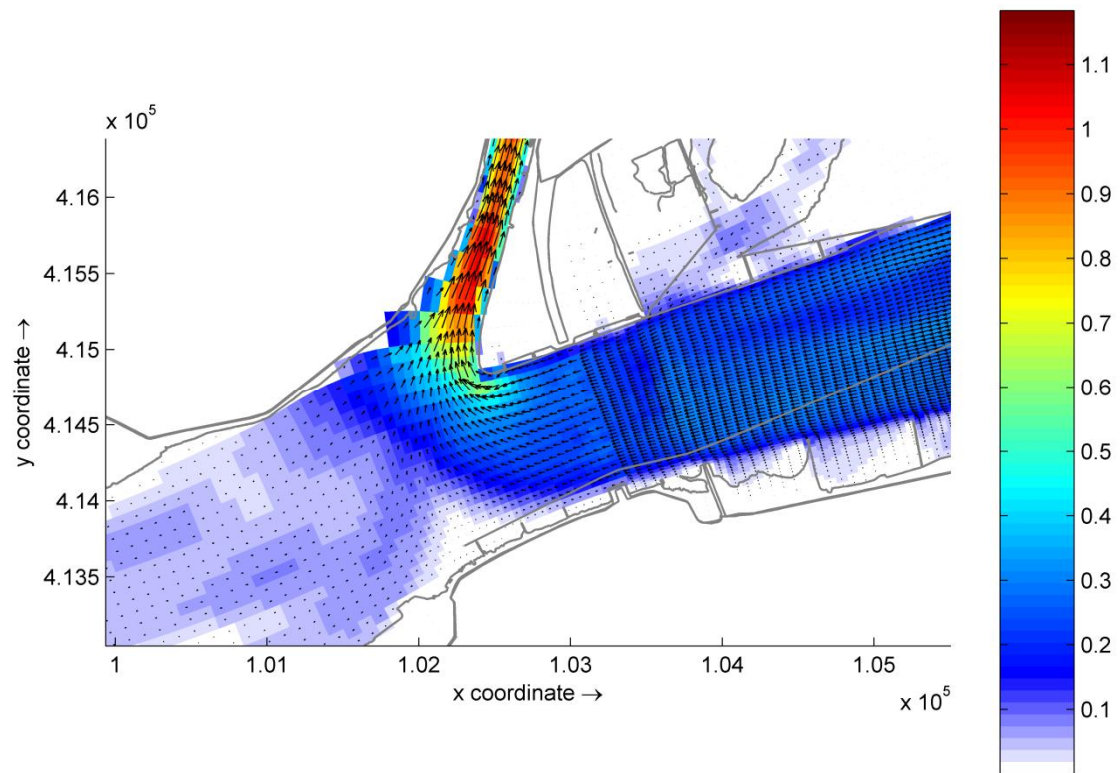


Figure 5.3 Depth-average velocity magnitude (m/s –scale color bar) and velocity vectors, computed for a low river discharge of  $2200 \text{ m}^3/\text{s}$  at Lobith, and lowering tide.

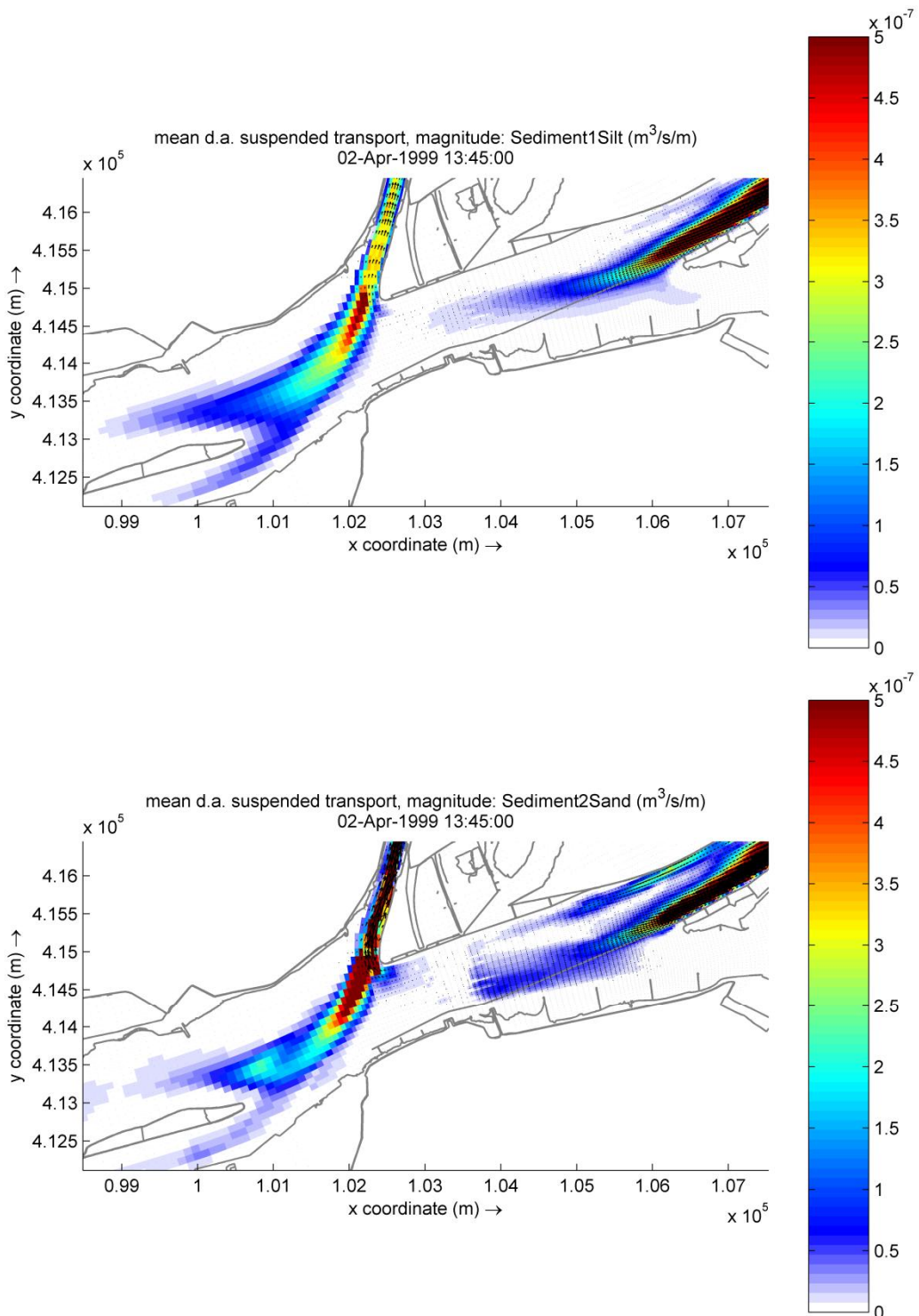


Figure 5.4 Suspended-sediment transport computed ( $\text{m}^3/\text{s}/\text{m}$ ), lowering tide with river inflow  $2200 \text{ m}^3/\text{s}$  at Lobith:  
Top silt fraction; Bottom sand fraction.

Suspended transport strongly decreases as the flow velocities drop at the mouth of the Dordtsche Kil. (1-2 cells were filled up ~1.4 m within 2 years at that specific location).

The relation between suspended and bed load sediment transport is about 4:1.

Hence suspended load should be the main cause for sedimentation.

At the deeper trench of the ‘Oversteek Moerdijk’, increasing bed levels are expected due to its impact on the flow field characteristics.

Dredging and dumping activities were observed throughout the first 5 years of morphodynamic simulation. In Figure 5.5 the computed bed-level change in the “Oversteek” has been presented.

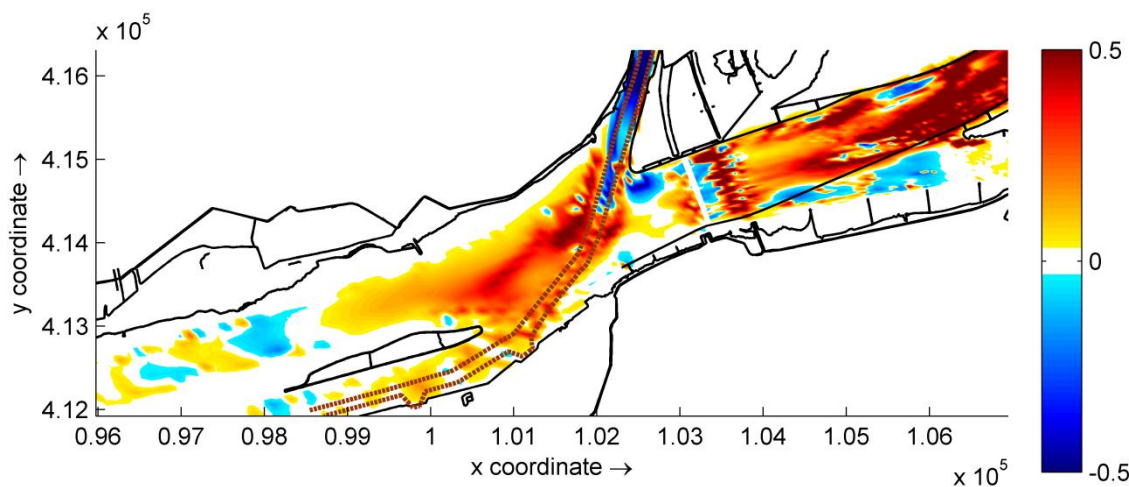


Figure 5.5 Bed-level development at the “oversteek”: positive values are sedimentation (red), negative values are erosion (blue).

Dredging volumes are reported in the following figure. They indicate that the dredged volume is increasing after the first year to a volume of roughly 20,000 m<sup>3</sup>/year, which is about 5 to 10 times smaller than the actual recorded dredging volumes. The dredged material mainly consists of sediment fractions ‘silt’ and ‘fine sand’: these are sediments that are delivered mostly by the rivers (not by erosion of substratum), and are present in the top layer in surrounding regions and at the inflow boundaries.

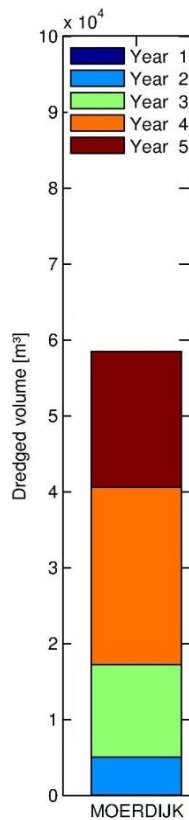


Figure 5.6 Dredging volumes for simulation years 1-5.

From Figure 5.5 can be seen that a lot of sediment from the rivers is depositing west of the Moerdijk bridges. It is possible that the over-exaggerated sedimentation in this section is causing relatively low supply of sediment to the 'Oversteek'. It is recommended to study somewhat more the details of these processes in the Hollandsch Diep to establish more insight in to the sediment balance and sediment trajectories. It is for instance possible to add some tracer material to a location in the Hollandsch Diep and another tracer in the Dordtsche Kil to see the path of these tracers and their net contribution to the sedimentation in the 'Oversteek'.

## 6 3D analysis of scour holes in the river Spui

### 6.1 Introduction

The Rhine-Meuse delta has been subject to several anthropogenic interventions. Hydraulic structures like the Haringvliet barrier changed the original character of the delta by controlling the flow characteristics. The measures of the Delta Works reduced the risk of flooding significantly. However, they also contributed to higher flow velocities in some branches. In earlier research projects, e.g. Smits (2011), erosion pits were investigated.

These pits were observed mainly in the Dordtsche Kil and the Spui, interconnecting branches that have to convey more water due to the closing of the Haringvliet.

Monitoring bed level changes give an indication that erosion is still on-going. If this erosion continues, these pits could reach dimensions that could endanger dike stability.

In this case study, the erosion pits are modelled with 3D hydrodynamic Delft3D simulations in order to evaluate the magnitude of the local shear stresses and the characteristics of the flow pattern around the pits. This way, we may be able to make statements about the nature of this local erosion phenomena and possible measures to counteract it.

In addition to the higher flow velocity, it was found that the river bed consists of different layers. At some locations, the upper layer is composed of fine bed material that is easily erodible. This way, local erosion also affects adjacent areas with higher bed stability, i.e. resistance against erosion. Moreover, the branches with local erosion pits are mainly undersupplied morphological systems which do not tend to fill up the holes.

Complicating factors in the analysis are the influence of tide and the discharge dependent operation of the Haringvliet barrier that have significant impact on the flow reversal and the orientation of the mean flow direction.

For reliable results, a sophisticated approach was chosen including the application of three different models, namely, a hydrostatic Z-layer model, a Sigma-layer model and a fully non-hydrostatic Z-layer model.

### 6.2 Model

#### 6.2.1 Grid extraction and refinement

The original grid of the river section was extracted from the corresponding domain as shown in the following figures. In order to increase the resolution for the 3D simulation the original grid was refined by a factor 9, leading to cells with one third of the original length and width. Because of the grid refinement, the time step had to be lowered as well (from 0.01 to 0.003 minutes).

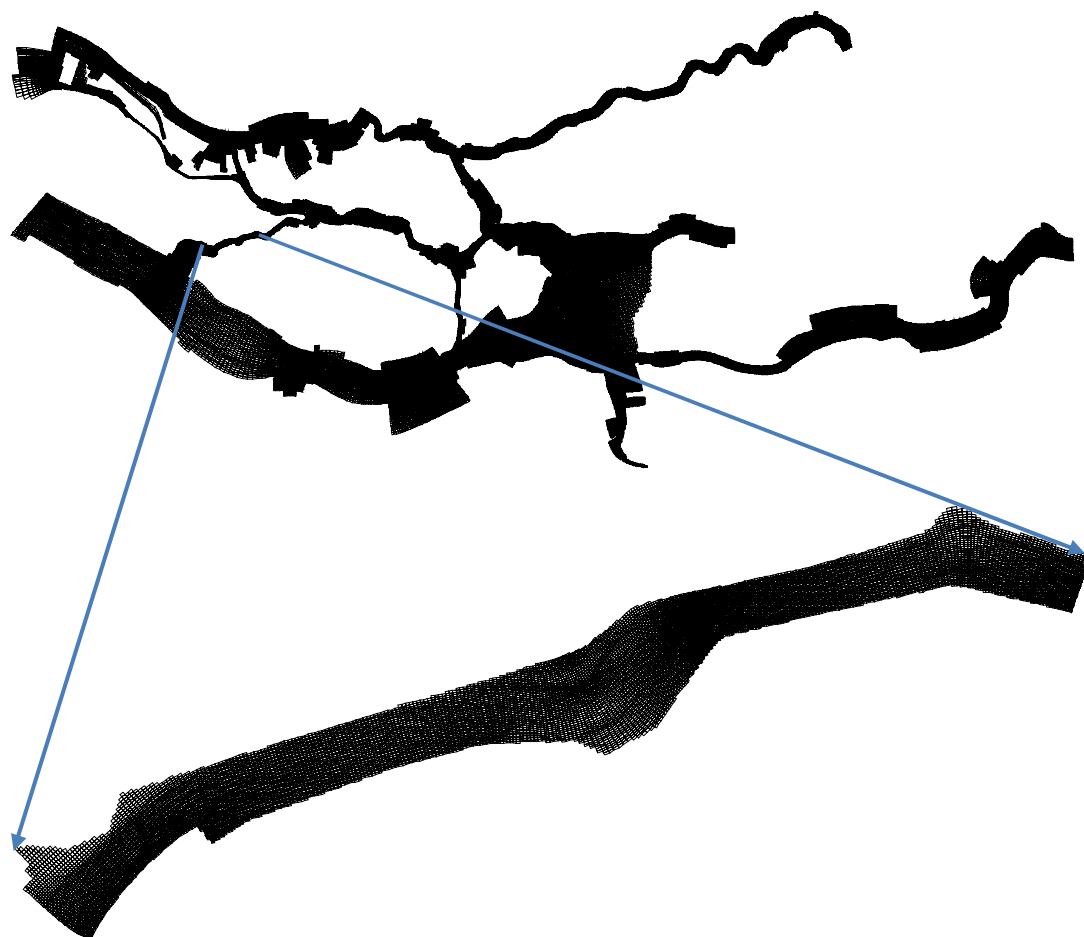


Figure 6.1 Indication of extraction of Spui river section from RMM model and refinement of computational grid.

## 6.2.2 Boundary conditions

The boundary conditions for the Spui River were extracted from the output of simulations of the RMM model. Three discharges are simulated, namely low, medium and high river flows.

The boundaries of the new domain were set at river kilometres 1001 and 1006 (see Figure 6.2).

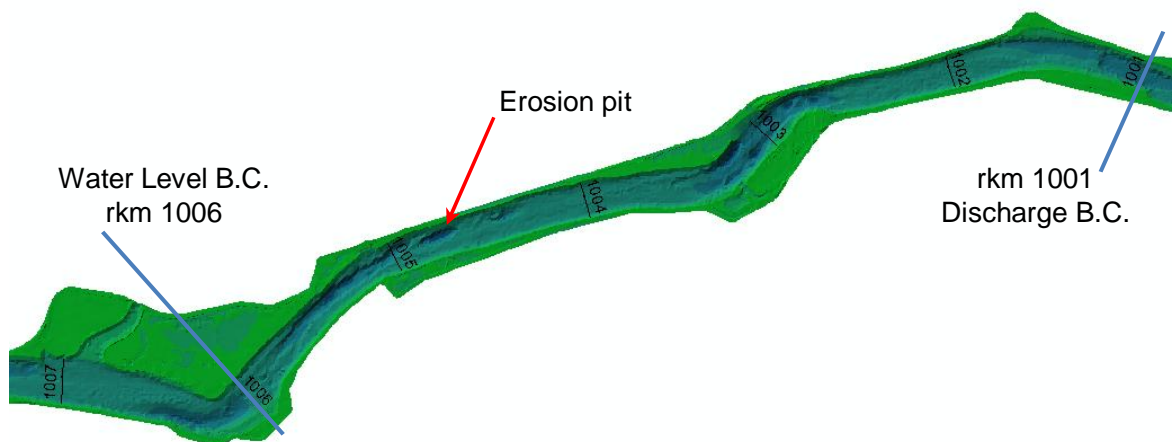


Figure 6.3 Section of the Spui River with erosion pit near river kilometre 1005.

The depth averaged discharge was determined based on the output data at the observation point at rkm 1001. For the local water level, data was taken from the cross-section at rkm 1006.

The simulation period was chosen to be 3 days to resolve a sufficient number of tidal cycles but also to account for the extensive simulation time of three-dimensional simulations.

In order to guarantee a smooth start with a short spin-up time, the start of the simulation is one day after the start of the obtained boundary conditions.



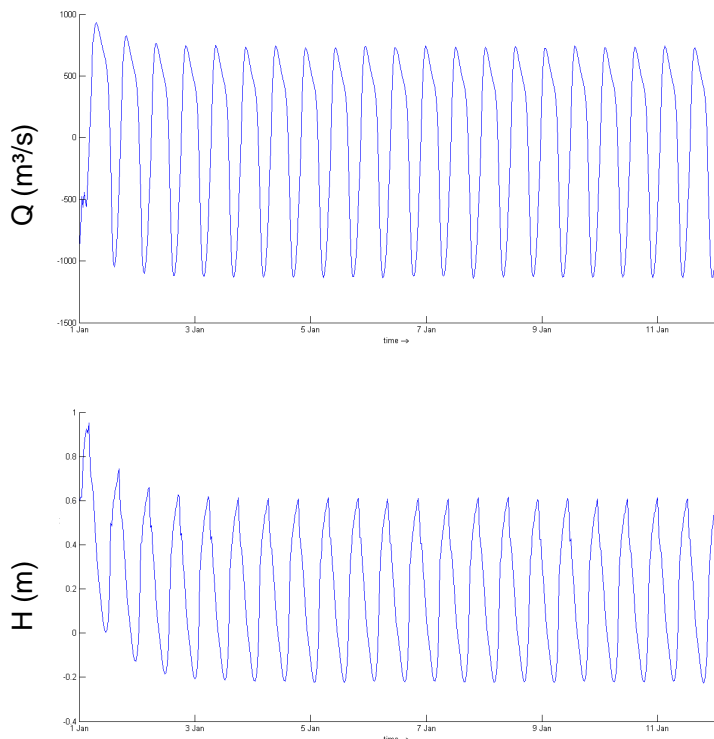


Figure 6.4 Discharge and water level boundary conditions for high river discharge scenario.

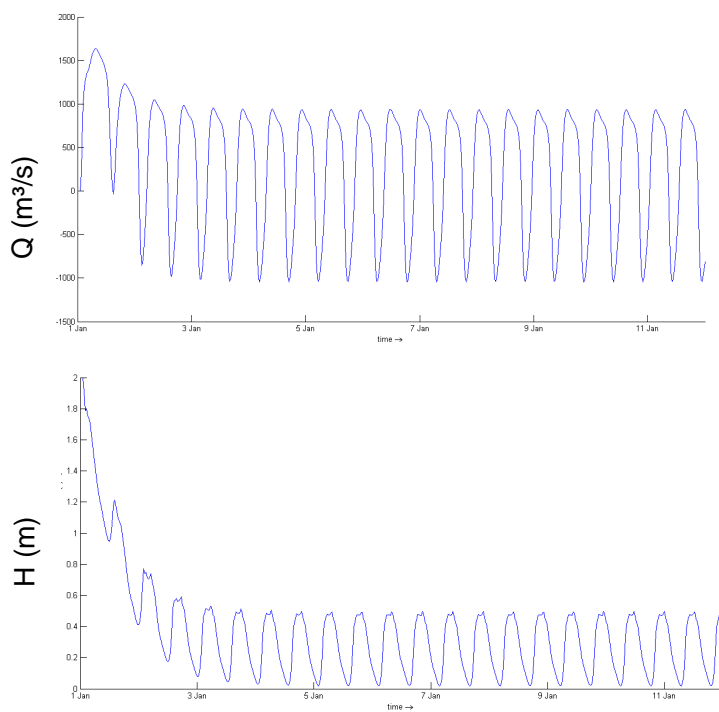


Figure 6.5 Discharge and water level boundary conditions for medium river discharge scenario.



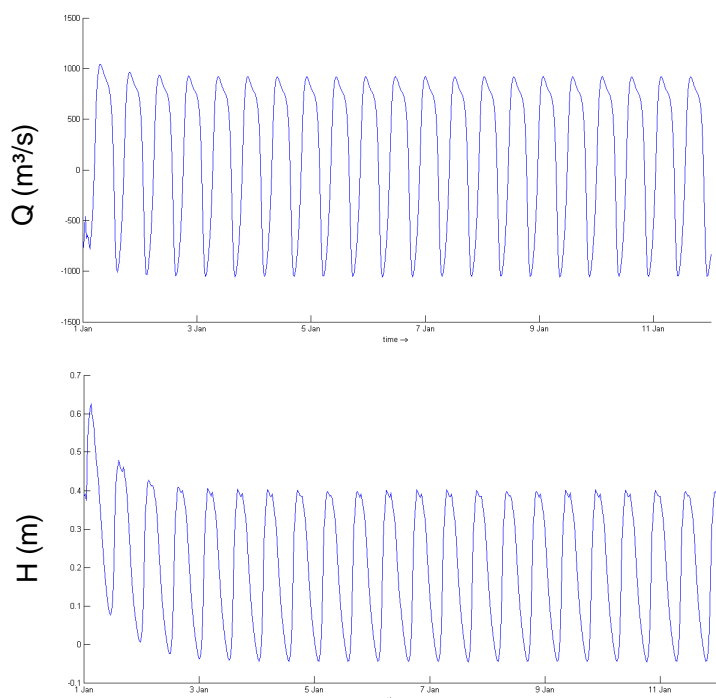


Figure 6.6 Discharge and water level boundary conditions for low river discharge scenario.

### 6.2.3 Initial conditions

The initial conditions were chosen to be the water level, which corresponds to the initial water level obtained through the RMM simulations. Hence, for the low, medium and high discharge scenarios the initial conditions were set to -0.1, 0.4 and 0.0 m, respectively.



#### 6.2.4 Vertical hydrodynamic grid

In Delft3D, two options are available to compute the vertical flow pattern:

- Sigma-layer and Z-layer.

The Sigma-layers are evenly distributed between the top layer (surface) and the bottom layer (bed) and adapt to the slope, whereas the Z-layer are completely horizontal.

Moreover, the Z-layer can be used to include non-hydrostatic flow conditions. A new version with full non-hydrostatic computation was used besides a normal, hydrostatic Z-layer model.

Non-hydrostatic flow should be considered, if the vertical component of the flow velocity is in the order of the horizontal flow velocity. Hence, this effect has been included given the depth and the steep slope of the scour holes.

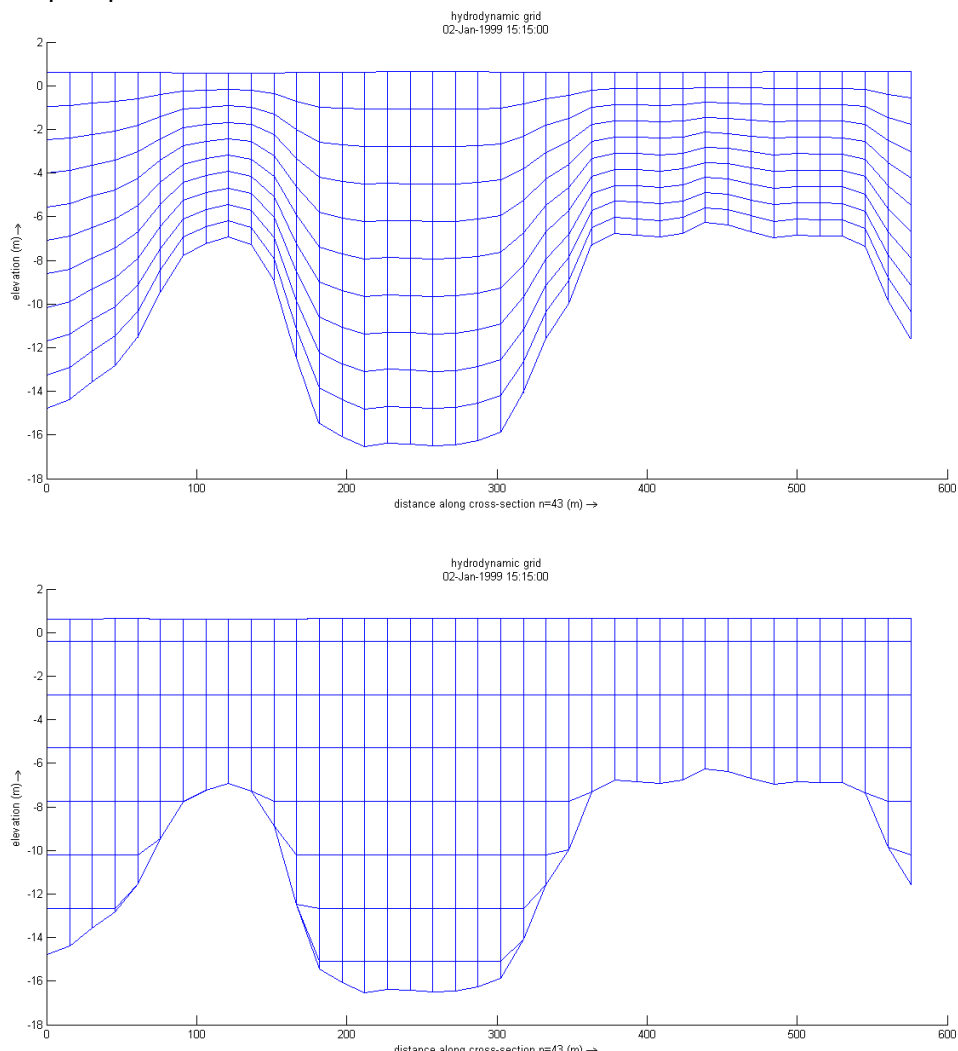


Figure 6.7 Longitudinal cross section of erosion pit modelled with Sigma-layer and Z-layer.

In the following table, all simulations are presented.

No.	Model (type of simulation)	Time step	Layer distribution	Boundary condition (river discharge)	Initial condition
01	Non-hydrostatic Z	0.003	10, 10% each	High	-0.10 m
02	Non-hydrostatic Z	0.003	10, 10% each	Medium	0.40 m
03	Non-hydrostatic Z	0.003	10, 10% each	Low	0.00 m
04	Hydrostatic Z	0.003	10, 10% each	High	-0.10 m
05	Hydrostatic Z	0.003	10, 10% each	Medium	0.40 m
06	Hydrostatic Z	0.003	10, 10% each	Low	0.00 m
07	Sigma	0.003	10, 10% each	High	-0.10 m
08	Sigma	0.003	10, 10% each	Medium	0.40 m
09	Sigma	0.003	10, 10% each	Low	0.00 m

All simulations are carried out with tidal boundary conditions as shown in section 6.2.2. The simulation time of the different 3D models for a period of three days is given below.

Expected simulation time:

- **Z non-hydrostatic**      **2d12h**
- **Z hydrostatic**            **1d12h**
- **Sigma**                    **5d 3h**

## 6.3 Results

The figures in this section show the distribution of bed shear stress ( $\text{N/m}^2$ ) from a top view and the flow field ( $\text{m/s}$ ) in a transverse and a longitudinal cross section for all three models. The medium discharge was chosen as reference scenario. Each simulation result is presented for the corresponding time step of the velocity peaks in both directions.

It is clearly visible that the tidal signal leads to a flow reversal and that the flow velocities towards the Oude Maas exceed the velocities of the flow towards the Haringvliet.

As can be seen later on, this does not hold for all scenarios, i.e. depending on the total river discharge, the time averaged discharge reverses. Moreover, in the transversal cross sections, secondary flow effects were observed, as well.

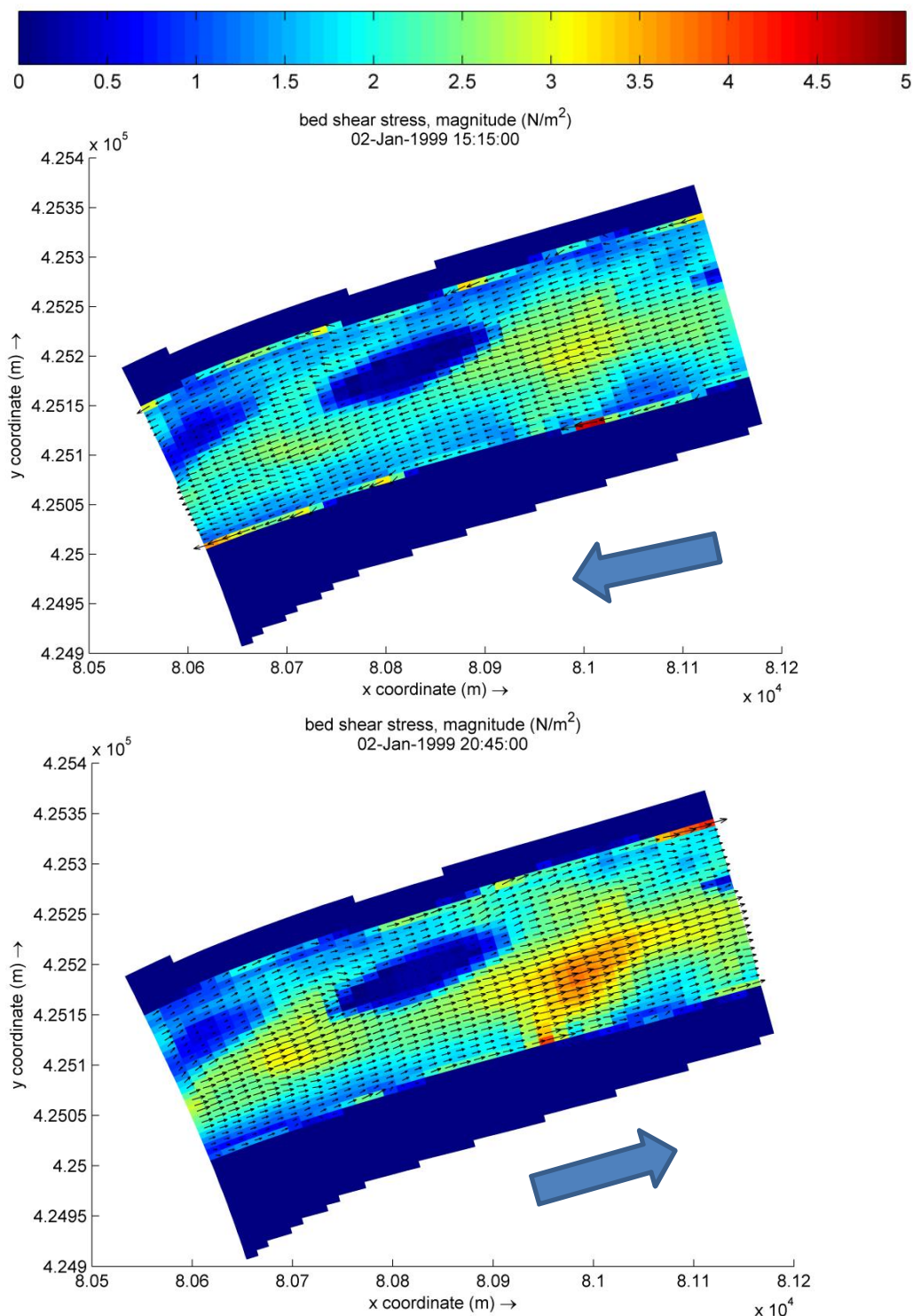


Figure 6.8 Non-hydrostatic Z-layer model, bed shear stress, medium discharge scenario.

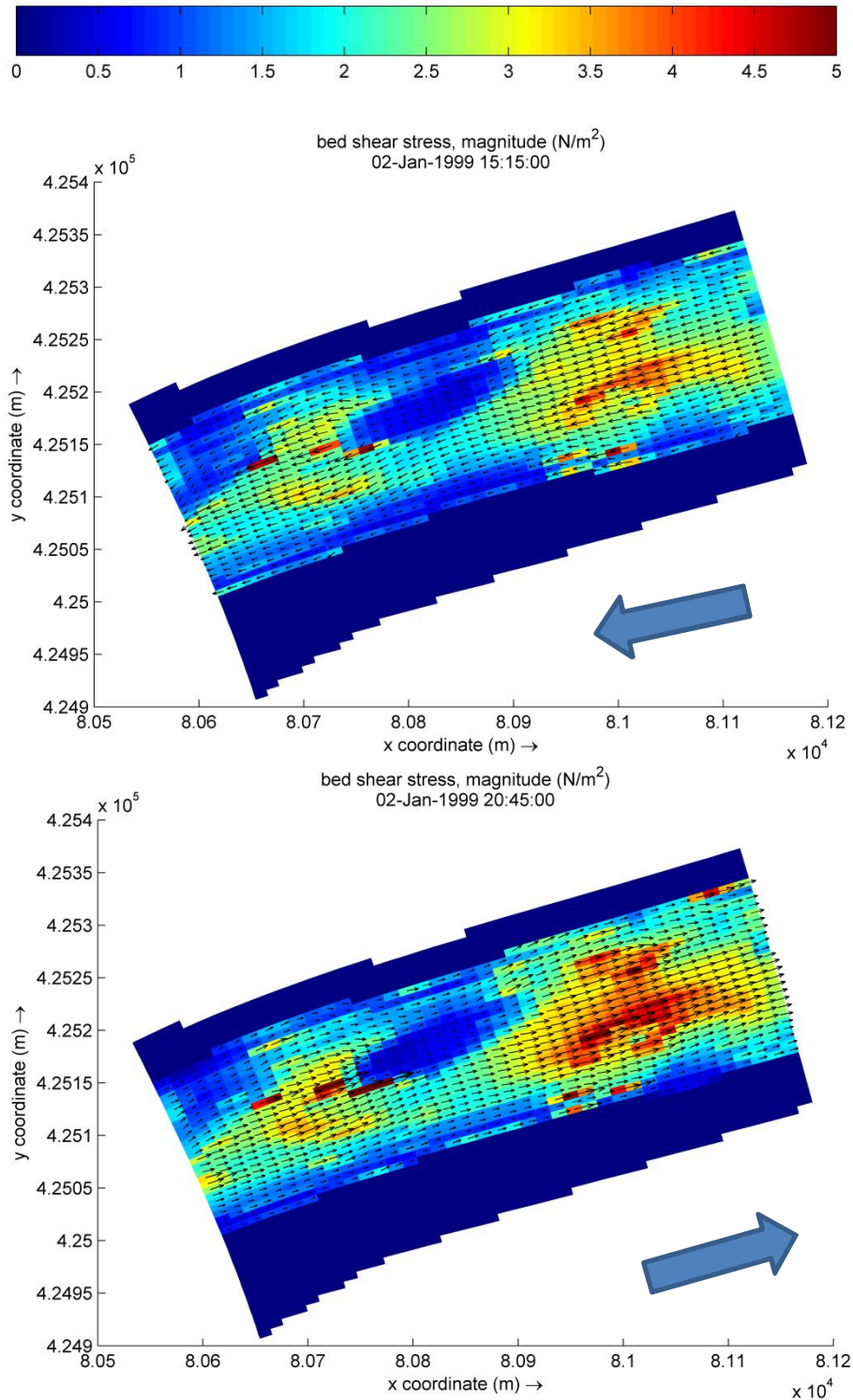


Figure 6.9 Hydrostatic Z-layer model, bed shear stress, medium discharge scenario.

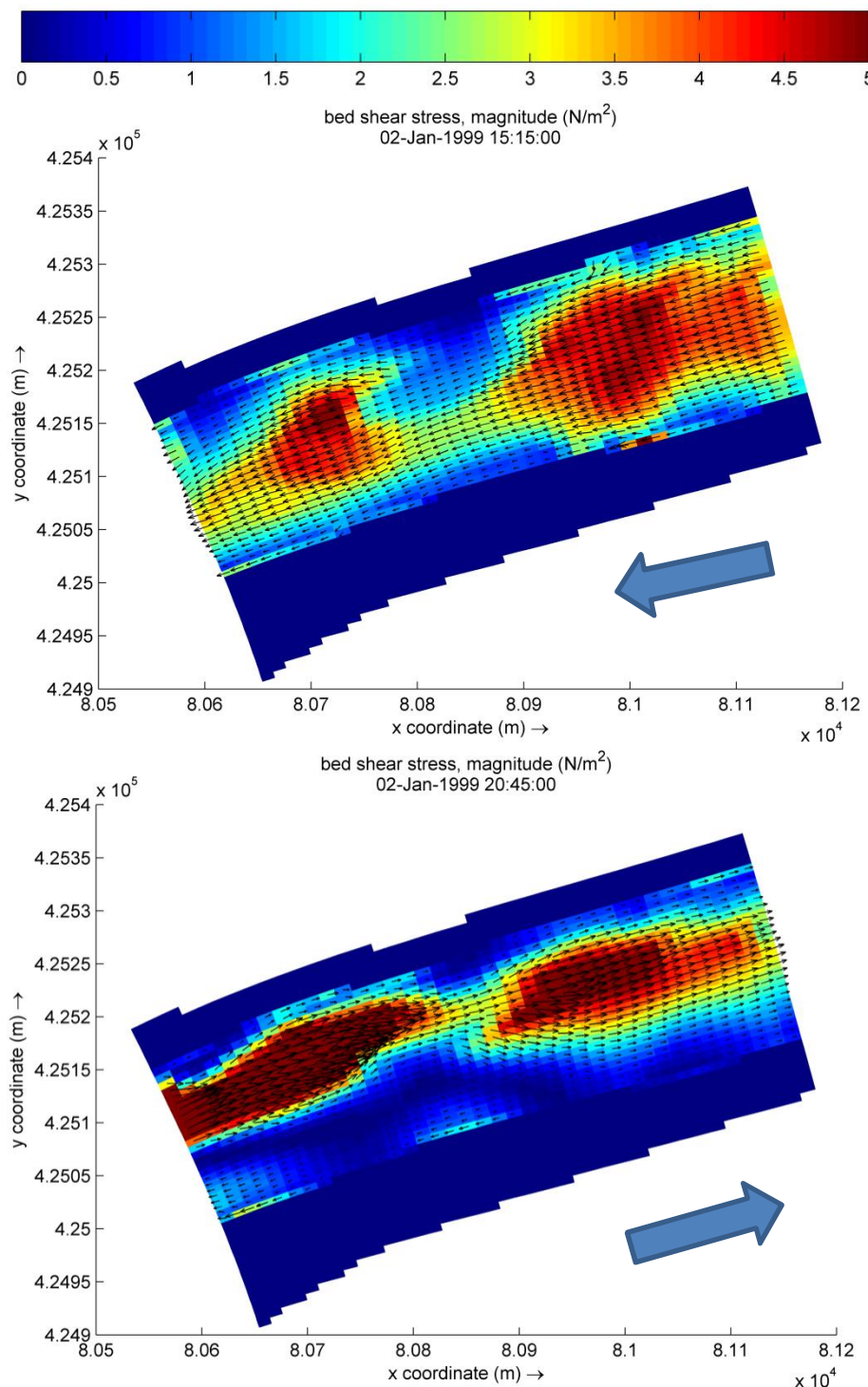


Figure 6.10 Sigma-layer model, bed shear stress, medium discharge scenario.

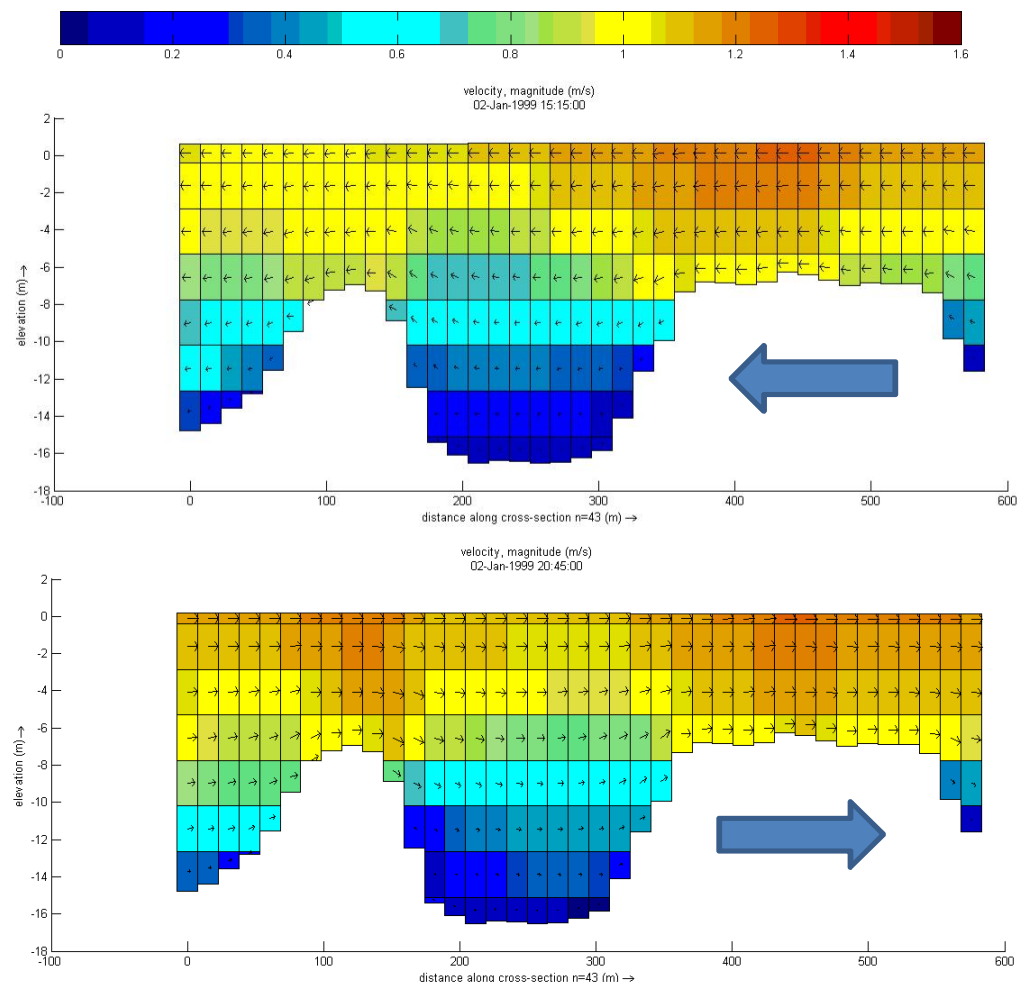


Figure 6.11 Non-hydrostatic Z-layer model, velocity magnitude longitudinal section, medium discharge scenario.

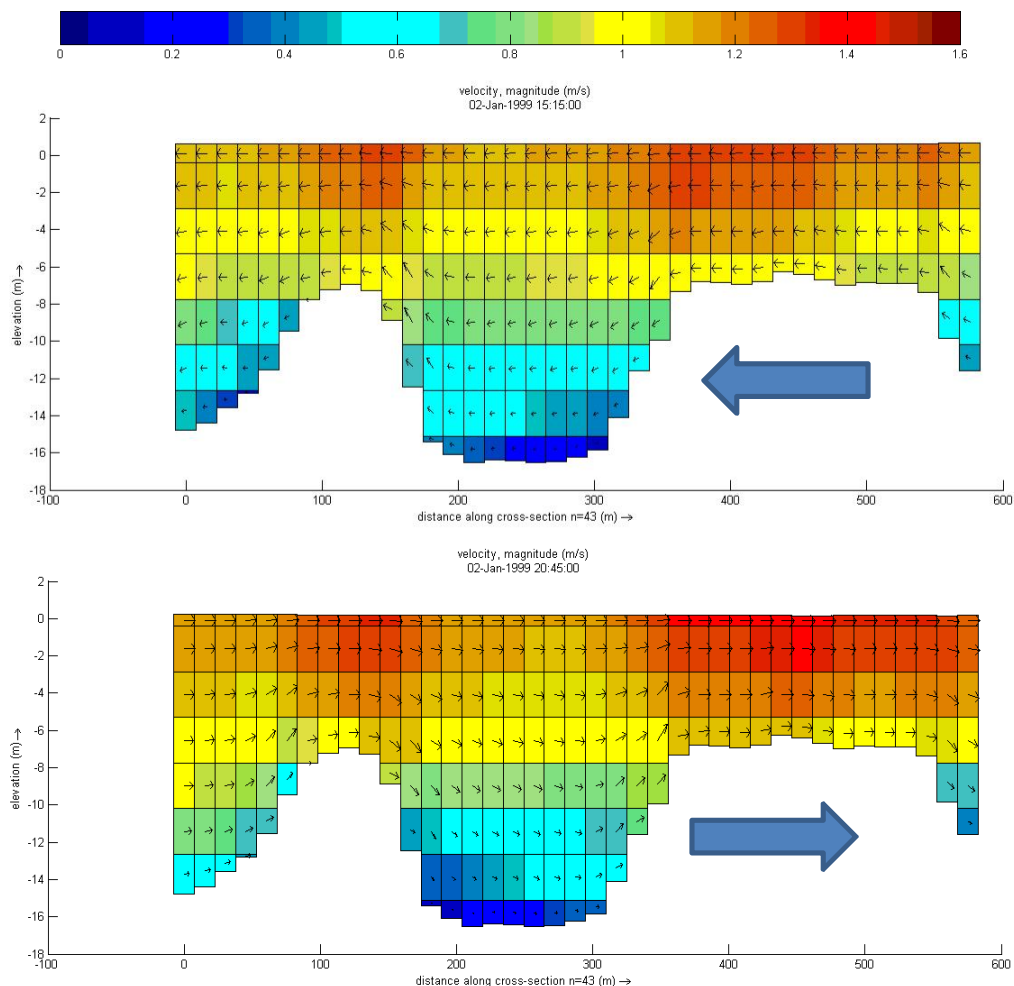


Figure 6.12 Hydrostatic Z-layer model, velocity magnitude longitudinal section, medium discharge scenario.

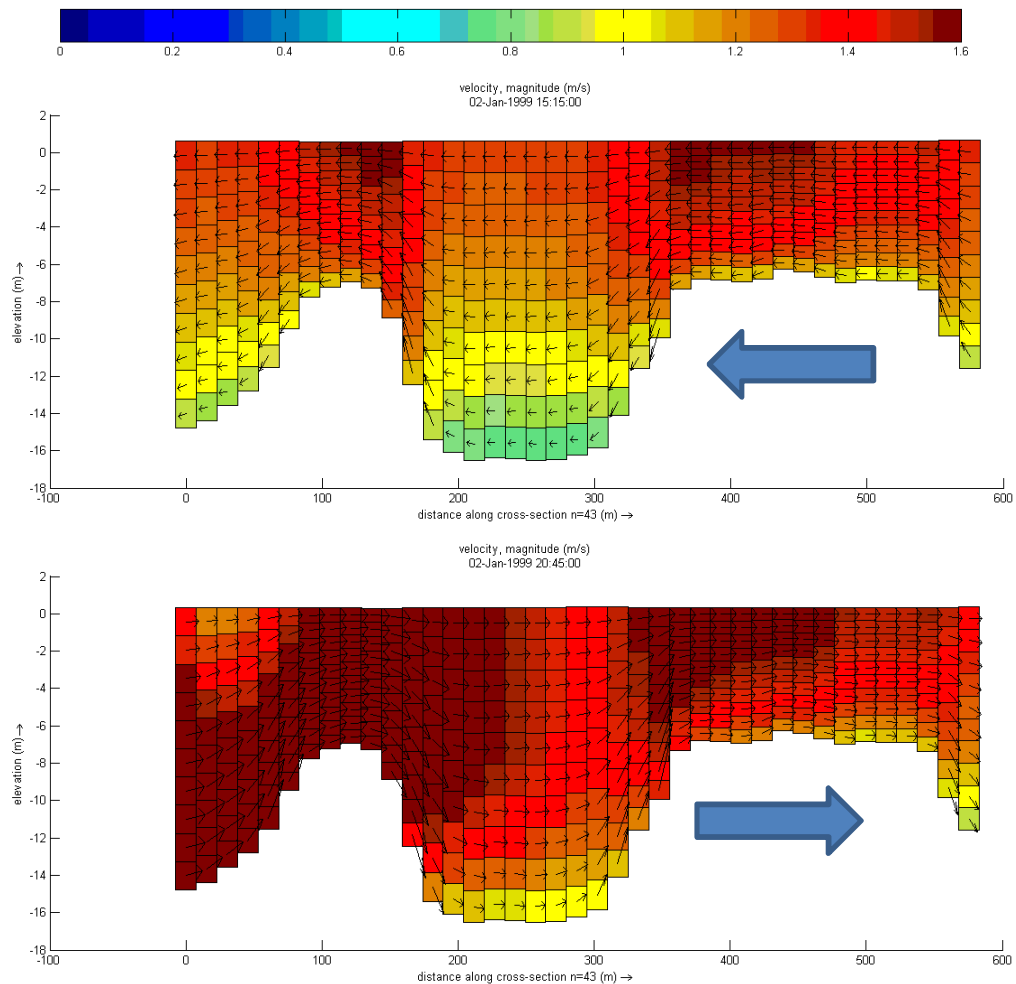


Figure 6.13 Sigma-layer model, velocity magnitude longitudinal section, medium discharge scenario.

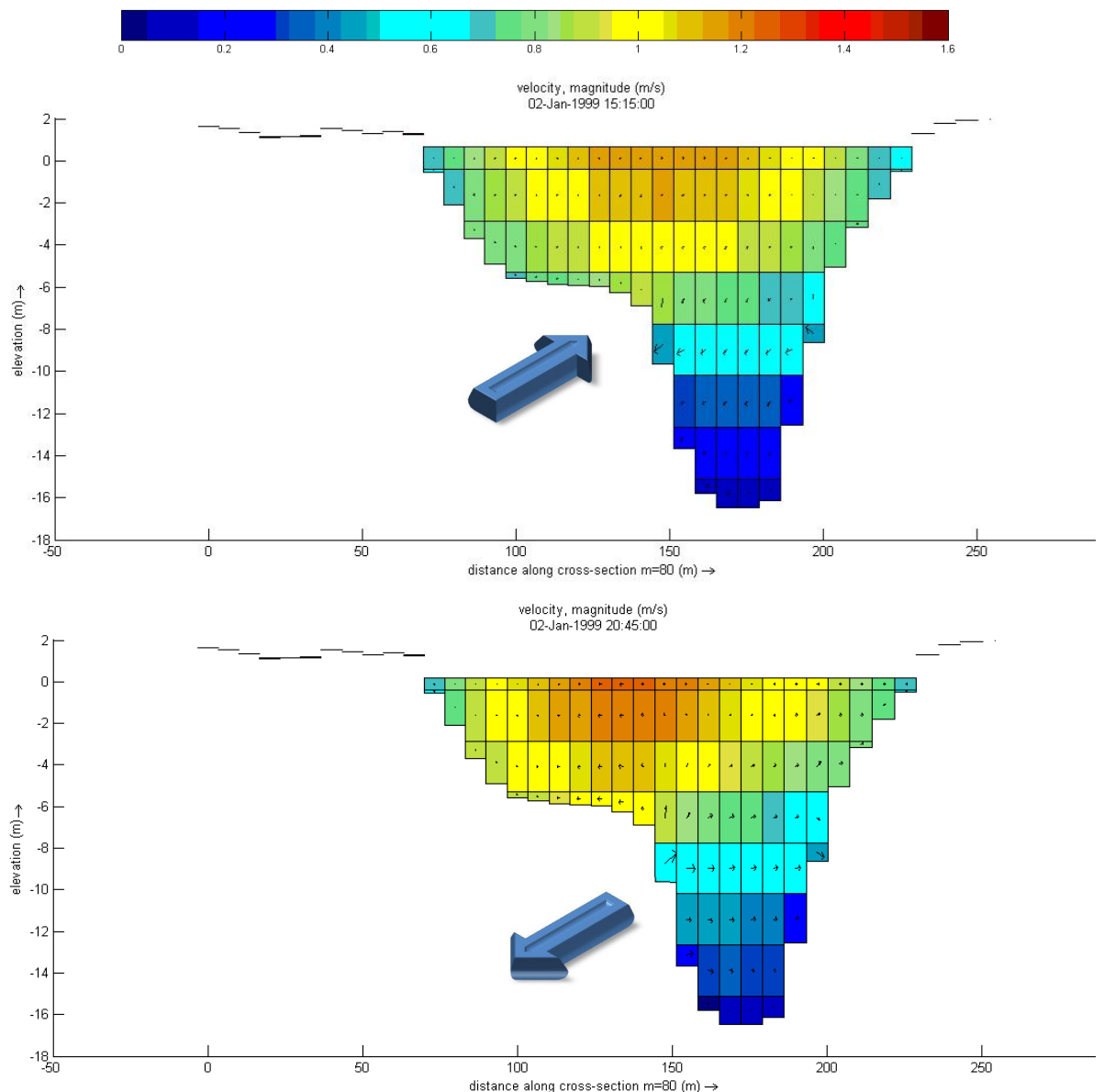


Figure 6.14 Non-hydrostatic Z-layer model, velocity magnitude, transverse section, medium discharge scenario.

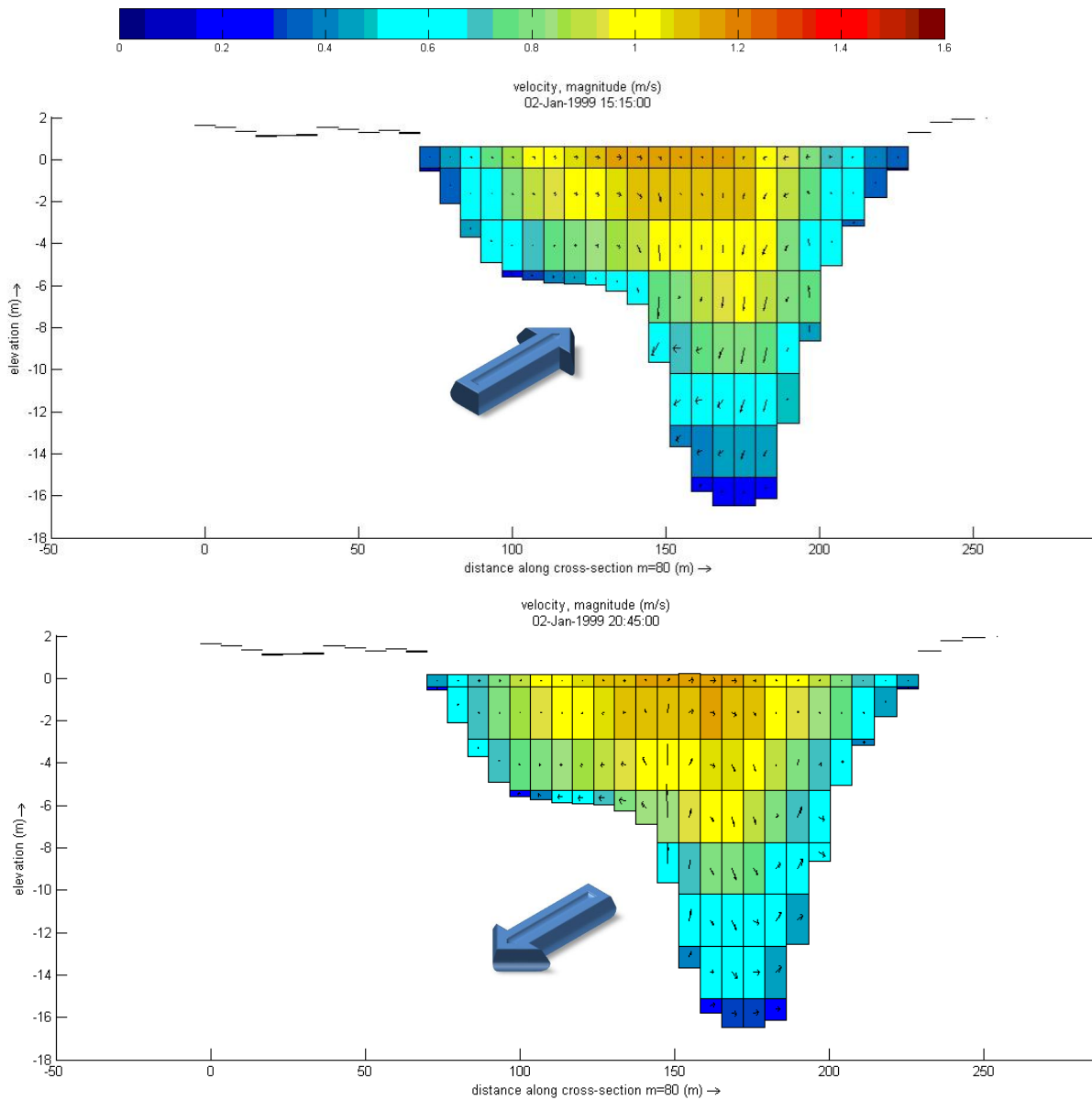


Figure 6.15 Hydrostatic Z-layer model, velocity magnitude longitudinal section, medium discharge scenario.

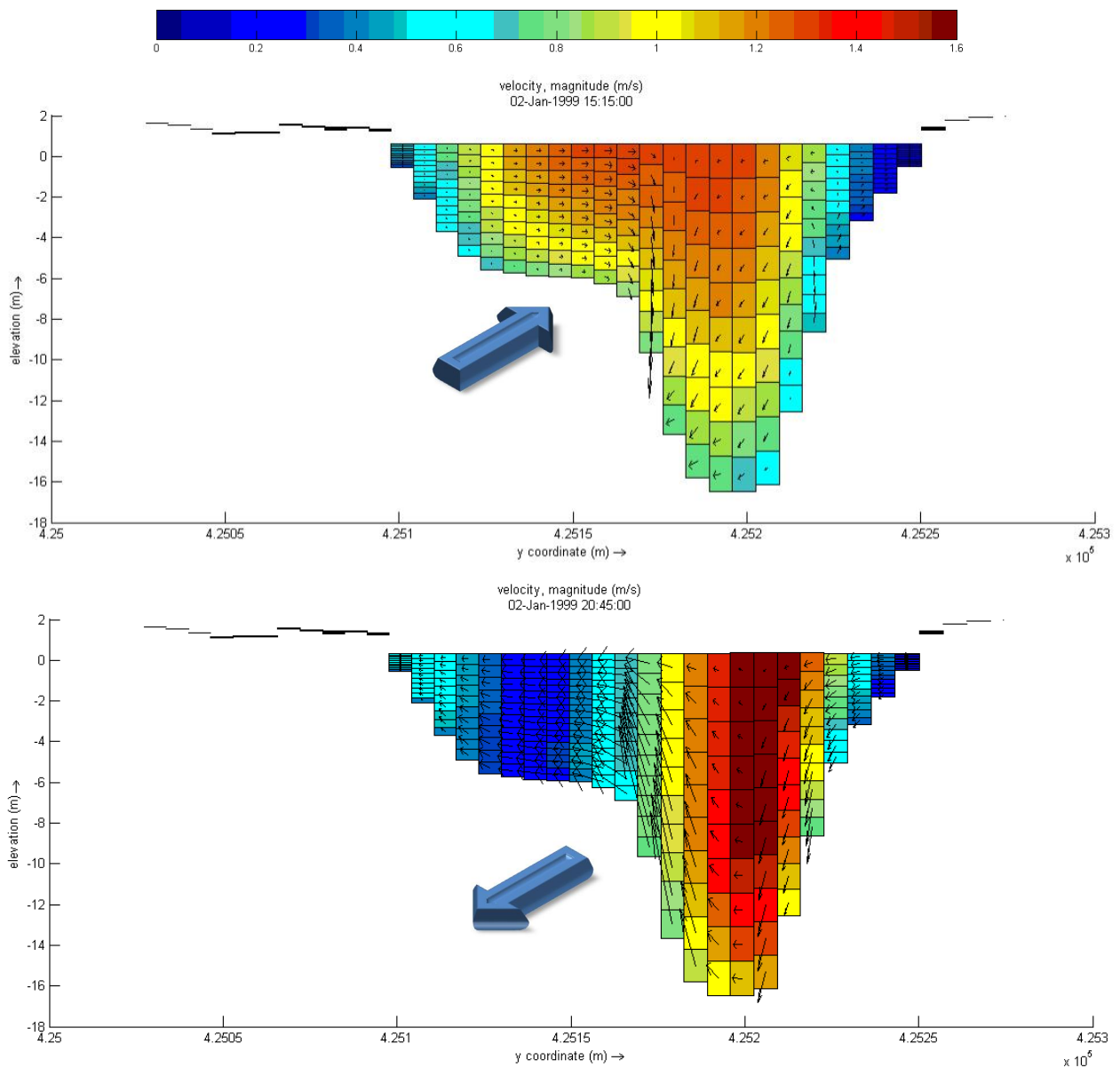


Figure 6.16 Sigma-layer model, velocity magnitude longitudinal section, medium discharge scenario.

In the Annex H, all results of the non-hydrostatic simulation are presented, i.e. for the low, medium and high river discharge scenario.

#### 6.4 Conclusions

After a comparison of the results of the different models, one comes to the conclusion that the non-hydrostatic model produced reasonably realistic results for shear stresses and flow velocities as expected.

The sigma-layer model led to high flow velocities, thereby high shear stresses. A closer analysis of the water levels showed significant deviations (overshoots, longer spin-up period). Corresponding figures of water level elevations can be found in the appendices. The inaccuracy may be a result from a relatively large time step. However, reducing the time step even further would lead to very expensive computations (the simulation time is already twice the simulation time of the non-hydrostatic Z-layer model).

The hydrostatic Z-layer model showed results comparable to those of the non-hydrostatic Z-layer model. However, it produced relatively large shear stresses at single computational cells without a clear indication of overshoots in the corresponding flow field. In those cases, the limitations of a purely hydrostatic model to resolve flow at locations with non-hydrostatic conditions might be the reason for these deviations.

Compared to the other models, the non-hydrostatic Z-layer model showed reliable results regarding both shear stresses and flow field. Of course, these results come at a cost in terms of simulation time. In this specific case study, the total simulation time was about 1.7 times higher. However, compared to the required simulation time and the accuracy of the sigma-layer model, this model still represents a fast solution.

The outcome of the simulation does not show a high bottom shear stress within the erosion pit. Also, the flow velocities are rather small. As a consequence, the original layer material must have had a relatively low resistance against erosion compared to the surrounding bed material. Once it is exposed to the flow velocities, erosion goes on as long as the critical shear stress is exceeded.

Obviously, the question remains, why the pit does not fill up with sediment that settles due to the low flow velocities. The most likely reason is that the Spui River is an undersupplied morphological system. There is no substantial amount of coarse sediments supplied to the pit from surrounding sections. This also explains why in the model runs no dredging activities were observed in the Spui River during a 10-year simulation of the entire model. However, in the prototype there might also be additional hydrodynamic phenomena that prevent sedimentation, and that are not included in the model (such as specific turbulence features, not captured by standard k- $\epsilon$  turbulence models).

When looking at the transverse section of the erosion pit, one can observe a secondary flow that reverses depending on the tidal influence. This flow shows vertical velocities of about 0.2 to 0.4 m/s, which on one hand could have an impact on the (on-going) erosion process of the pit and on the other hand could hold sediment in suspension.

For further analysis, it is recommended to carry out a morphodynamic 3D simulation in order to get more insight into the actual transport mechanisms within and near erosion pits.

## 7 Conclusions and recommendations

This report presents the results for improving tools for morphological modelling in the Rhine-Meuse Delta, as obtained in the KPP project “Rivierkunde 2012”, sub-theme “Stabiele keringen”. This Chapter presents the most relevant conclusions and recommendations for all the different tasks in this project.

The model has been set-up and extended for the full RMM area. Conclusions with respect to the model domain are:

- The morphological Delft3D model of the Rhine Meuse estuary now covers the Lek, Maas (starting from Lith), the Bergsche Maas, Amer, Boven Merwede, Nieuwe Merwede, Beneden Merwede, Dorstische Kil, Hollands Diep, Haringvliet, Spui, Oude Maas, the Noord, Nieuwe Maas, Hartelkanaal, Calandkanaal and the Nieuwe Waterweg.
- The RMM consists of 8 domains, each domain having a separate numerical grid:
  - The computational grids for the Lek, Boven Merwede, Nieuwe Merwede, Oude Maas and Dordtsche Kil were obtained from previous DVR and RMM work.
  - The computational grid of the Nieuwe Merwede was adjusted to incorporate the Biesbosch and the Amer. The grid for the Oude Maas was extended.
  - The computational grids for the Bersgsche Maas, Maas (from Lith), Haringvliet, Spui, Noord, Nieuwe Maas, Hartelkanaal, Calandkanaal and Nieuwe Waterweg were constructed for this study.

Conclusions on the set-up and verification of the hydraulic model:

- Three inflow discharge hydrographs were constructed, for inflow in the Lek, Waal and Meuse River. The Meuse discharge is assumed to be fully correlated with the Waal (Rhine) discharge. The discharge hydrograph at the Waal was leading in the schematization. Due to the tidal boundary downstream, the time period of a discharge step is a multiple of approximately 26 days.
- At the downstream boundary a waterlevel is imposed composed of an increased M2, the M4 and M6 components for Hoek van Holland. This representative tide is a form of input reduction.
- A lateral discharge withdrawal is implemented for the Haringvlietbarrier, based on 1D simulations that included the correct rules for water releases at the barrier ('lozingsprogramma LPH84').
- In a verification of the Delft3D model with the SOBEK NDB1\_1\_0 it was found that the overall behavior was in agreement. However a discharge preference for the Beneden Merwede and the Oude Maas was observed. It is recommended to reduce velocities in these branches by increasing the roughness of the summer bed.

Conclusions and recommendations on the construction and analyses of the morphological model and its results:

- Four sediment fractions are implemented, namely two sand fractions (sand and coarse sand) and two cohesive fractions (silt and clay). At the inflow boundaries suspended sediment concentrations are applied, the total inflow load is in good agreement with the values from literature.

- Fixed layers are included at locations of tunnels and pipelines.
- A Matlab tool is developed to facilitate the automatic interpretation of lithographic profiles into Delft3D bed stratigraphic input. For the Noord, Oude Maas, Dordtsche Kil and Spui, subsoil data is implemented in the Delft3d model.
- A parameterization of the 3D effects of the salt wedge on sediment transport has been implemented for the sand fractions in the Delft3d code. The outcomes of the model show that stable results can be obtained when limiting the complexity of this approach (by selecting appropriate coefficients). The correct settings of these coefficients is still to be determined. An extension is also needed for correction for cohesive sediments (accounting for development of a turbidity maximum, etc).
- A general technique for morphological simulations for tidal rivers has been developed. Including several time reduction techniques. We replaced the tidal boundary condition, with full spring-neap cycle, by a single representative tidal cycle. Although this simplifies and speeds-up the calculation, it is still necessary to verify what loss of accuracy of the morphological changes is caused by this simplification, and how relevant this loss is compared to other uncertainties.
- It is also recommended to investigate the possibility of a time dependent morphological factor, localize and resolve problematic areas in the computational grid to increase the time step. The hardware and simulation architecture were found to be quite optimal.
- During the construction of the model experts from the estuarine hydraulics and morphology have been consulted for advice. For the acceptance of the model, it is recommended to discuss the model as a whole including the results with the experts in these fields. This discussion can give input for further research.

In relation to development of an overall morphological model for the Dutch River system for the project *Deltamodel*, further extension of the RMM model and testing has been performed in 2012 and begin 2013. The testresults are presented in Sloff et al, 2013. From these test we concluded that (see Sloff et al, 2013):

- The locations of erosion and sedimentation are correctly predicted, but the magnitude is not accurate at all locations (erosion trends are larger than measured). Partially this is caused by play-in effects of bed composition, and partially by insufficient adjustment of calibration parameters and sediment supply from inflow boundaries. It is recommended to adjust these for more accuracy.
- There are unrealistic bar-pool patterns calculated in the river bed at the connection between Oude Maas and Nieuwe Waterweg, and at the Boven-Merwede. It is expected that these problems are caused by settings of the transport model, in combination with graded sediment. For practical applications it is recommended to solve these problems.
- It is recommended to make some effort to further speed-up the calculations (at this moment 1 month is needed to simulate 10 years).

Conclusions on the application of the model for the “Oversteek Moerdijk”:

- The model is simulating sedimentation in the navigation channel, but the total dredging volume to maintain this channel is much less than in reality.
- It is recommended to study somewhat more the details of these processes in the Hollandsch Diep to establish more insight in the sediment balance and sediment trajectories. It looks in the model for instance that much of the sediment coming from the East is depositing upstream of the Moerdijk-bridge, while it may deposit more downstream in prototype.

Conclusions on the model test for local scour:

- The non-hydrostatic z-layer model produced reasonably good results for shear stresses and flow velocities as expected.
- The sigma-layer model led to high flow velocities and, this way, to high shear stresses. A closer analysis of the water levels showed significant deviations (overshoots, longer spin-up period).
- The hydrostatic Z-layer model showed results comparable to those of the non-hydrostatic Z-layer model. However, it produced relatively large shear stresses (overshoots) at single computational cells.
- The outcome of the simulation does not show a high bottom shear stress within the erosion pit. Further erosion of the pit is not expected, while refill of the pit is limited, since in the area mostly under-supplied conditions occur (most of the bed is non-erodible)
- It is recommended to extend the model simulations with sediment transport and morphology, and study the sedimentary processes in more detail.



## 8 References

- Abraham, G., 1982, International Course in Hydraulic Engineering, reference notes on density currents and transport processes – WL | Delft Hydraulics
- Becker, A., 2012a, Maas-modellen 5de generatie, Modelopzet, kalibratie en verificatie. Deltires, Report 1204280-000.
- Becker, A., 2012b, Rijn-modellen 5de generatie, Modelopzet, kalibratie en verificatie. Deltires, Report 1205994-002.
- Chu, A., Wang, Z.B., De Vriend, H.J., Stive, M.J.F. 2010, A process-based approach to sediment transport in the Yangtze Estuary. 32nd International Conference on Coastal Engineering, ICCE 2010, June 30 – July 5 2010, Shanghai, China.
- Giri, S. 2011, Dredging strategy in the Waal: Morphological study with Delft3D. Memo, Deltires, Delft.
- Hijma, M.P. 2009, From river valley to estuary. The early-mid Holocene transgression of the Rhine-Meuse valley, The Netherlands. PhD thesis KNAG/Faculty of Geographical Sciences, Utrecht University, Netherlands Geographical Studies 389, 192p.
- Van der Kaaij, T., H.F.P. van den Boogaard, C. Kuijper, C.J. Sloff, J.W. van Zetten 2010, Herstel van de "trapjeslijn" in de Nieuwe Waterweg en de Nieuwe Maas (Fase 2), Vervolgstudie naar de effecten op de zoutindringing. Deltires, Report 1002366-000 ZKS.
- Lesser, G., 2009, An approach to medium-term coastal morphological modelling, PhD thesis, Delft University of Technology.
- Van Maren, D.S. , J.C. Winterwerp and R.E. Uittenbogaard 2007, New developments in the mud transport module of Delft3D. WL | Delft Hydraulics Report Z3824.55.
- Van der Mark, C.F., S. Giri, C.J. Sloff, E. Mosselman, 2010, Development of a 2D morphological model of the Nederrijn-Lek river. Deltires, Report 1201089-000 ZWS
- Meijers, E., J. Icke, 2006, Zwevende stofmodellering : nevengeulen bij Gameren en Rijn-Maasmonding. WL | Delft Hydraulics, Report Q4201.
- Mosselman, E. C. J. Sloff , B. Jagers, 2005, Voorspelinstrument duurzame vaarweg: voorbereiding, Delft: WL | Delft Hydraulics, Report Q3963.00
- De Nijs, M.A.J., J.C. Winterwerp, J.D. Pietrzak, 2010, The Effects of the Internal Flow Structure on SPM Entrapment in the Rotterdam Waterway. J. Phys. Oceanogr – (2011) 40, 2357–2380.
- Prandle, D., 2009, Estuaries, Dynamics, Mixing, Sedimentation and Morphology. Cambridge University Press.
- Roelvink, D., A. Reniers, 2012, A guide to modelling coastal morphology. Advances in coastal and ocean Engineering, volume 12, World Scientific, Singapore.
- Savenije, H.H.G. 2005,– Salinity and tides in Alluvial Estuaries – Elsevier
- Sloff, C.J., C. Erdbink, 2008, Onderzoek Morfologie Rijn, Maas en Benedenrivieren; bezinning op slib, WL | Delft Hydraulics, Report Q4400.20.
- Sloff, C. J. , S. Giri, 2009a, TO-Rivkunde. Deltires, Report 1200186.
- Sloff, C.J., S. Giri en W. van Dijk, 2009b, Onderzoek morfologie Rijn, Maas en Benedenrivieren : 2D modellering Merwedes, Deltires Report 1002004-004
- Sloff, C.J., R. van der Sligte, T. Visser 2013, Riviermorphologisch Deltamodel; Testen RMD. Deltires, Report 1207054-000-ZWS-0013.

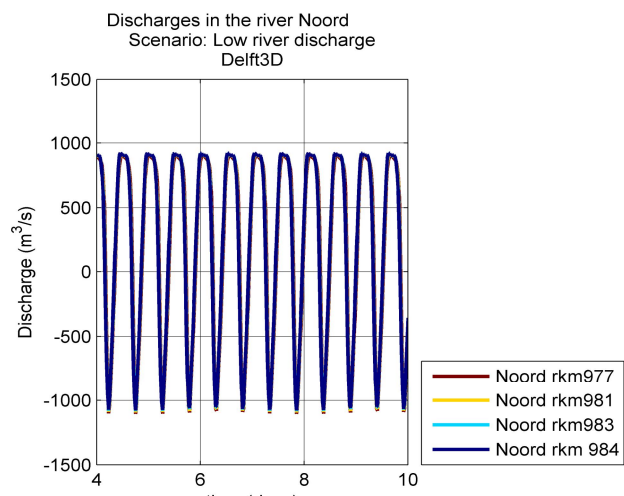
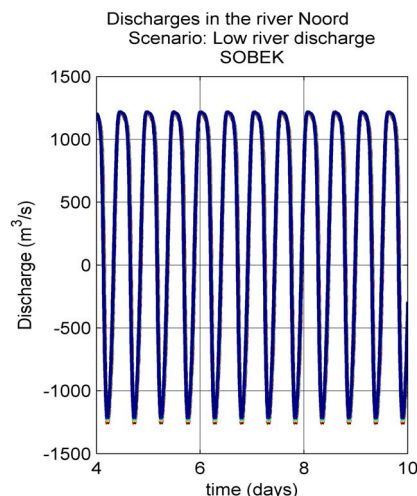
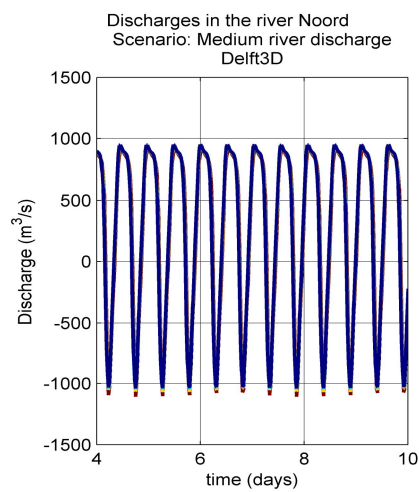
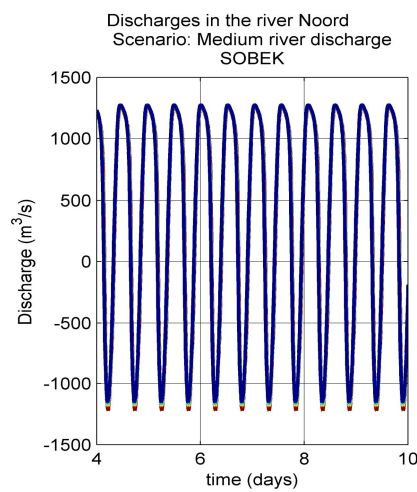
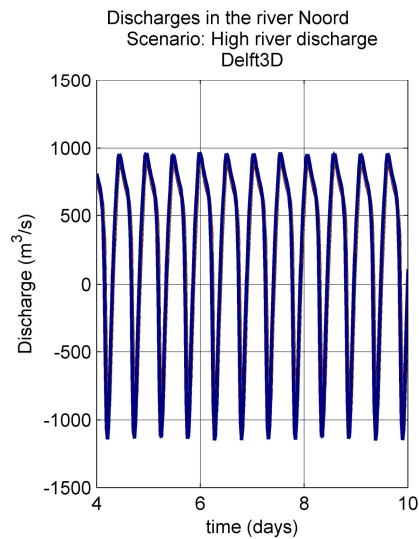
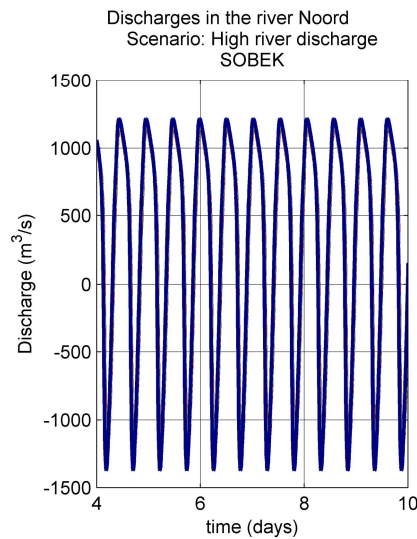
- Smits, T.C. 2011, Erosion processes and bed level maintenance strategies in the tide influenced branches of the Rhine-Meuse delta. MSc Thesis, Delft University of Technology, Faculty of Civil Engineering and Geosciences, Section Hydraulic Engineering, Delft, 2011.
- Snippen, E., 2005, Sedimentbalans Rijn-Maasmonding periode 1990-2000, Sediment in (be)weging, Memo RIZA
- Struijk, R., Plan van aanpak B&O WAQUA-RMM 2013. Rijkswaterstaat Dienst Zuid Holland.
- Van Rijn, L. C. (1984a). "Sediment Transport, Part I: Bed Load Transport" Journal of Hydraulic Engineering, ASCE, 110(10), 1431-1456.
- Van Rijn, L. C. (1984b). "Sediment Transport, Part II: Suspended Load Transport" Journal of Hydraulic Engineering, ASCE, 110(11), 1613-1641.
- Van Rijn, L. C. (1984c). "Sediment Transport, Part III: Bed Forms and Alluvial Roughness" Journal of Hydraulic Engineering, ASCE, 110(12), 1733-1754.
- Van Rijn, 1993 Principles of sediment transport in rivers estuaries and coastal seas, Aqua publishing, The Netherlands
- Winterwerp, J.C., W.G.M. van Kesteren, 2004, Introduction to the physics of cohesive sediment dynamics in the marine environment. Elsevier, Amsterdam
- Yossef, M.F.M., E. Mosselman, H.R.A. Jagers, C.J. Sloff, S. van Vuren, B. Vermeulen, 2006, Voorspelinstrument duurzame vaarweg : innovatieve aspecten. WL | Delft Hydraulics, Report Q4082.00
- Zagonjolli, M., 2012. WAQUA-model Rijn-Maasmonding: JAM 2012 en BenO. Deltares, projectnummer 1205994.003
- Zijl, F., D. Kerkhoven, A.Z. Visser, T. van der Kaaij, 2011, WAQUA-model Rijn-Maasmonding: modelopzet, calibratie en verificatie, Deltares, Report 1202199-005 ZKS

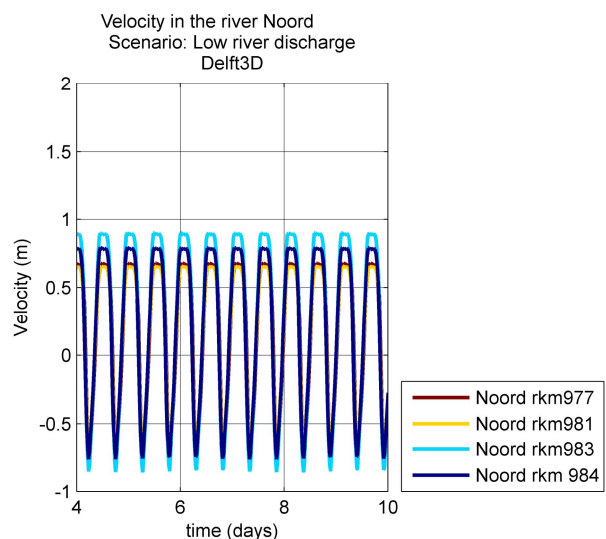
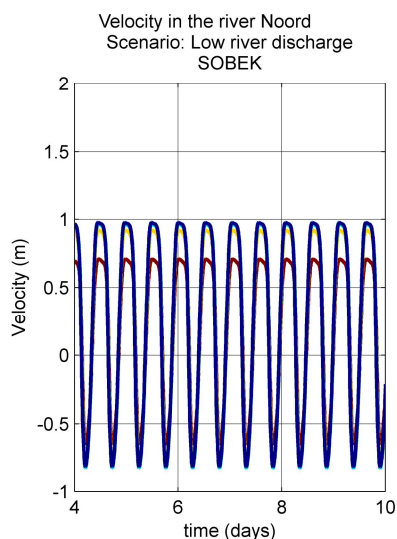
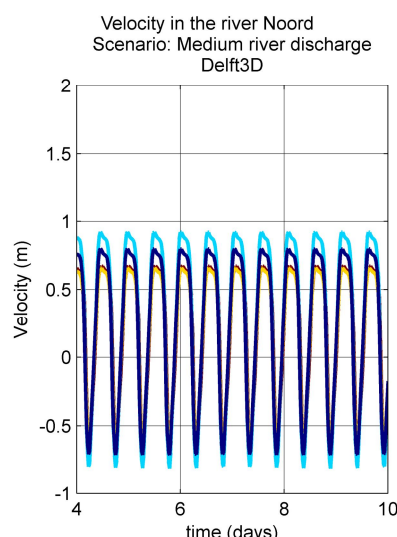
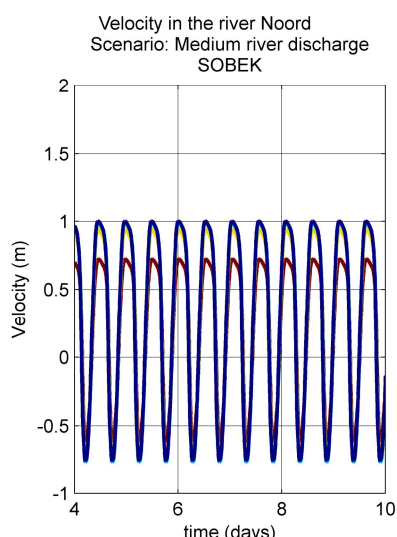
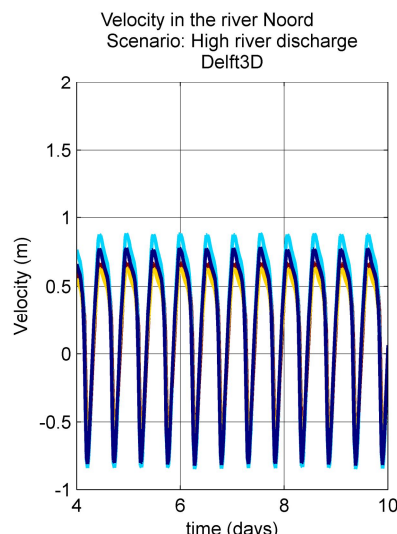
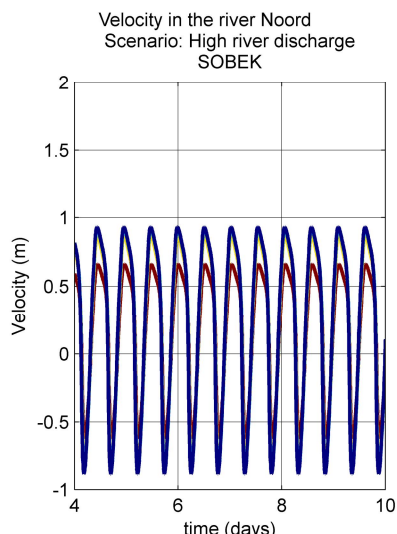
## A Hydraulic verification results

The discharge, velocity and water level for the important branches are presented in the figures below.

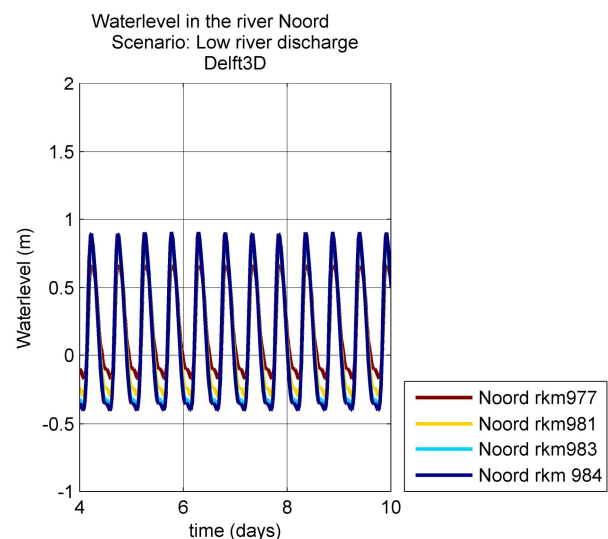
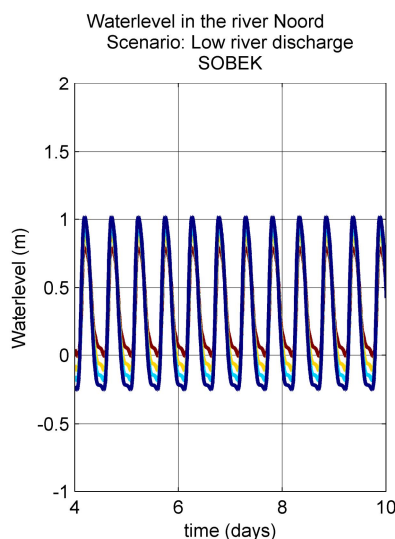
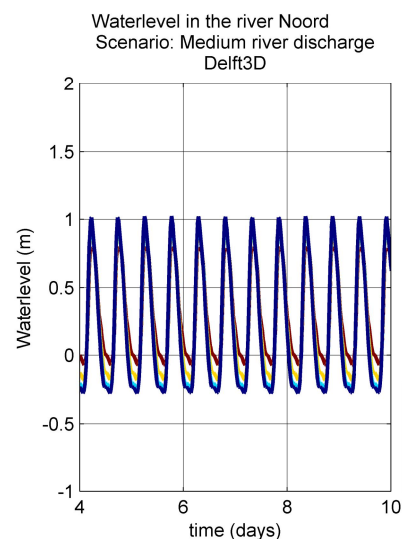
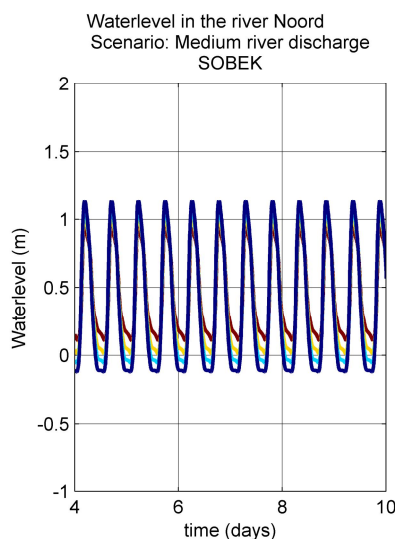
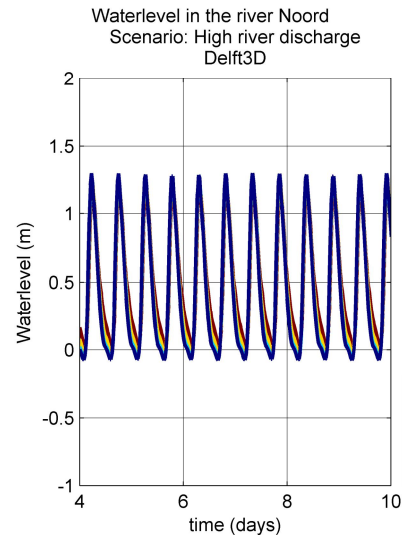
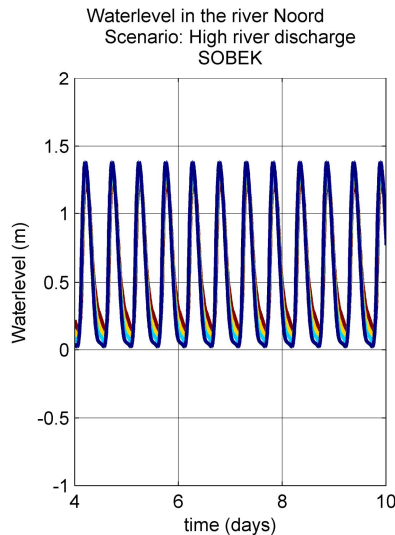
Content:

- 1 Noord
- 2 Oude Maas
- 3 Dordtsche Kil
- 4 Spui

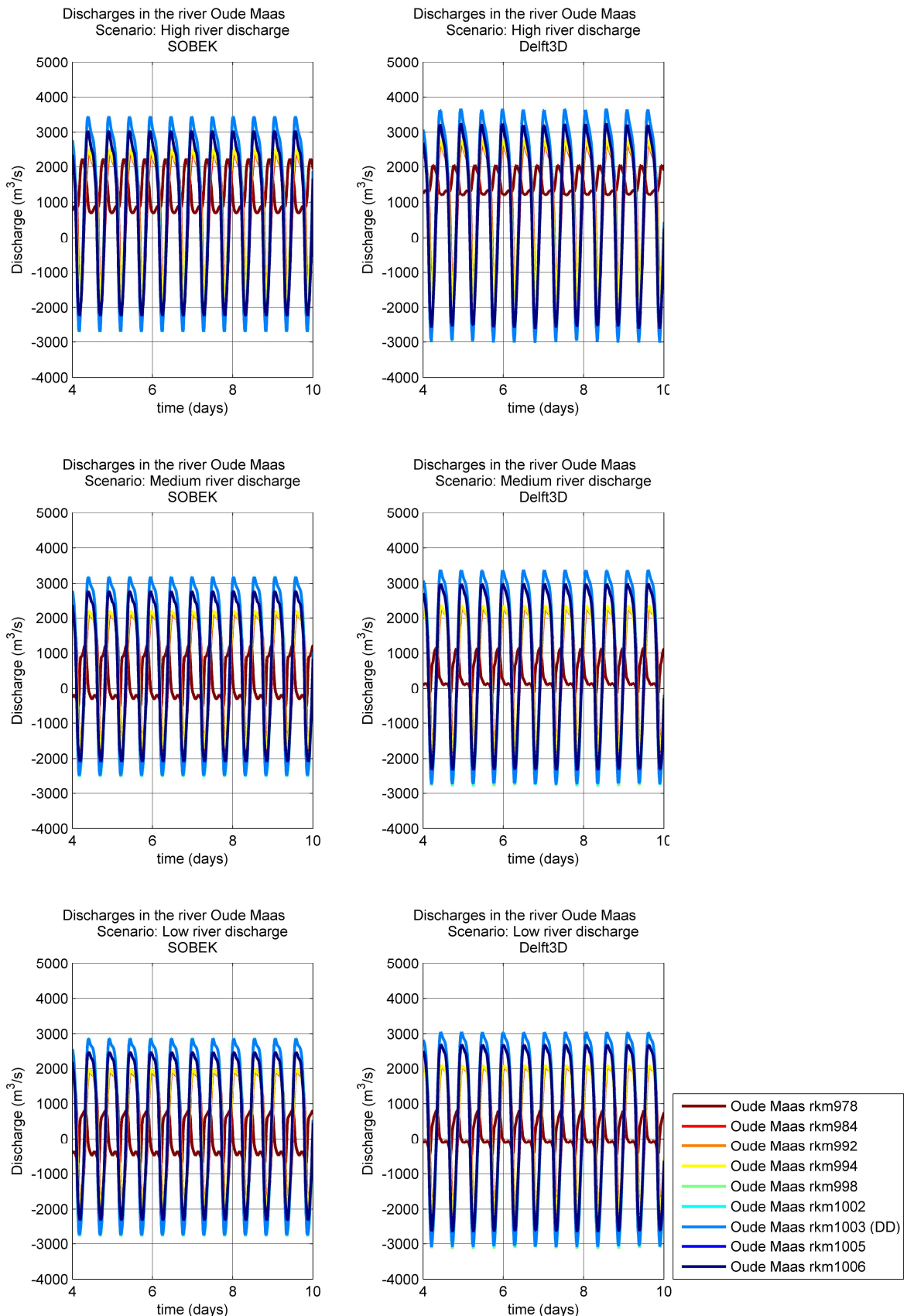


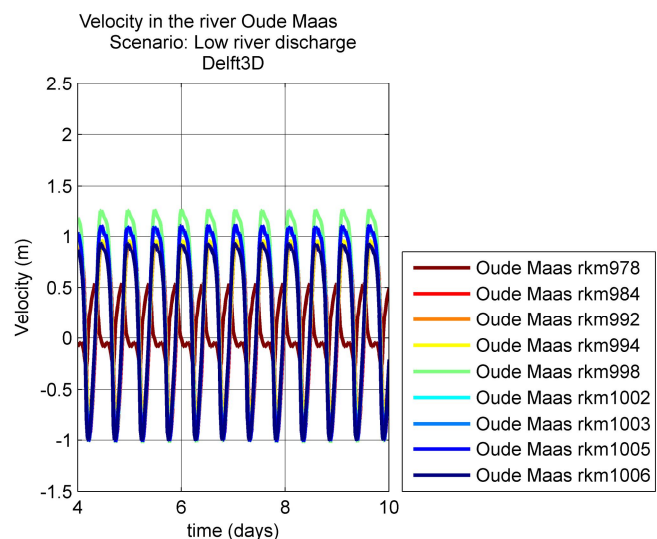
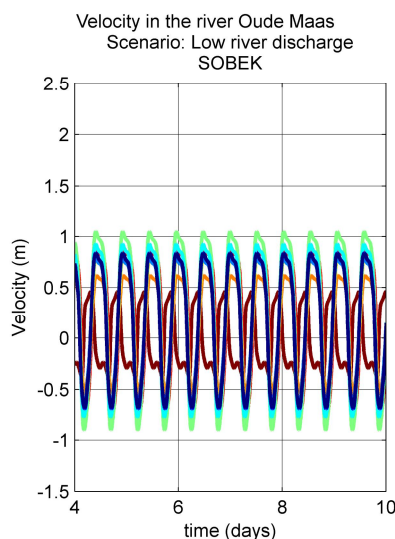
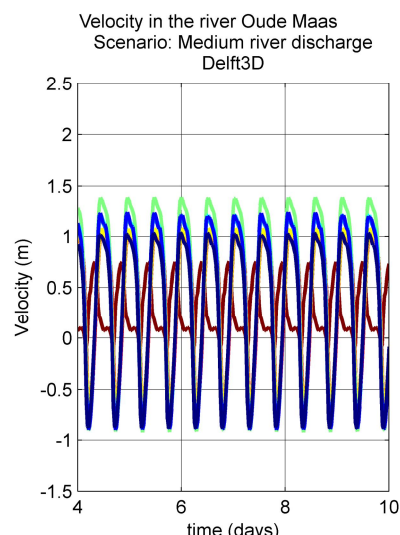
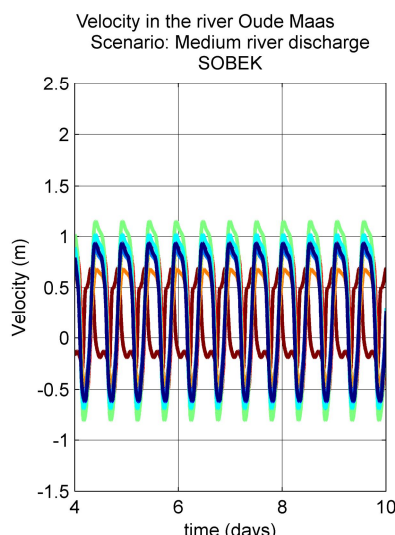
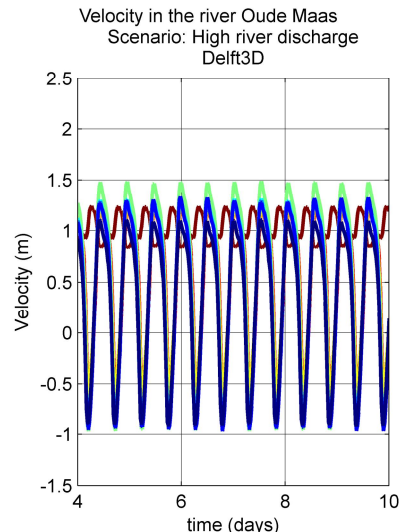
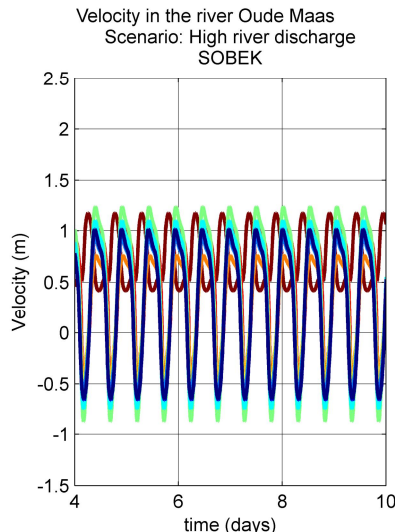


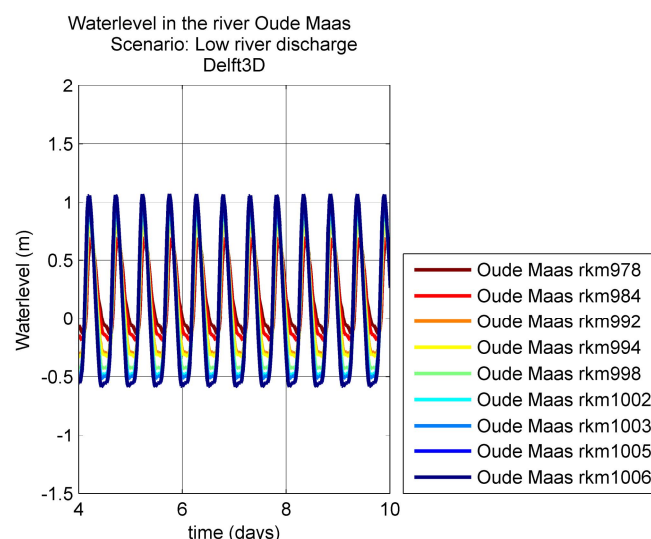
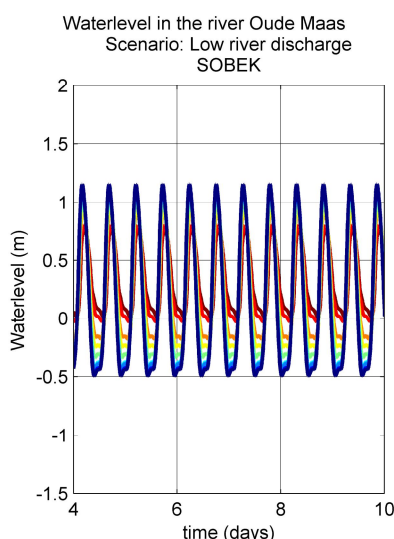
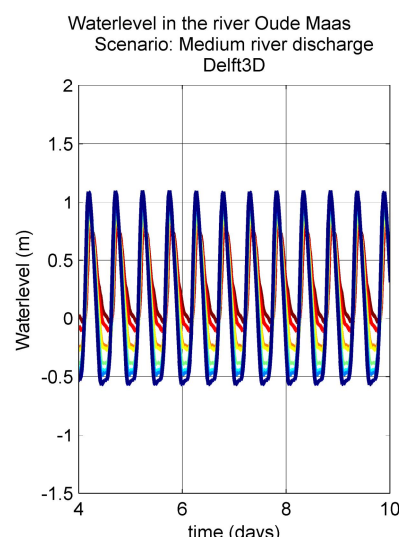
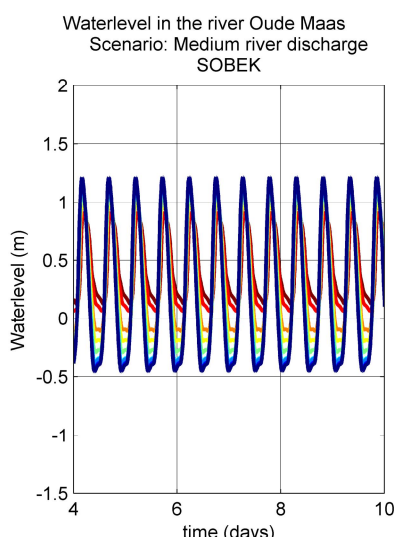
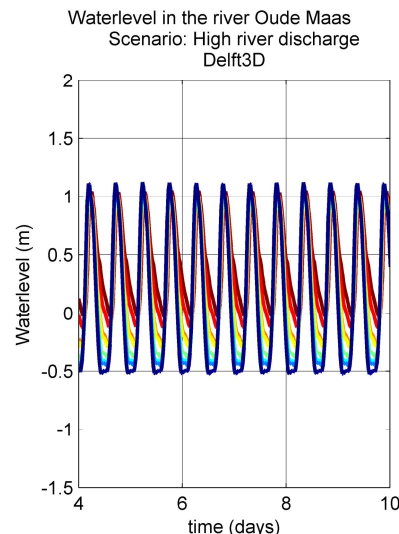
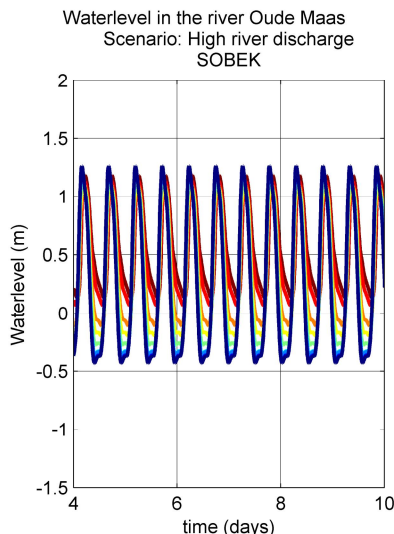
Noord rkm977
Noord rkm981
Noord rkm983
Noord rkm 984

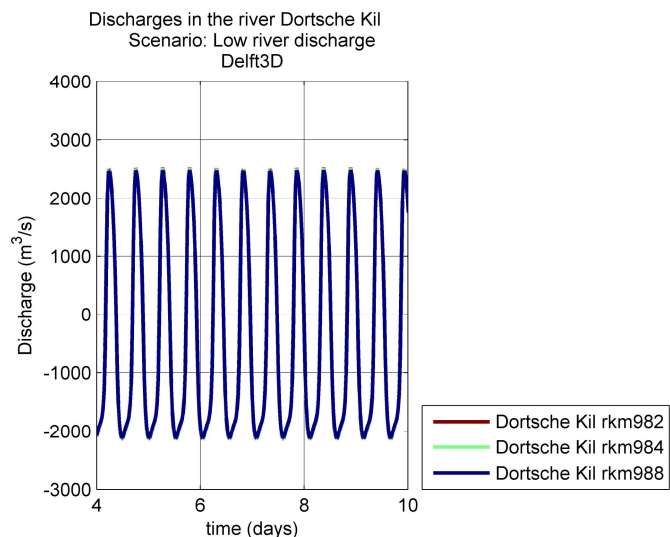
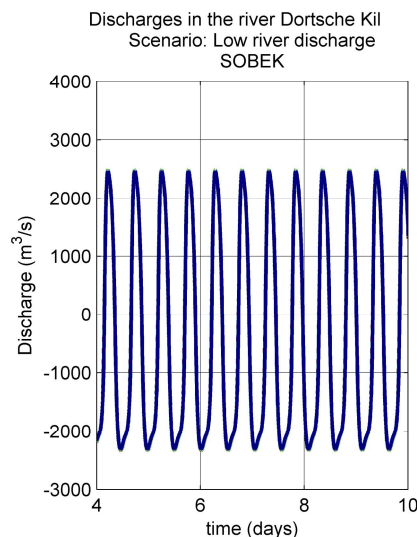
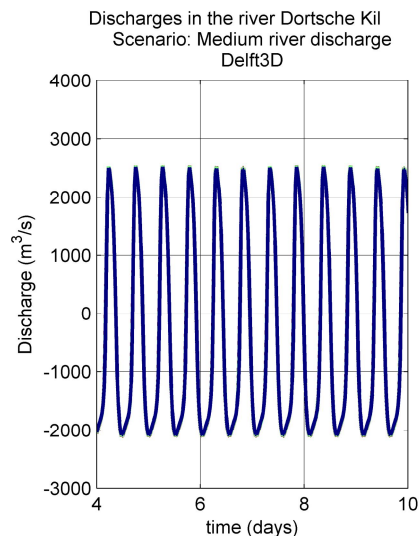
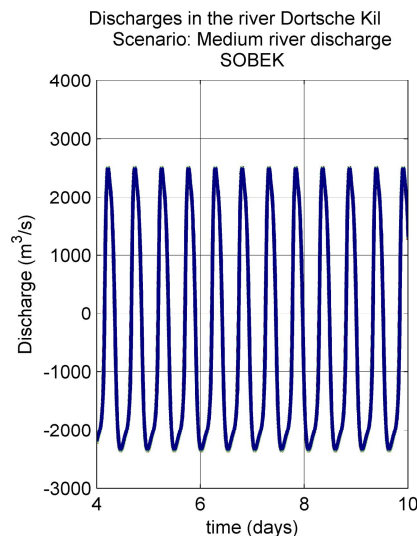
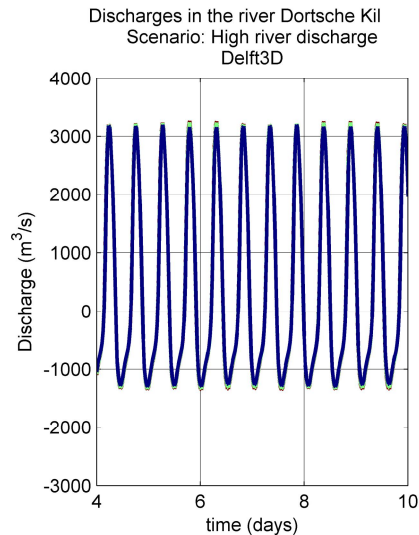
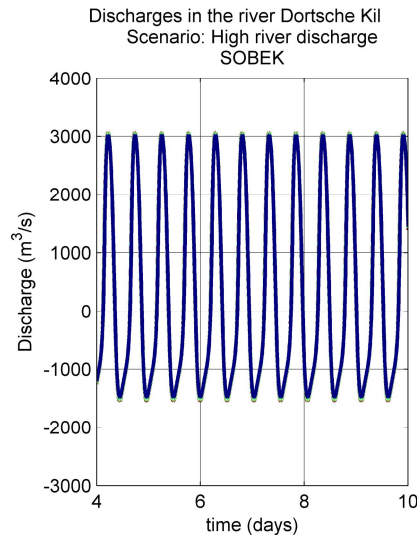


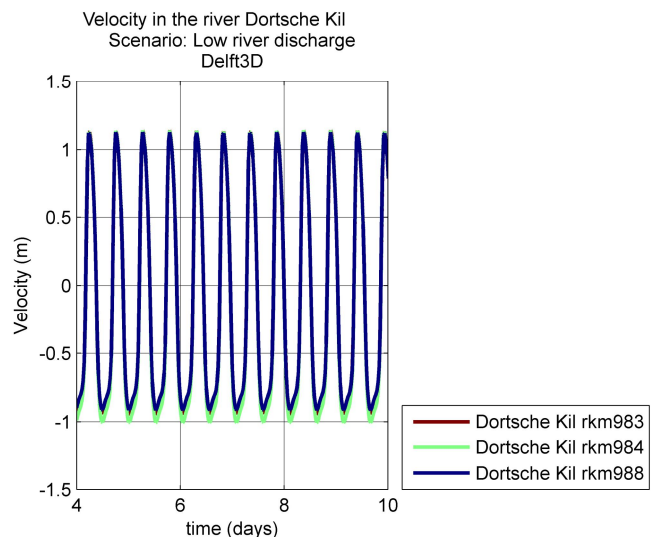
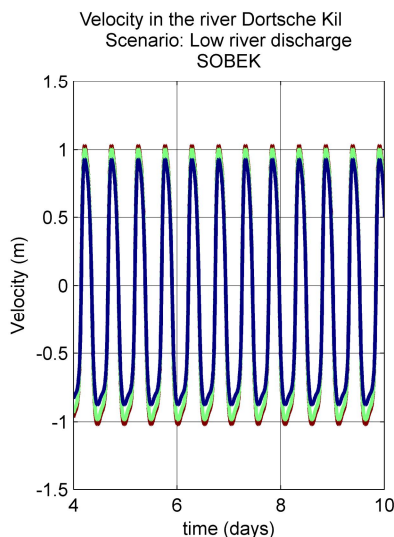
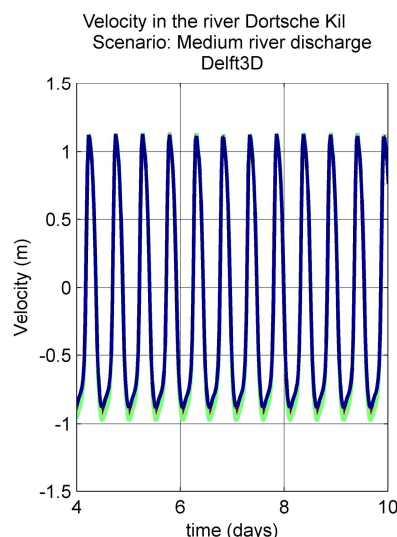
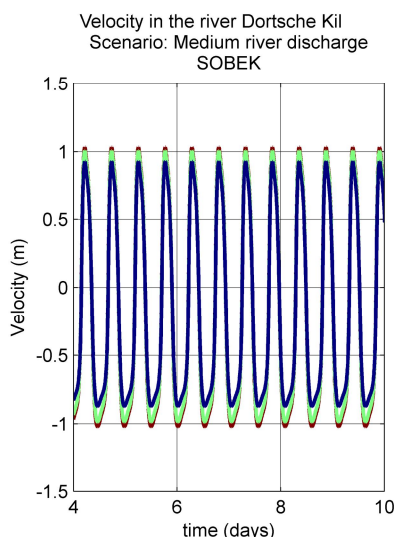
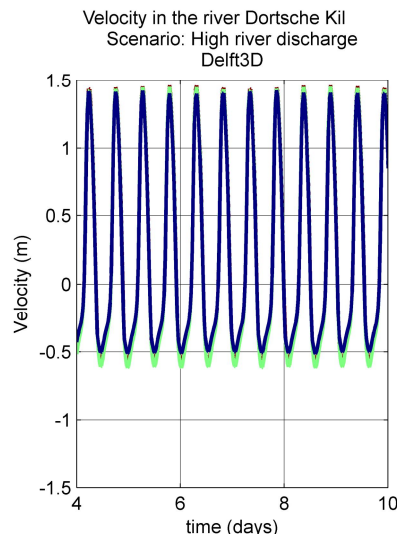
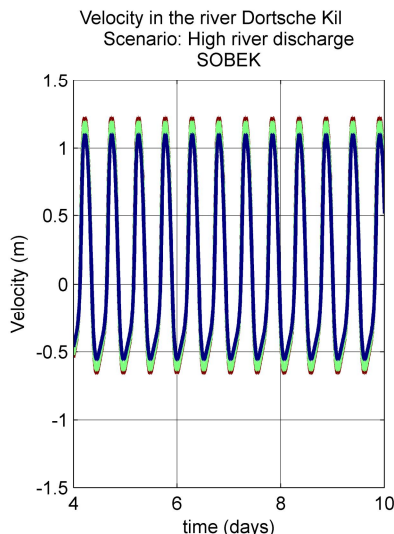
Noord rkm977
Noord rkm981
Noord rkm983
Noord rkm 984

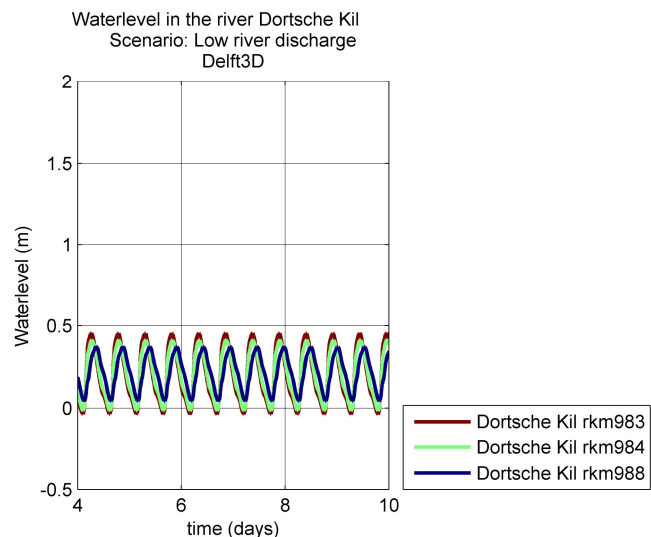
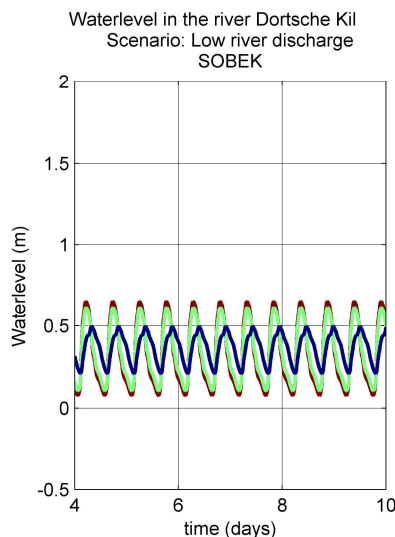
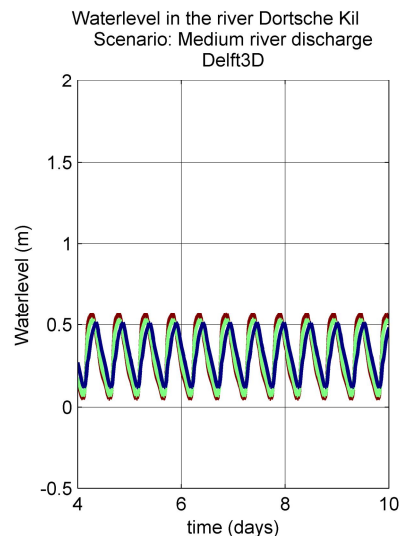
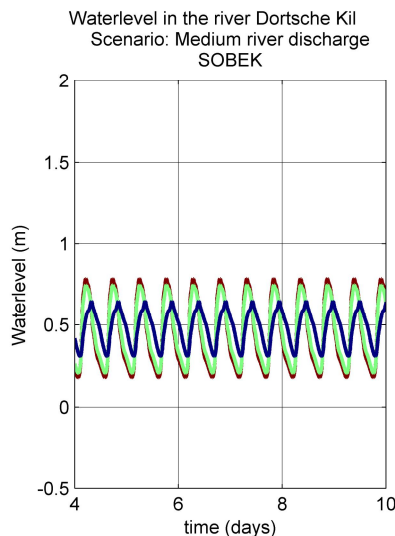
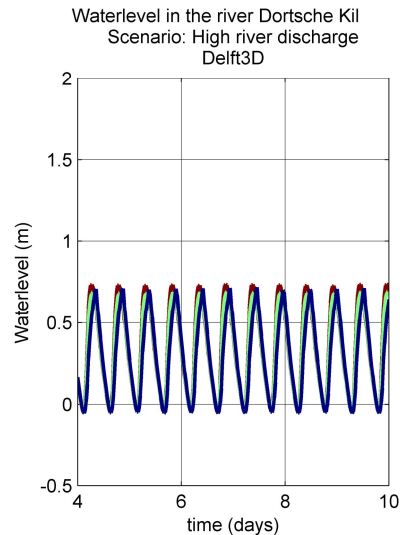
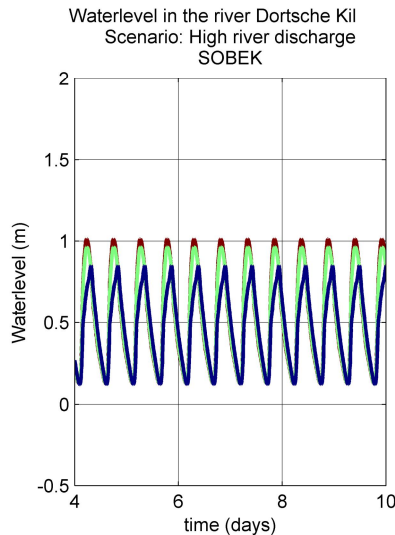


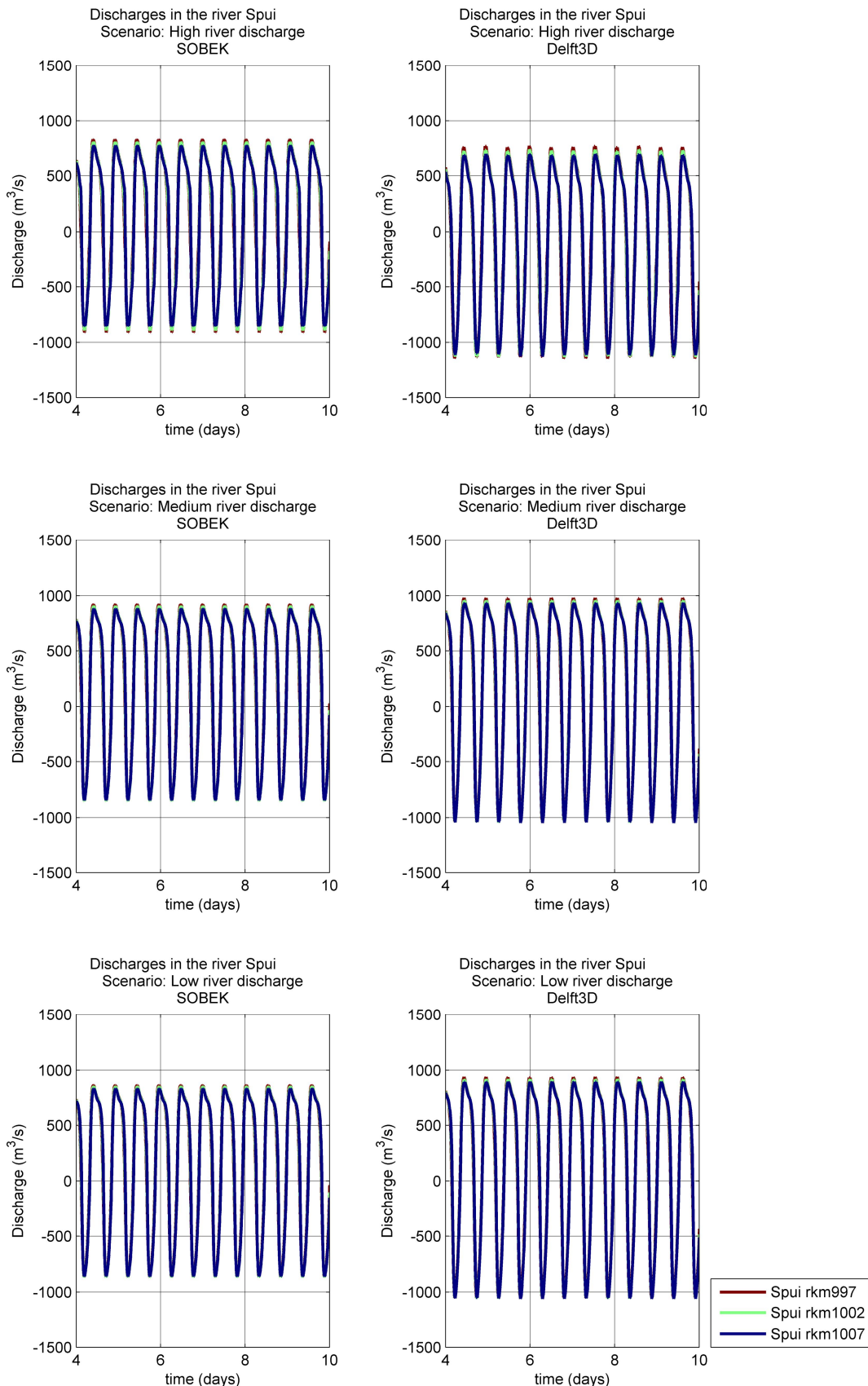


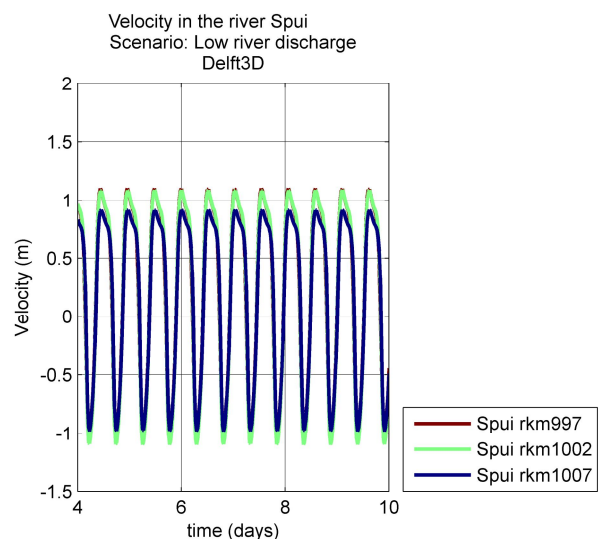
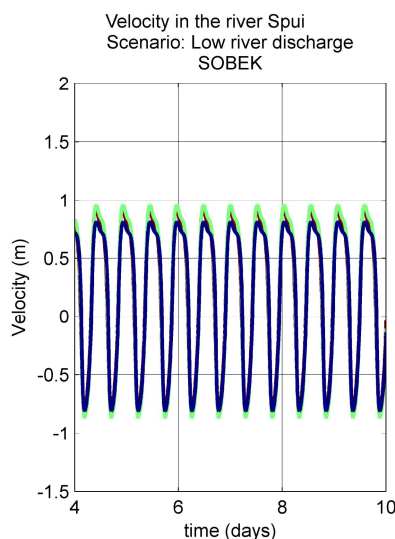
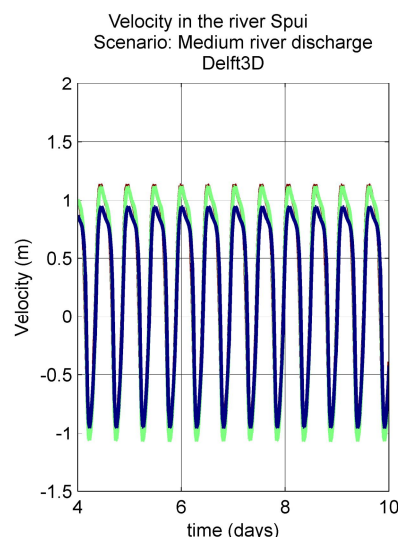
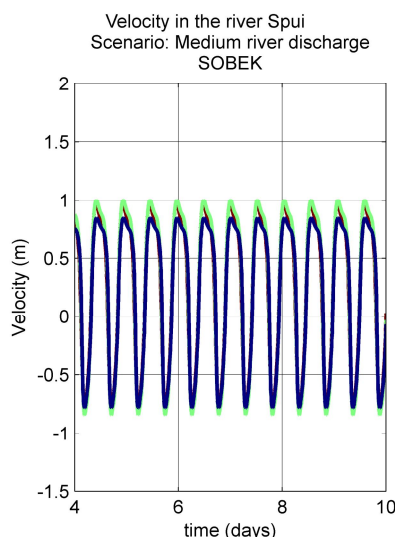
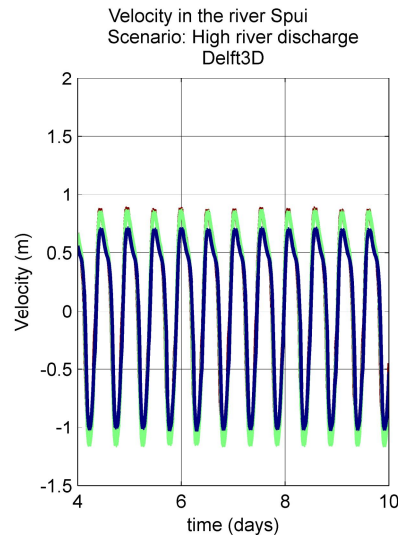
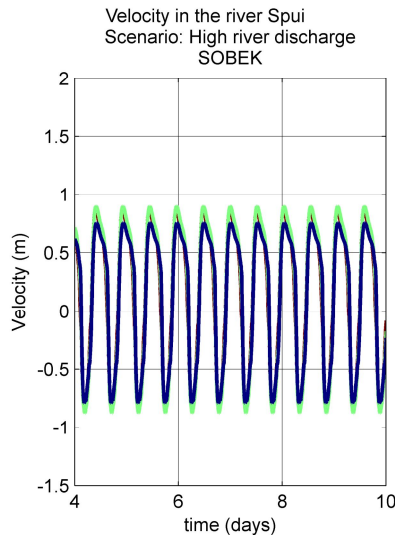


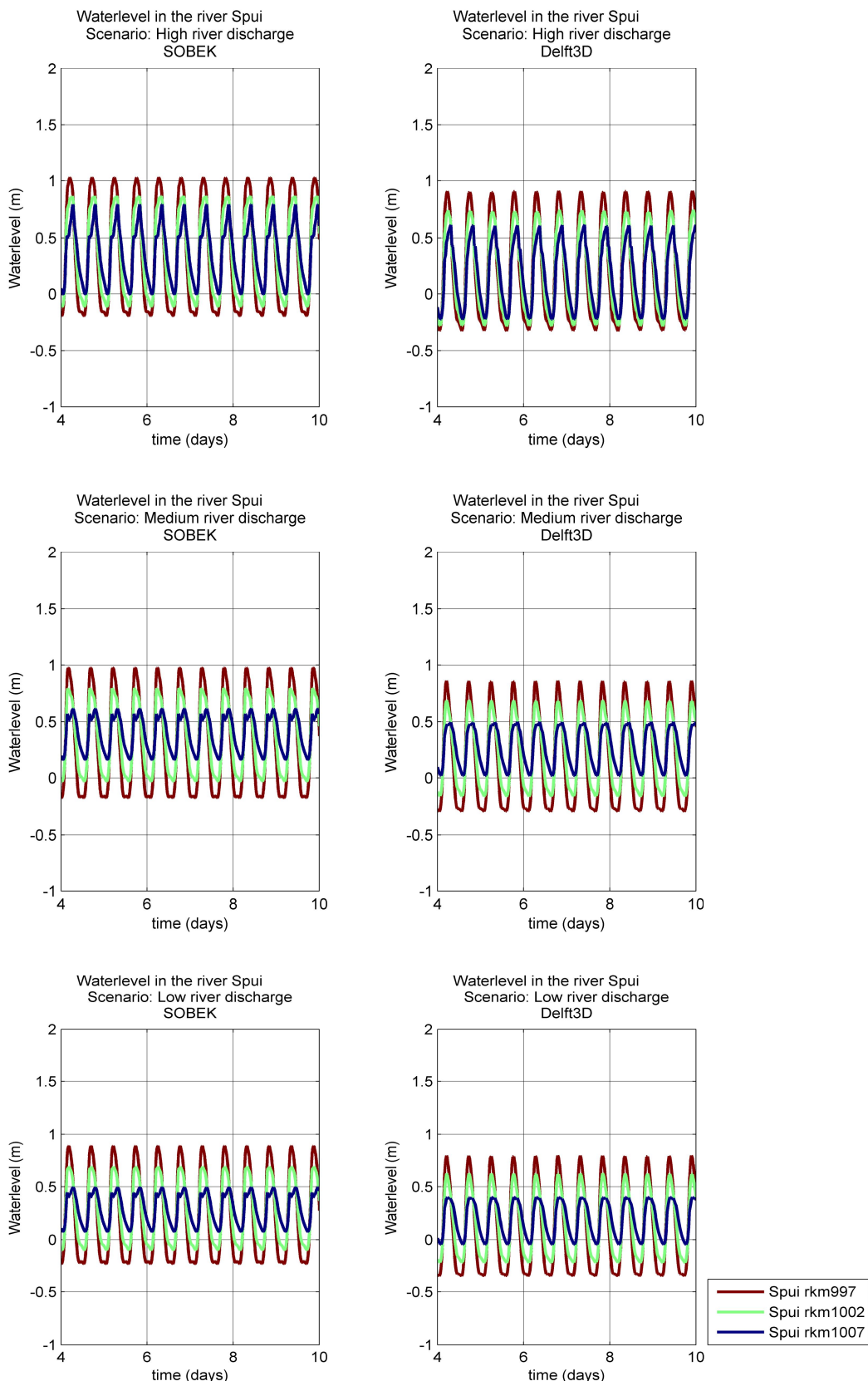














## B Roughness definition file (ruw-karak)

A selection of the summerbed roughness values as used in the hydraulic verification.

The roughness files from the hydraulic calibration of the RMM, Maas and Rijntakken were combined and transformed into a Delft3D format. The roughnessfile is given below.

```
#=====
=====
#
# CODE 301-500 : Ruwheids formulering volgens de formule van Manning
# r_code      : de ruwheids code
# a          : Manning (normaal of eb)      (0.001 - 0.0263 - 100.)
# b          : Manning (vloed)            (0.001 - 0.0263 - 100.)
# c          : geen betekenis
# d          : geen betekenis
# Simple area trachytype, 53, see p.272 Delft3D Manual 2011
# default waarde
301 53 0.0263
# diepe meerbodem
302 53 0.0263
# ondiepe meerbodem
303 53 0.0283
# diep getijdewater
304 53 0.024
# ondiep getijdewater
305 53 0.022
#
# Rijn-MaasMonding, kalibratie 5e generatie
#
# Noordzee
# noordzee
307 53 0.026
# noordzee kust
308 53 0.028
# Nieuwe Maas
# KrimpadLek-Rotterdam
320 53 0.0240
# Rotterdam-Parksluis
321 53 0.0225
# Parksluis-Eemhaven
322 53 0.0225
# Eemhaven-Vlaardingen
323 53 0.0225
# Vlaardingen-Geulhavn
324 53 0.016
#
# Nieuwe Waterweg
# Geulhaven-Maassluis
325 53 0.0160
```

```
# HoekvHoll-Maasmond
326 53 0.0180
# Moerdijk - Rak noord
327 53 0.0220
# Hollandsch Diep
331 53 0.0200
# Haringvliet
# Rak rnd-Hellevoetsl
332 53 0.0200
# Hellevoetsl - Hvsl
333 53 0.0200
# Oude Maas
# Dordrecht-Goidschalx
335 53 0.0200
# Goidschalx-Spijkenis
336 53 0.0200
# Spijkenisse-Geulhavn
337 53 0.0210
# Spui
# splOMSpui - Zuidland
339 53 0.0200
# Zuidland-splSpuiHV
340 53 0.0200
# Dordtsche Kil
# Dordtsche Kil
341 53 0.0260
# Noord
# Dordt-Krimp ad Lek
342 53 0.0270
# Hollandsche IJssel (gedeelte)
# KrimpadIJssl-splHYNM
343 53 0.0160
# Hartelkanaal
# Hartelbrug-Harmsnbrg
344 53 0.0240
# Harmsnbrg-HrtlKuwait
345 53 0.0240
# HrtlKuwait-Hartlhavn
346 53 0.0240
# Beerkanaal
# Mississiphvn-Beerkan
347 53 0.0240
# eb en vloed (voorbeeld)
#499 53 0.0273
#
=====
```

=====

```
# CODE 501-600 : Chezy waarde
# r_code      : de ruwheids code
# a          : Chezy (normale of eb)           (0.01 - 45. - 100.)
```

```

# b      : Chezy (vloed)          (0.01 - 45. - 100.)
# c      : geen betekenis
# d      : geen betekenis
# Simple area trachytype, 52, see p.272 Delft3D Manual 2011
# default waarde
501 52 45.0
# eb en vloed (voorbeeld)
#599 52 45.0    40.0
#
#=====

=====
#
# CODE 601-900 : Ruwheids methode voor het zomerbed van een rivier
# r_code   : de ruwheids code
# a       : alfa (normaal of eb)      (0.001 - 0.1 - 1.)
# b       : beta (normaal of eb)       (0.1 - 2.5 - 100.)
# c       : alfa (vloed) (alleen voor testen) (0.001 - 0.1 - 1.)
# d       : beta (vloed) (alleen voor testen) (0.1 - 2.5 - 100.)
# Alluvial area trachytype, 101, see pp.272, 625 Delft3D Manual 2011
# zomerbed default
601 101 0.1 2.5
# Rijn-MaasMonding, kalibratie 5e generatie
#
# Beneden Merwede
# Hardinxveld-Dordrecht
801 101 0.028 2.5
# Nieuwe Merwede
# Hardinxveld-Deeneplaat
802 101 0.025 2.5
# Deeneplaat-Moerdijk
803 101 0.025 2.5
# Amer
# Keizersv-splNiMwAmer
804 101 0.023 2.5
#
#=====

=====
#
# Einde rough.karak
#
#=====

=====

```



## C Haringvliet barrier

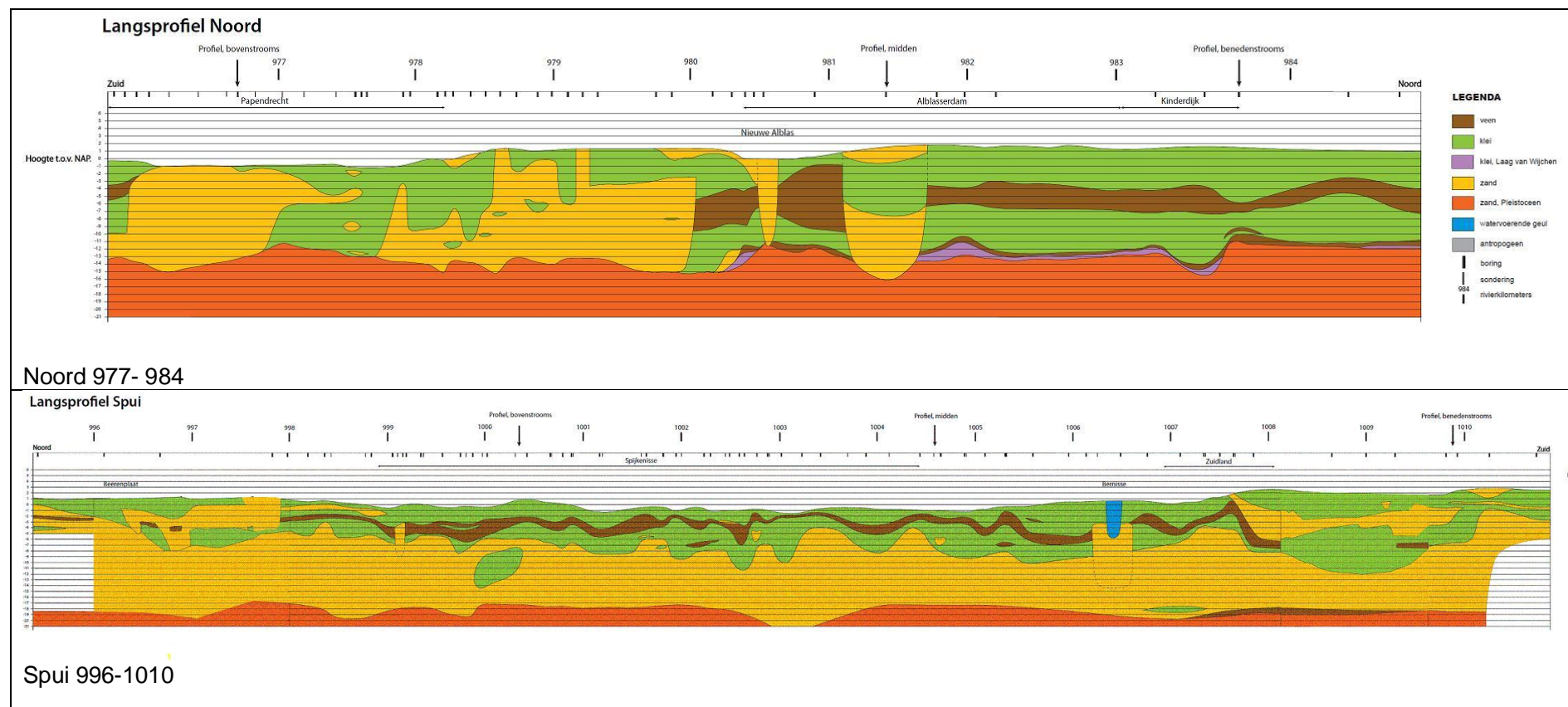
The conveyance of fresh water into the North Sea from the Haringvliet is modeled by means of thirteen sinks. The tidal signal is a cosine function whose phase shift approximately leads to the characteristics of a sine function (around -7 cm at t=0 s). In order to impose a discharge time series at the Haringvliet barrier, first the phase lag between the water levels at Maasmond and at Haringvliet were compared. They were obtained by subtracting the time step of the water level peak at Haringvliet from the foregoing flood peak at Maasmond.<sup>1</sup> The phase lag of water levels between Maasmond and the Haringvliet barrier was found to be approximately 5 hours.

In addition to the water level phase lag, it is also important to consider the phase lag between water level and discharge at the Haringvliet barrier because the imposed boundary condition is ought to be a discharge boundary representing the operation of the outlets. In order to carry out the analysis, representative discharge output data from SOBEK was selected and compared to the corresponding local water level. It was found, that the discharge peak occurs around 7 time steps after the water level shows its maximum. In correspondence with the water levels, also the discharge peaks did not deviate significantly from each other.

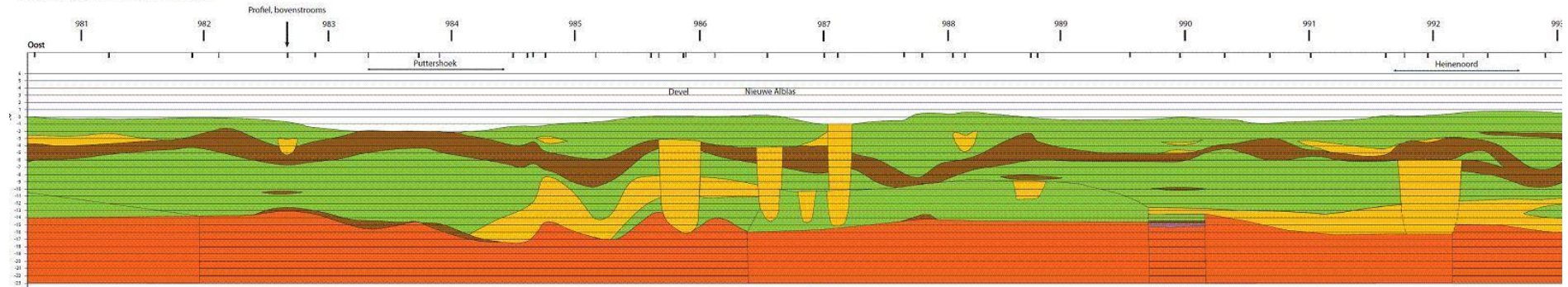
When adding up the phase lag between water levels and the additional phase lag of the discharge at Haringvliet, this results in total phase lag of approximately half a tidal cycle. This leads to the conclusion that the water level signal at the Maasmond is out-of-phase with the discharge at the Haringvliet barrier. To reduce the amount of data, the discharge time series at Haringvliet were discretized with non-equidistant time stepping.



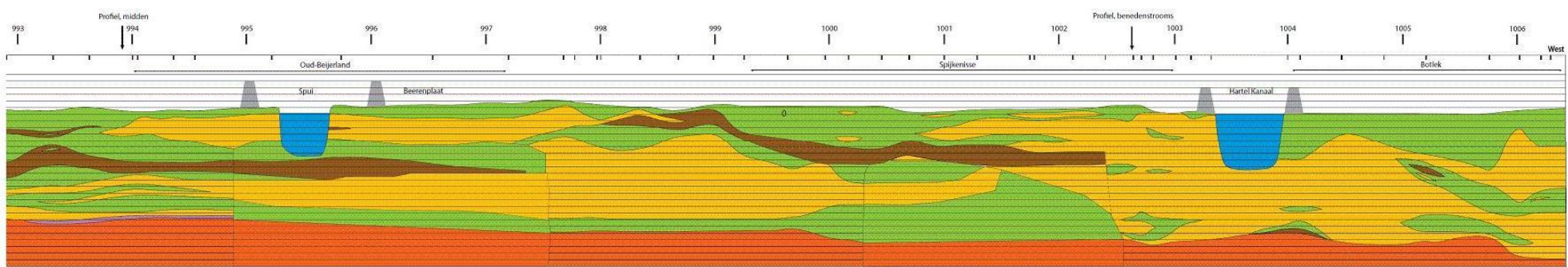
## D Subsoil Noord, Oude Maas, Spui



**Langsprofiel Oude Maas**



Oude Maas 981-993



Oude Maas 993 - 1006

## E Toplayer RMM south

The toplayer of the southern part of the Rijn Meuse estuary, figures obtained from Sloff 2008 and Snippen 2005.

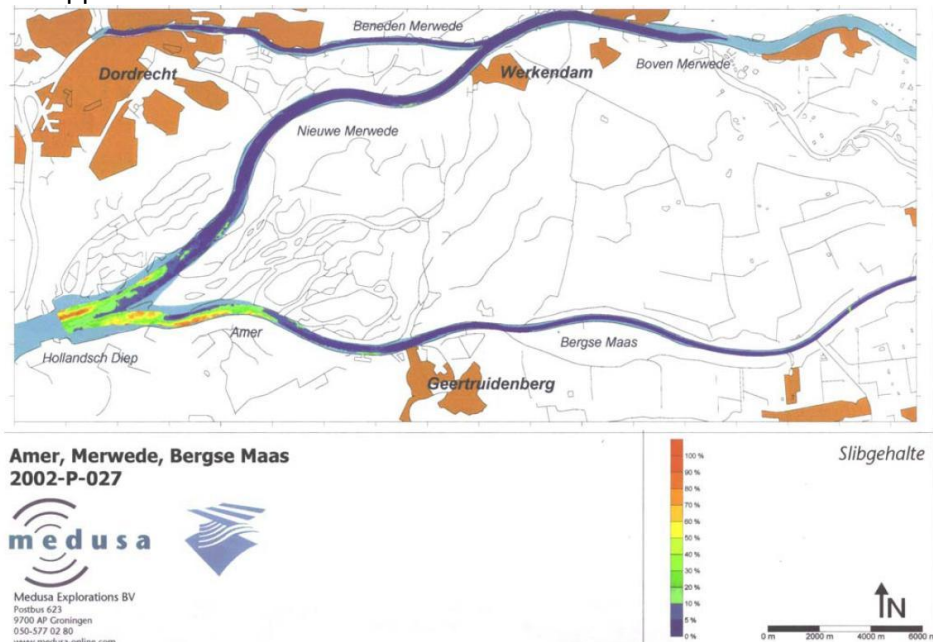


Figure 8.1 Silt content in the Hollandsch Diep, Amer, and Merwedes.

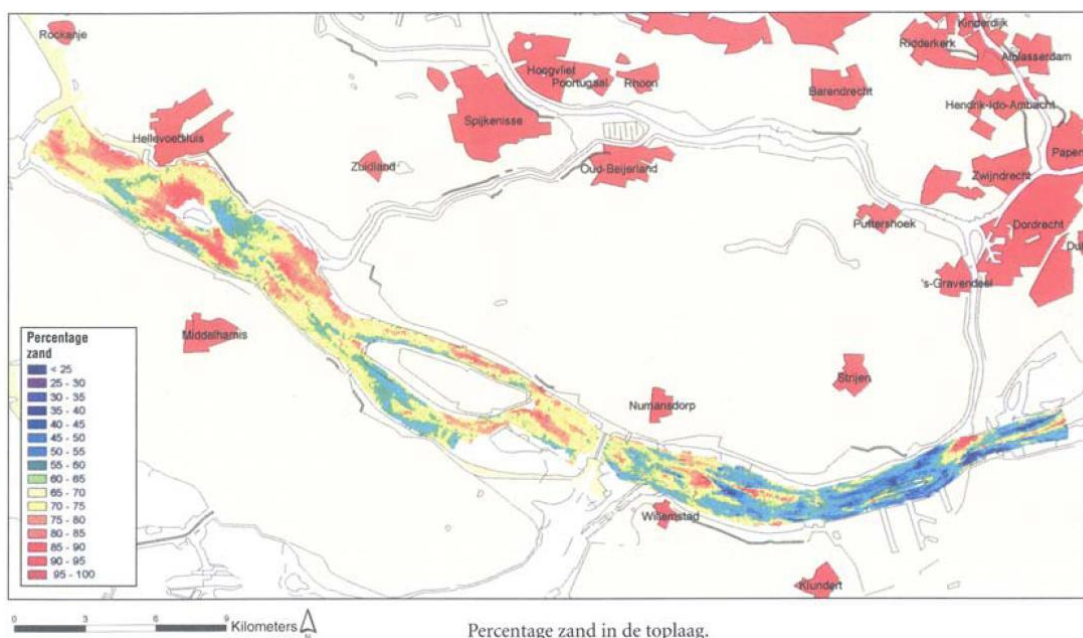


Figure 8.2 Sand content in the Hollandsch Diep and Haringvliet.



## F Van Rijn (1984); adjusted

The formula of Van Rijn (1984) takes the form:

$$S = S_s + S_b \quad (\text{F.1})$$

where:

$$S_b = \begin{cases} 0.053\sqrt{\Delta g D_{50}^3} D_*^{-0.3} T^{2.1} & \text{for } T < 3.0 \\ 0.1 \sqrt{\Delta g D_{50}^3} D_*^{-0.3} T^{1.5} & \text{for } T \geq 3.0 \end{cases} \quad (\text{F.2})$$

First the bed-load transport expression will be explained. In Eq. F.2  $T$  is a dimensionless bed shear parameter, written as:

$$T = \frac{\mu_c \tau_{bc} - \tau_{bcr}}{\tau_{bcr}} \quad (\text{F.3})$$

It is normalised with the critical bed shear stress according to Shields ( $\tau_{bcr}$ ), the term  $\mu_c \tau_{bc}$  is the effective shear stress. The formulas of the shear stresses are:

$$\tau_{bc} = \frac{1}{8} \rho_w f_{cb} u^2 \quad (\text{F.4})$$

$$f_{cb} = \frac{0.24}{[\log_{10}(12h/\xi_c)]^2} \quad (\text{F.5})$$

$$\mu_c = \left( \frac{18 \log_{10}(12h/\xi_c)}{C'} \right)^2 \quad (\text{F.6})$$

where  $C_{g,90}$  is the grain related Chézy coefficient:

$$C' = 18 \log_{10} \left( \frac{12h}{3D_{90}} \right) \quad (\text{F.7})$$

The critical shear stress is written according to Shields:

$$\tau_{bcr} = \rho_w \Delta g D_{50} \theta_{cr} \quad (\text{F.8})$$

in which  $\theta_{cr}$  is the critical Shields parameter for initiation of motion, which is a function of the dimensionless particle parameter  $D_*$ :

$$D_* = D_{50} \left( \frac{\Delta g}{V^2} \right)^{\frac{1}{3}} \quad (\text{F.9})$$

The suspended transport formulation reads:

$$S_s = f_{cs} u h C_a \quad (\text{F.10})$$

In which  $C_a$  is the reference concentration,  $u$  depth averaged velocity,  $h$  the water depth and  $f_{cs}$  is a shape factor of which only an approximate solution exists:

$$f_{cs} = \begin{cases} f_0(z_c) & \text{if } z_c \neq 1.2 \\ f_1(z_c) & \text{if } z_c = 1.2 \end{cases} \quad (\text{F.11})$$

$$f_0(z_c) = \frac{(\xi_c/h)^{z_c} - (\xi_c/h)^{1.2}}{(1 - \xi_c/h)^{z_c} (1.2 - z_c)} \quad (\text{F.12})$$

$$f_1(z_c) = \left( \frac{\xi_c/h}{1 - \xi_c/h} \right)^{1.2} \log_e (\xi_c/h) \quad (\text{F.13})$$

where  $\xi_c$  is the reference level or roughness height (can be interpreted as the bed-load layer thickness) and  $z_c$  the suspension number:

$$z_c = \min \left( 20, \frac{w_s}{\beta \kappa u_*} + \phi \right) \quad (\text{F.14})$$

$$u_* = u \sqrt{\frac{f_{cb}}{8}} \quad (\text{F.15})$$

$$\beta = \min \left( 1.5, 1 + 2 \left( \frac{w_s}{u_*} \right)^2 \right) \quad (\text{F.16})$$

$$\phi = 2.5 \left( \frac{w_s}{u_*} \right)^{0.8} \left( \frac{C_a}{0.65} \right)^{0.4} \quad (\text{F.17})$$

The reference concentration is written as:

$$C_a = 0.015 \alpha_1 \frac{d_{50}}{\xi_c} \frac{T^{1.5}}{D_*^{0.3}} \quad (\text{F.18})$$

The following formula specific parameters have to be specified as input to the model.

$w_s$	the settling velocity of the sediment [m/s]
$\alpha_1$	coefficient (should be $O(1)$ )
$\xi_c$	reference level (bed load layer thickness) or roughness height [m]
$d_{90}$	$D_{90}$ -particle diameter [m]

In the adjusted Van Rijn the following changes are introduced:

1. Reduce Eq. F.2 to

$$S_b = \alpha_{BED} \cdot 0.1 \sqrt{\Delta g D_{50}^3} D_*^{-0.3} T^{1.5} \quad (\text{F.19})$$

with  $\alpha_{BED}$  calibration parameter for bed load transport component, and for consistency we use  $\alpha_{SUS}$  instead of  $\alpha_1$  as a calibration parameter for suspended load transport component. Both calibration parameters are user specified inputs.

2. Use a variable fall velocity ( $w_s$ ) that is internally calculated based on the sediment size rather than using a user specified input value.
3. Introduce the possibility to specify a user defined critical Shields parameter  $\theta_{cr}$ . This option is introduced inline with the experience from modelling the Bovenrijn, where a rather low critical Shields parameter is needed to reproduce its morphological behaviour correctly.



## G Riemann boundaries and sea level rise

In Delft3D the open boundary conditions can be specified by either a water level, a velocity, a discharge, a Neumann number or a adjusted linearized Riemann invariant. In the Zeedelta model the open boundary condition for the sea boundary is given by the latter (Delft3D-Flow user manual September 2011, paragraph 9.4.1.2, page 213):

$$F_R(t) = U \pm \zeta \sqrt{\frac{g}{d}} \quad (7.1)$$

Where the sign is dependent on the direction of propagation and with,

$U$  = velocity in normal direction [m/s]

$\zeta$  = the variation in water level [m]

$g$  = the gravitational acceleration [m/s<sup>2</sup>]

$d$  = depth [m]

Imposing new boundary conditions as a result of sea level rise ( $h_{slr}$ ), is straightforward if the boundary condition is given in water levels. For the adjusted Riemann invariant, derivation of new boundary conditions is a little bit more complicated, but can be done as follows:

$$\begin{aligned} F_{R2}(t) &= U_2 \pm (\zeta + h_{slr}) \sqrt{\frac{g}{d}} \\ F_{R1}(t) &= U_1 \pm (\zeta) \sqrt{\frac{g}{d}} \end{aligned} \quad (7.2)$$

$$\Delta F = F_{R2} - F_{R1} = U_2 - U_1 \pm h_{slr} \sqrt{\frac{g}{d}} = \pm h_{slr} \sqrt{\frac{g}{d}} \quad (7.3)$$

In Equation (1.2)  $F_{R2}$  is the new value for the Riemann boundary,  $U_2$  its corresponding velocity and  $h_{slr}$  the amount of sea level rise.  $F_{R1}$  is the original Riemann value and  $U_1$  its velocity. The value for  $d$  can be derived from the model and upon assuming that the velocities before and after sea level rise will not significantly change ( $U_1 \approx U_2$ ), equation (1.3) can be obtained which is an expression for the difference in  $F_R$  values. Consequently the value for  $F_{R2}$  is:

$$F_{R2} = F_{R1} \pm h_{slr} \sqrt{\frac{g}{d}} \quad (7.4)$$

Model results with the new Riemann boundary conditions, show that this procedure is successful and that the assumption  $U_1 \approx U_2$  is justified.

## H Results 3D analysis scour holes

### H.1 Water-level results

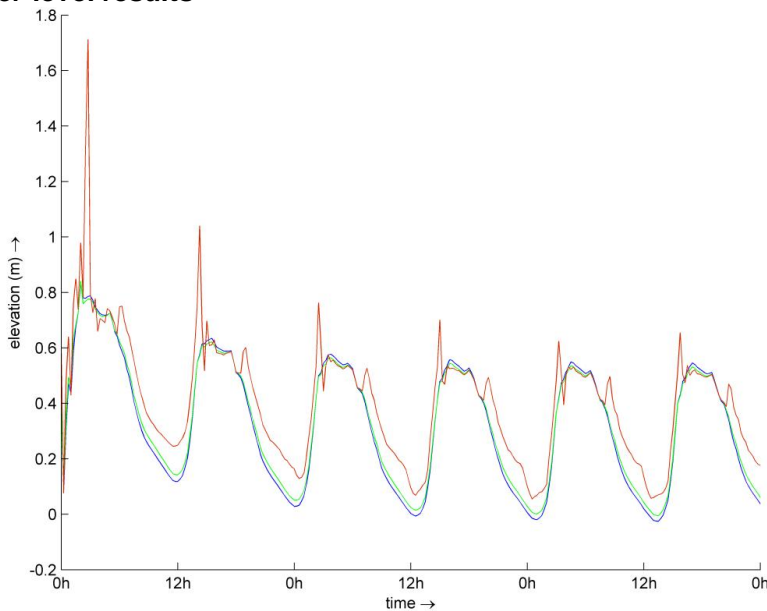


Figure H.1 Water level elevation taken from observation point at rkm 1005 of Spui River (sigma layer model: red, hydrostatic model: green, non-hydrostatic model: blue).

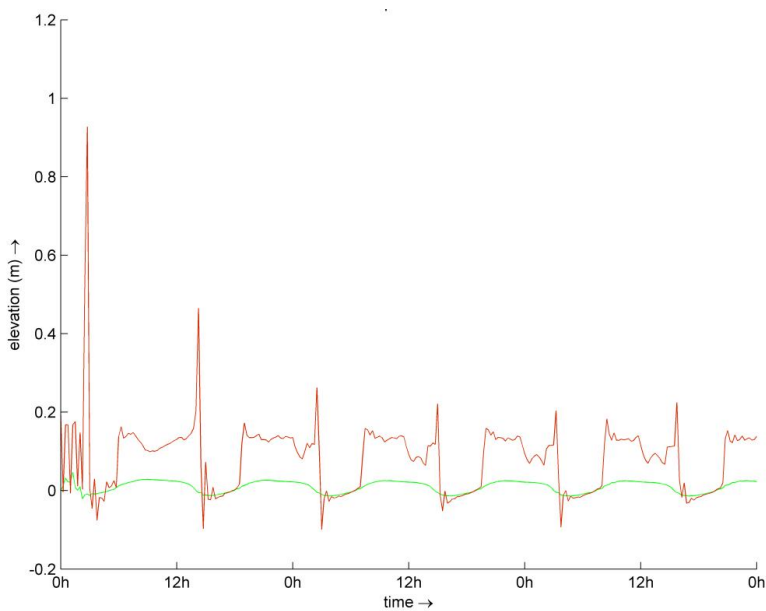


Figure H.2 Water level difference taken from observation point at rkm 1005 of Spui River with non hydrostatic model as reference situation (sigma layer model: red, hydrostatic model: green).

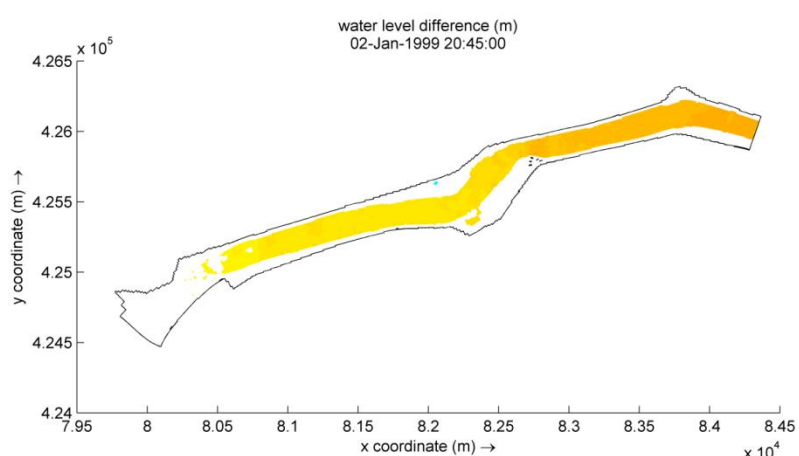
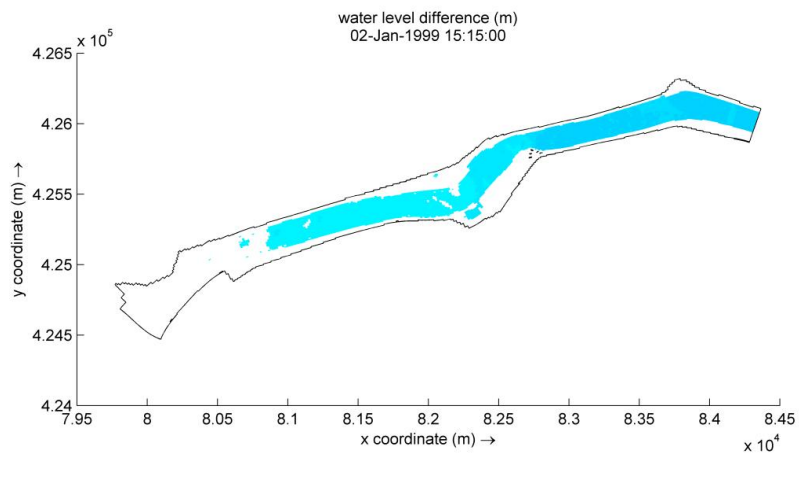


Figure H.3 Water level difference between hydrostatic and non-hydrostatic simulation at defined time steps.

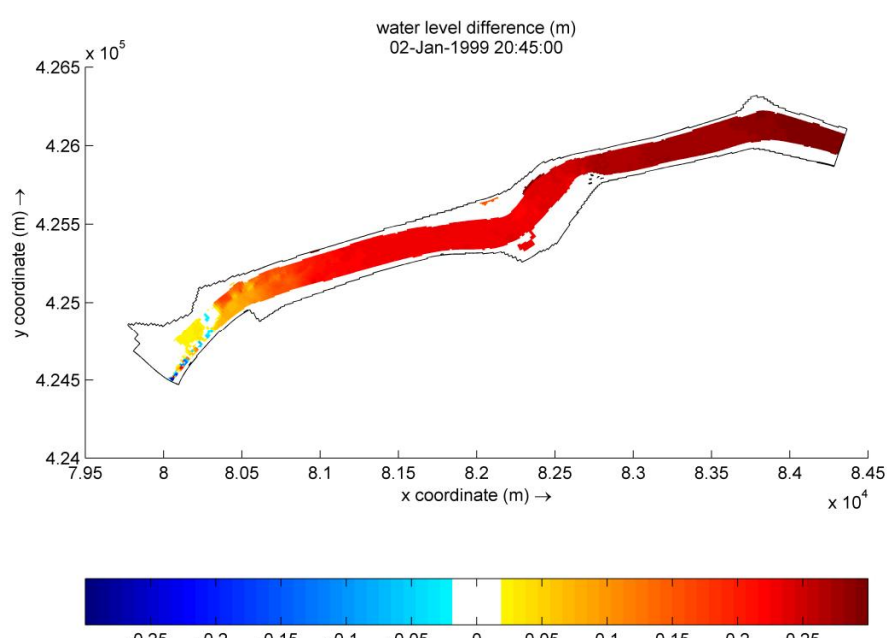
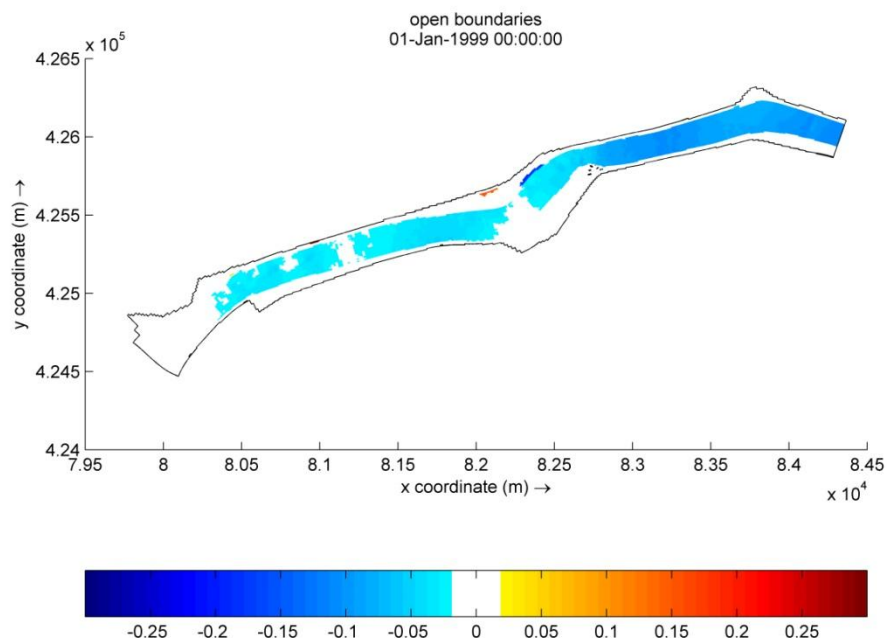


Figure H.4 Water level difference between sigma layer model and non-hydrostatic simulation at defined time steps.

## H.2 Computed stresses and velocities for different discharge scenario's

In the following, all results of the non-hydrostatic simulation are presented, i.e. for the low, medium and high river discharge scenario.

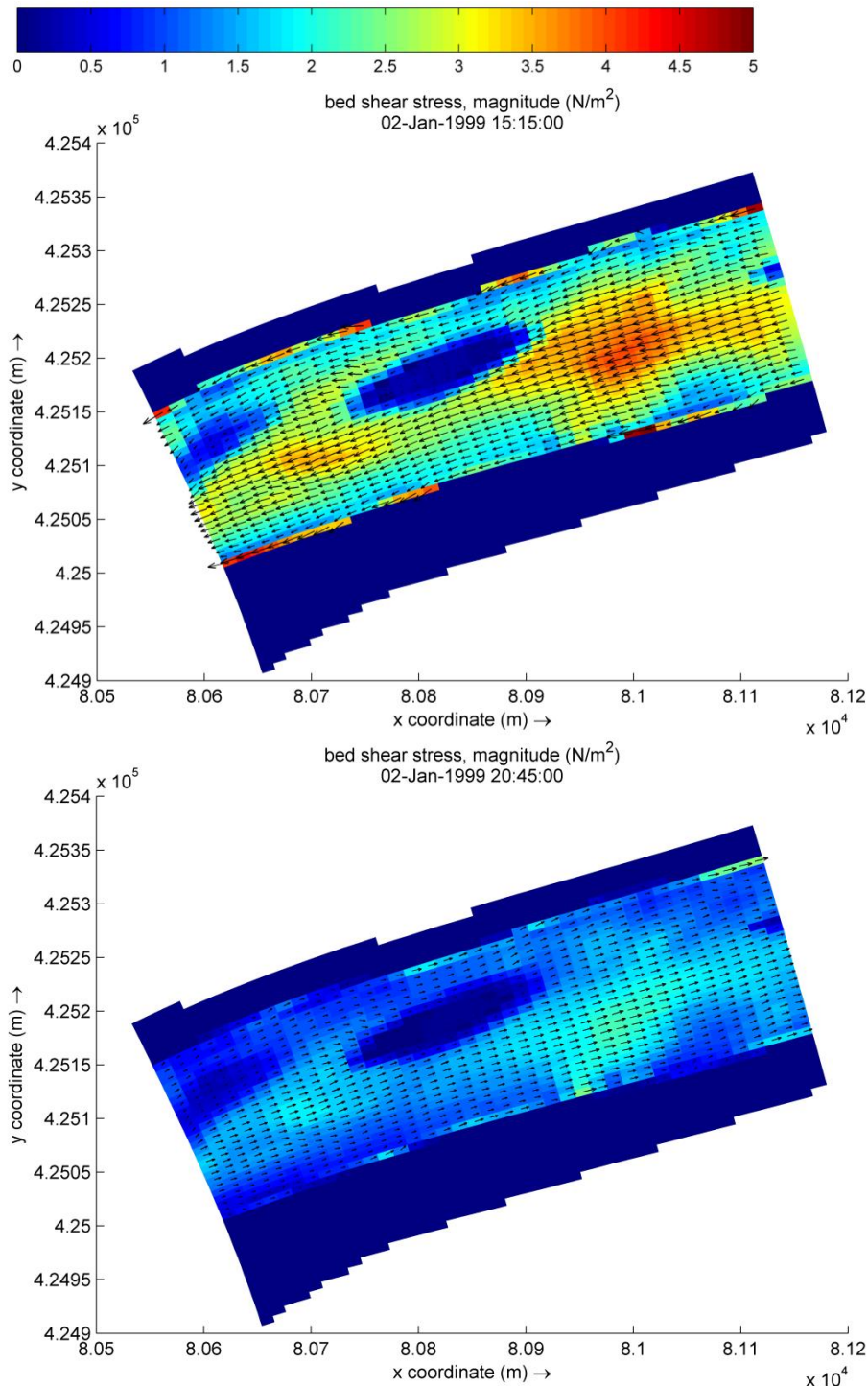


Figure H.5 Non-hydrostatic Z-layer model, bed shear stress, low discharge scenario.

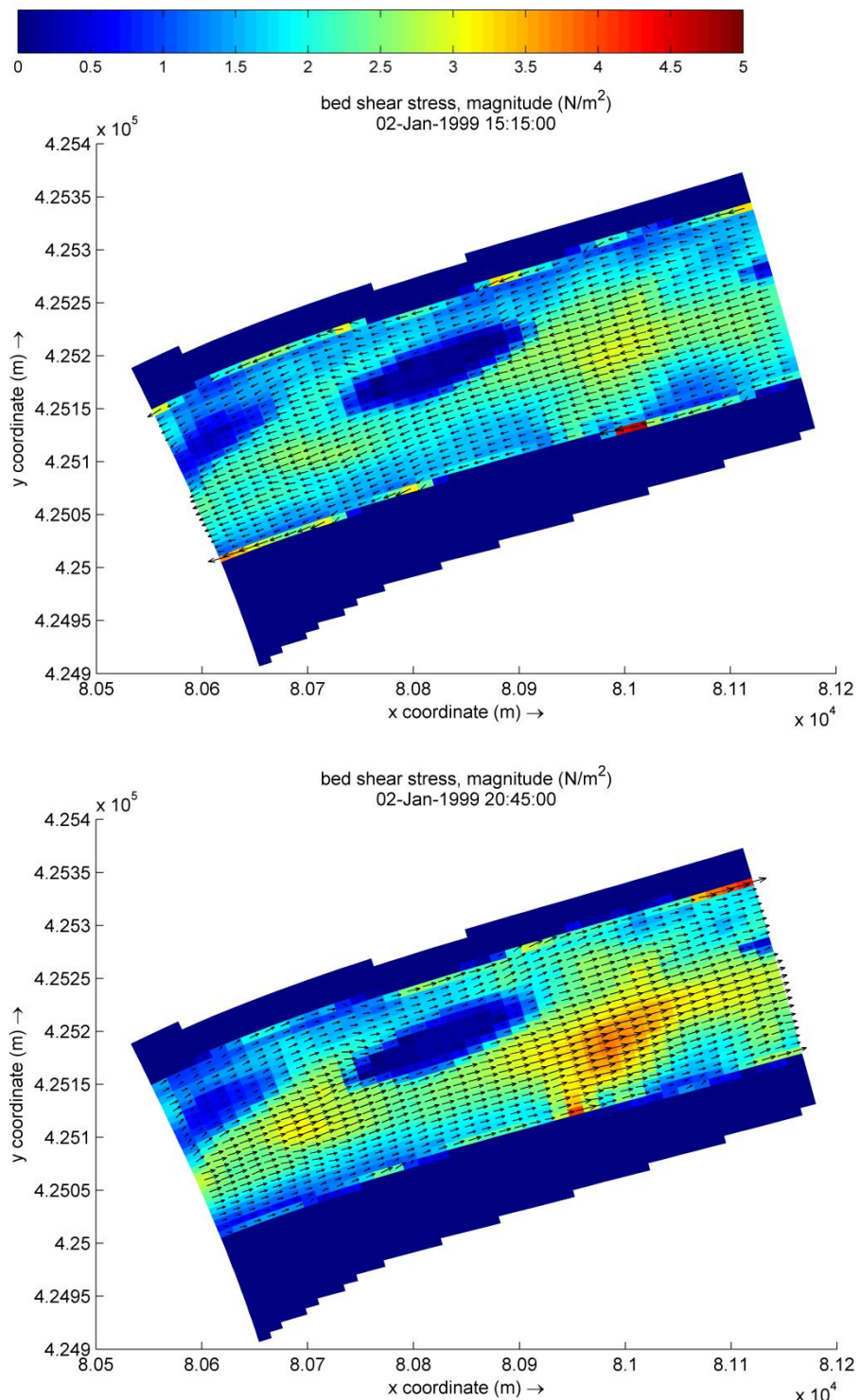


Figure H.6 Non-hydrostatic Z-layer model, bed shear stress, medium discharge scenario.

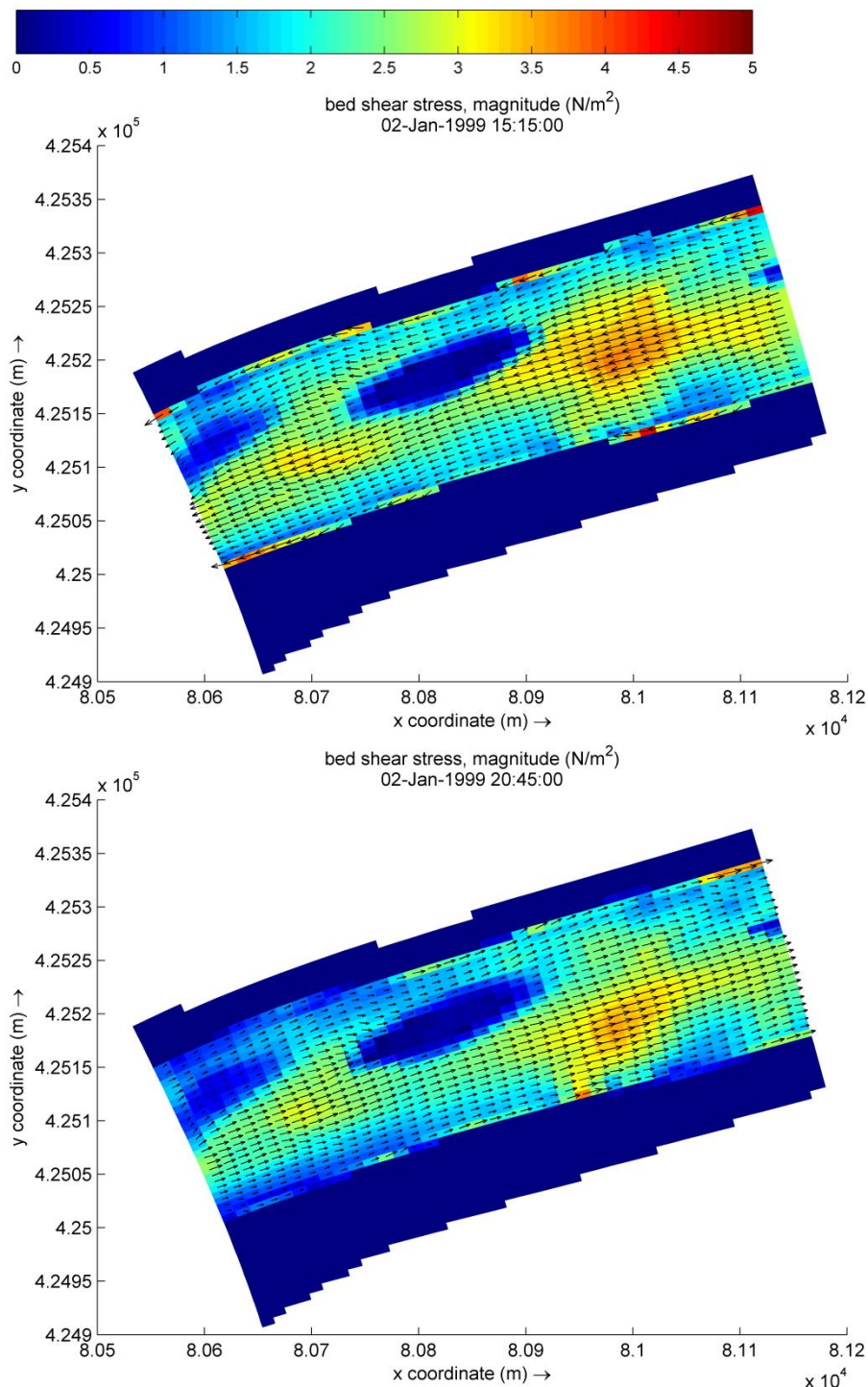


Figure H.7 Non-hydrostatic Z-layer model, bed shear stress, high discharge scenario.

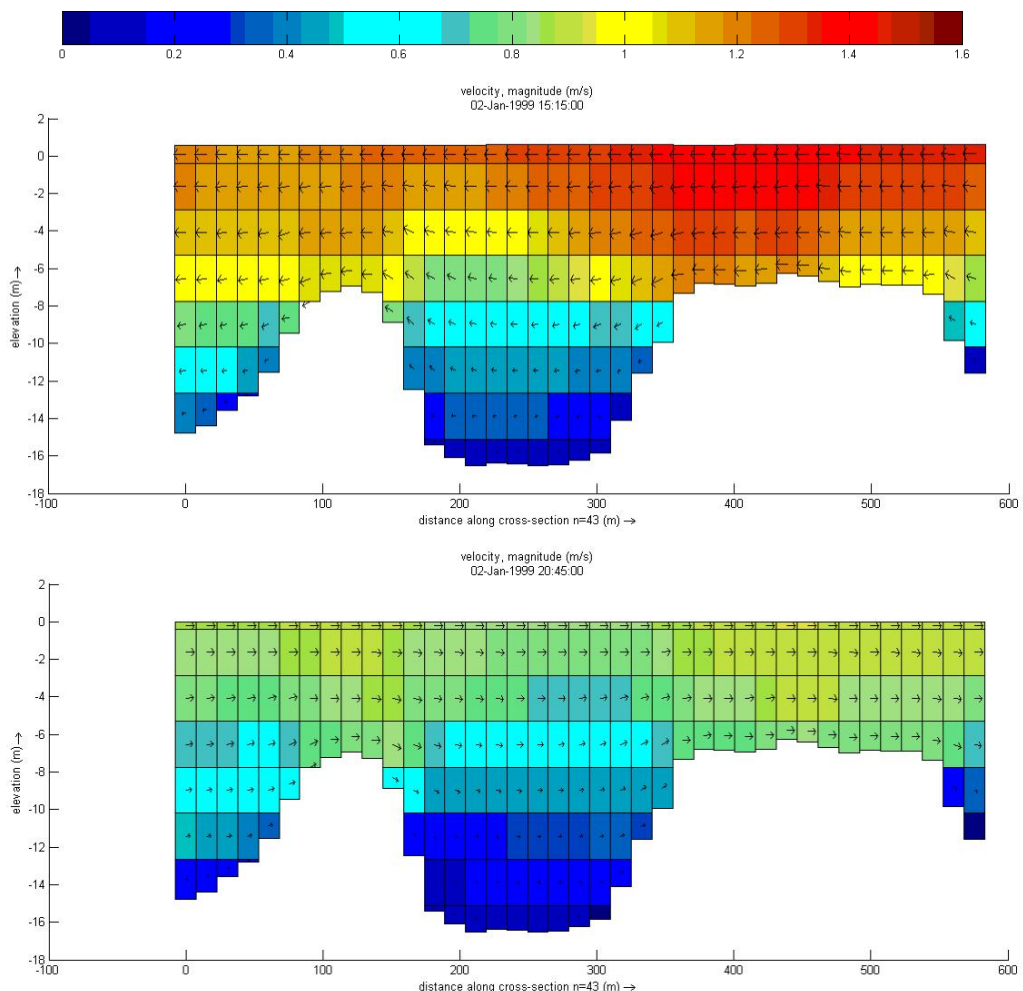


Figure H.8 Hydrostatic Z-layer model, velocity magnitude longitudinal cross section, medium discharge scenario.

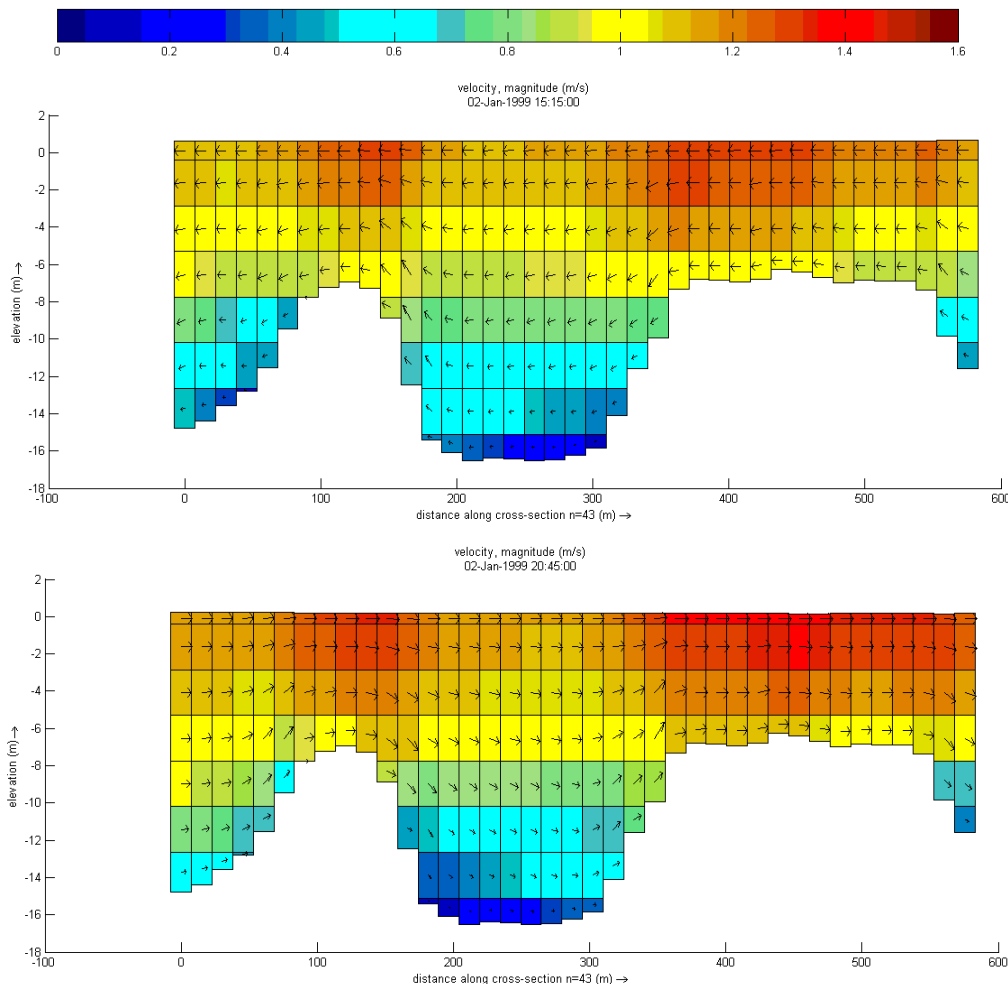


Figure H.9 Hydrostatic Z-layer model, velocity magnitude longitudinal cross section, medium discharge scenario.

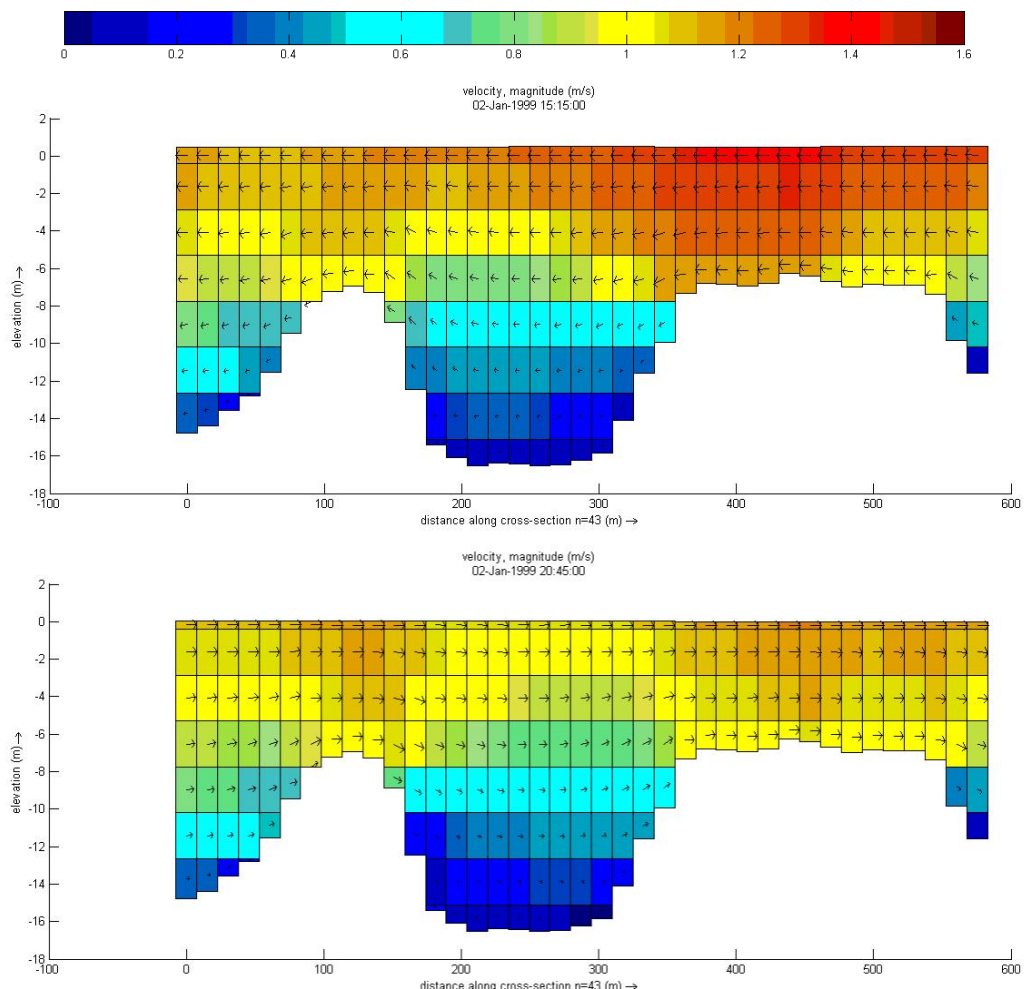


Figure H.10 Hydrostatic Z-layer model, velocity magnitude longitudinal cross section, high discharge scenario.

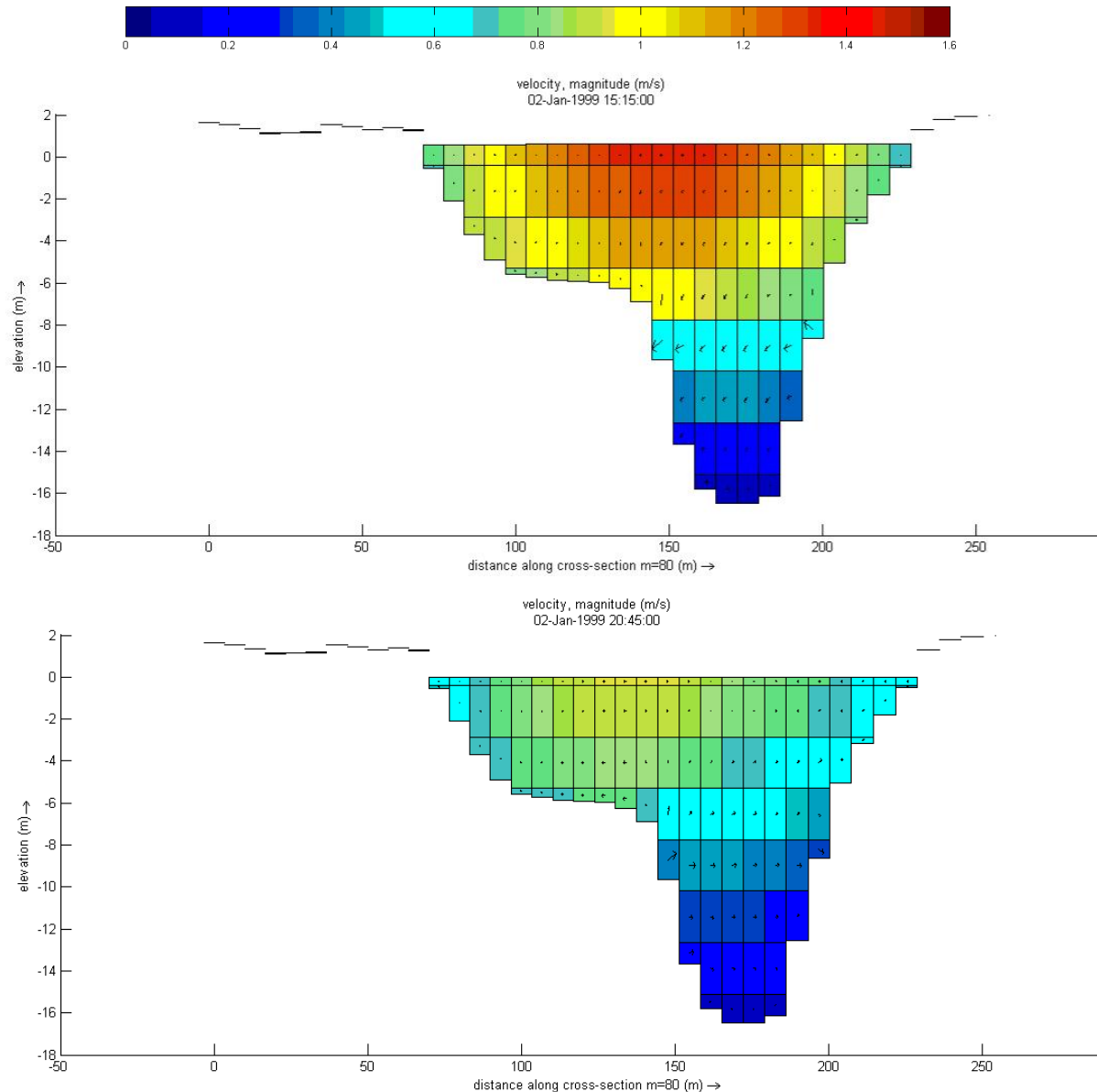


Figure H.11 Non-hydrostatic Z-layer model, velocity magnitude, transverse cross section, low discharge scenario.

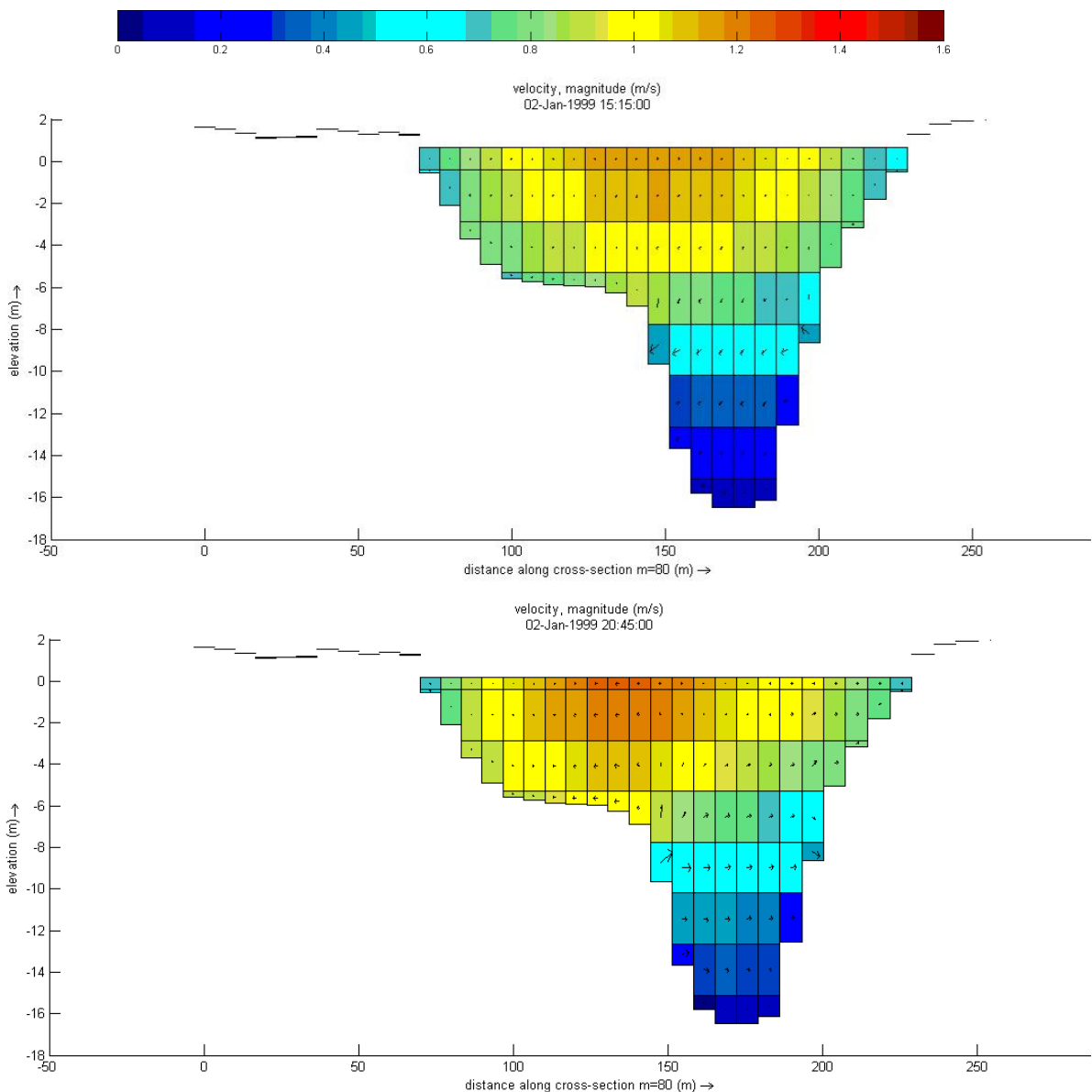


Figure H.12 Non-hydrostatic Z-layer model, velocity magnitude, transverse cross section, medium discharge scenario.

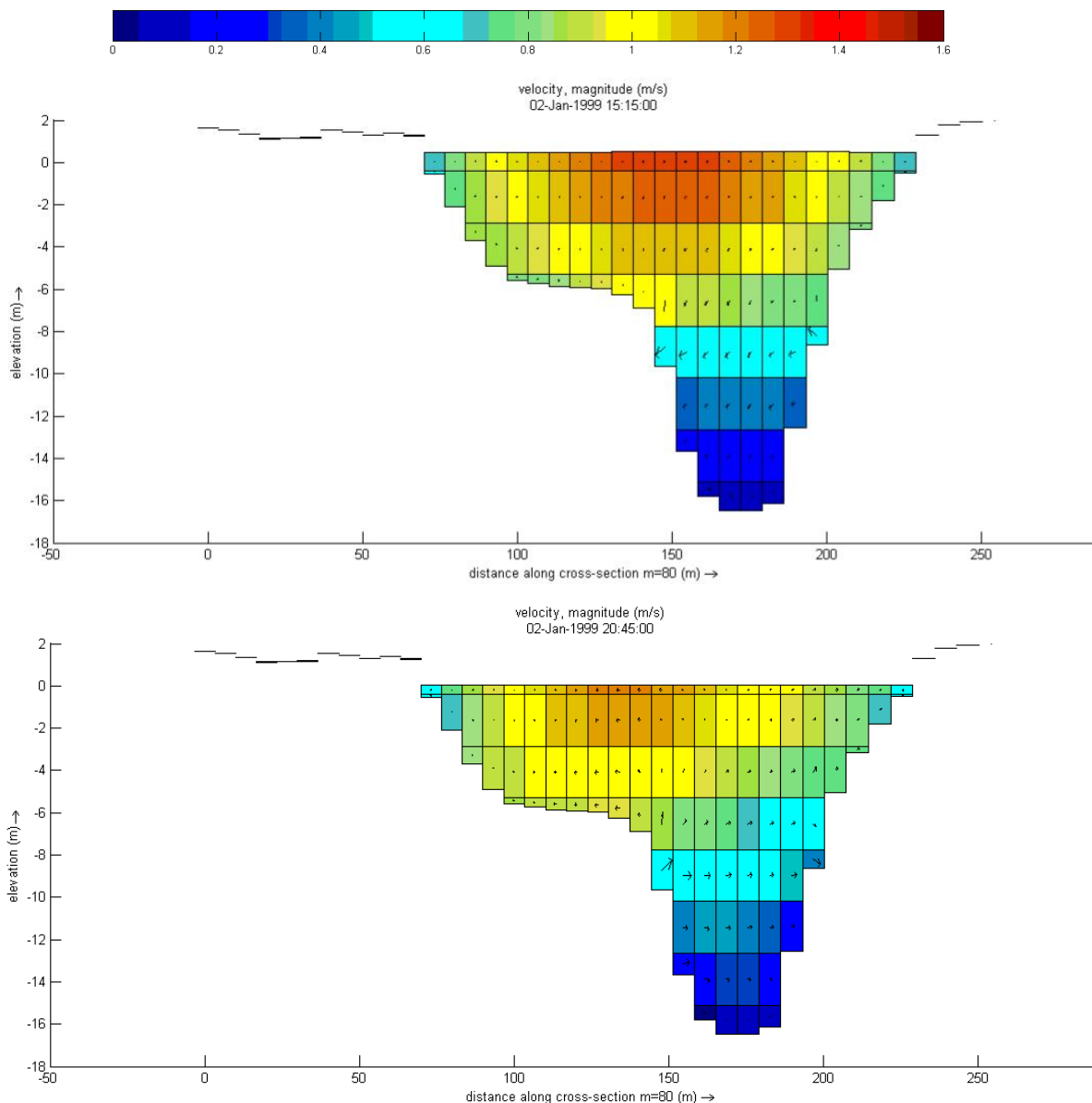


Figure H.13 Non-hydrostatic Z-layer model, velocity magnitude, transverse cross section, high discharge scenario.